

Alma Mater Studiorum – Università di Bologna

School of Engineering and Architecture

Master of Science in Electrical and Energy Engineering

TESI DILAUREA

In

TECHNOLOGICAL MANAGEMENT OF ELECTRICAL INFRASTRUCTURES M.C.I.

Reliability of Interfaces for HVDC Cable Accessories

Supervisor : Prof. Andrea Cavallini

Prof. Jerome Castellon

Submitted by

Adepu Rasagna

Matricula 0000851160

1st graduation session Academic

year 2019/20

PREFACE

This Master Research thesis was developed within the framework of the research project proposed by **Prof. Andrea Cavallini** and financially supported by **University of Bologna**.

The project was focused on the study of the TSM method for space charge measurement in dielectric materials employed for HVDC cables which was carried out in **University of Montpellier**. The Research activity was mainly developed at the **IES - Institute of Electronics and Systems (IES - Institut d'Electronique et des Systèmes)** Montpellier, France. Under the Supervisor of **Prof. Jerome Castellon**. He gave me the most valuable inputs for the project and supported me for the entire period. He has been very supportive and a source of motivation when at times the task has seemed unsurmountable.

During this research activity, for almost six months, the other three months of research has been carried out at the University of Bologna, under the prestigious supervision of **Prof. Andrea Cavallini**. Here mainly the project is focused on the study of Partial Discharge Injection in AC/DC, Leakage Measurement test on HVDC Cables and the Space charge measurements in PEA Method. I would like to thank **Prof. Andrea Cavallini** for giving an opportunity to do my Internship in France and for willing to help me when confronted with problems during the analysis. I benefited greatly from his expertise within the field and been encouraged by his enthusiasm. It has been my great privilege to work under his inspiring guidance.

Last but not least, I would like to thank my Friends, Fellow students, for their love and encouragement.

To my loving family ...

To my parents: for their continuous and unparalleled love, support, and encouragement.

To my brother: for always being there to support me.

... To my respected Supervisor ...

To Dr. Andrea Cavallini & Dr. Jerome Castellon for their continuous assistance and unlimited trust and support.

... To my colleagues ...

Who were companions through my journey

Declaration

I hereby declare that except where specific reference is made to the work of others, the contents of this dissertation are original and have not been submitted in whole or in part for consideration for any other degree or qualification in this, or any other university. This dissertation is my own work and contains nothing which is the outcome of work done in collaboration, except as specified in the text and Acknowledgements.

Ms. Rasagna Adepu
July 2020

Abstract

Cross-linked polyethylene (XLPE) and polypropylene (PP) insulations in HVDC cable systems are widely used in modern transmission networks. The focus of this project is mainly on the interfaces of the accessories (joints and terminations) with the cable body. The interface can be studied using techniques from elastic-plastic mechanics, reaching the conclusion that cavities will always exist where the two dielectric surfaces mate. The situation is greatly improved by using rubbery material (typically, silicon rubber) and oiling the surfaces, but the existence of free spaces makes the interfaces the most vulnerable points in a cable system.

The goal of this thesis is to understand breakdown mechanisms of interfaces through the analysis of partial discharges, space charge accumulation and leakage current measurement. Common non-destructive methods to determine the space charge distribution in cables for HVDC transmission are the Thermal Step Method (TSM) and the Pulsed Electro-Acoustic (PEA) Method. The present contribution concerns space charge distribution measurements in insulation samples and HVDC cable interface models. For interfaces, it highlights that there exists a critical voltage at which the space charge shifts from homo- to hetero-charge.

The conductivity characteristics of the XLPE insulation of HVDC cable are investigated under different applied mechanical stress and the breakdown voltage which could be affected by crosslinking byproducts within the insulation of the material.

Partial Discharge is a key tool to ensure the reliability and perform life extension of High Voltage electrical equipment. For cable interfaces, it is generally assumed that surface partial discharges create carbonized tracks at the contact between the cable insulation and the accessory body, both in AC and DC, leading to breakdown. In this thesis, it was not possible to reproduce this condition. Breakdown occurred through a mechanism that remains to be unraveled. A possible connection with the shifts mentioned above, from homo to hetero charge at the interface, seems to exist.

Keywords: Space Charge, Partial Discharges, Leakage Measurement Current, Temperature, Young's Modulus.

Table of contents

PREFACE.....	1
Declaration.....	3
Abstract.....	4
List of Figures.....	9
List of Tables	13
1. INTRODUCTION.....	14
1.1. The Aims of thesis were as follows:.....	17
1.2. Contributions:	17
1.3. Context:	18
2. DESIGN AND STRUCTURE OF HVDC CABLE.....	19
2.1. Preface:	19
2.2. HV Underground Cable Partial Discharge (PD) Box:.....	20
2.3. Technologies for HVDC Cable Accessories	21
2.3.1 Heat Shrink Accessories:	21
2.3.2 . Cold-Shrink Accessories:.....	22
2.3.3 Push on Accessories:.....	22
2.3.4 Hybrid Accessories:	23
2.4. Types of Cables for HVDC transmission:.....	23
2.4.1 Mass-Impregnated (MI) Cable:.....	23
2.4.2 Oil-Filled (OF) Cable:.....	24
2.4.3 Polypropylene Paper Laminate or Lapped Thin Film Insulated Cable:	25
2.4.4 Polymer-insulated or Extruded-insulation Cable:	25
2.5. HVDC cable insulation in AC and DC:.....	26
2.6. DC Characteristics of DC-XLPE Insulation Material:	26
2.6.1 XLPE Technology:.....	27
2.6.2 Polypropylene Technology:	27
2.6.3 Mechanical properties of polypropylene Nano composites:.....	28
2.6.4 Medium Voltage Polypropylene Compounds by HV Cable:.....	29
2.7. Power cables in High Voltages:.....	29
2.8. Use of PP in cable applications:	30
3. PARTIAL DISCHARGES IN HVDC CABLES.....	31
3.1. Preface:	31
3.2. Detection of PD:	31

3.3.	Type of Partial Discharges:	32
3.3.1	Internal Discharge:	32
3.3.2	Corona Discharge:	32
3.3.3	Surface Discharge:	32
3.4.	PD Background Noise:	33
3.5.	Performance of Insulation to PD:	33
3.6.	Partial Discharge Recurrence Pulses:	33
3.7.	Plasma PD Models:	35
3.8.	Partial Discharges in DC Insulation:	36
3.9.	Surface Discharge Distribution:	39
3.10.	Measurement Set-up:	39
3.10.1	Discussion of PD Monitoring for HVDC equipment:	40
3.10.2	Sensors:	40
3.10.3	Signal acquisition:	41
3.10.4	PD Analyzer:	41
3.10.5	Synchronous timestamping:	42
3.10.6	Voltage measurement:	42
3.10.7	Environmental sensors:	43
3.10.8	Oscilloscope:	43
3.10.9	Phase Resolved PD:	44
4.	REVIEW OF SPACE CHARGE MEASUREMENTS	45
4.1.	Preface:	45
4.2.	History behind the Thermal Step Measurement:	46
4.3.	Thermal methods:	49
4.4.	Principle of the Thermal Step Method:	49
4.5.	The thermal step method under applied DC field:	51
4.5.1	Experimental Set up:	52
4.6.	Space Charge in PEA Method:	52
4.6.1	Acoustic group:	53
4.7.	The Pulsed Electro Acoustic method:	54
4.7.1	Basic principle of PEA:	54
4.8.	De-Convolution process:	56
4.9.	Measurement Errors:	58
4.9.1	Random error:	58

4.9.2	Systematic error:	58
4.9.3	Errors in signal detection and data acquisition:	58
4.9.4	Errors in numerical processing of the signal:	59
5.	INTERFACES IN CABLE JOINTS	60
5.1.	Preface:	60
5.2.	Elastic modulus (Young's modulus or modulus of elasticity):	60
5.3.	Solid-Solid interfaces:	61
5.4.	Co-Relation between the surface and Breakdown strength:	63
5.5.	Interface Contact Model:	64
	XLPE-XLPE Interface:	67
6.	EXPERIMENTAL SETUP	68
6.1.	Measuring Setup:	68
6.1.1	Sample Preparation:	68
6.1.2	Experimental Set-up:	68
6.1.3	Thermal Diffuser:	69
6.1.4	pico-Amperometer:	69
6.1.5	DC Voltage Supply:	70
6.1.6	Computer:	70
6.1.7	Experimental Procedure:	71
6.2.	PEA Method:	71
6.2.1	Sample Preparation:	71
6.2.2	PEA System:	71
6.2.3	PEA Cell:	72
6.2.4	Pulse Generator	73
6.2.5	Device Casing:	74
6.2.6	Acoustic Signal Detector:	74
6.2.7	Signal Acquisition System:	75
6.2.8	Test Procedure:	75
6.3.	Partial Discharges in AC/DC:	75
6.3.1	Measuring Setup:	75
6.3.2	DC Voltage Power Supply:	76
6.3.3	Leakage Current Measurement:	77
6.4.	Partial discharge Acquisition:	77
6.5.	PD Waveform Viewer:	78

6.6.	Test Procedure:	79
6.7.	Specimen:	80
6.8.	Test Object:.....	81
6.9.	Mechanical pressure calculation:.....	82
7.	TEST RESULTS AND ANALYSIS	85
7.1.	Space Charge in XLPE and PP:.....	85
7.1.1	Type-2:	85
7.1.2	Type-1:	88
7.1.3	Space charge in polypropylene samples (TSM).....	89
7.2.	Space charge in XLPE samples (PEA):.....	90
7.2.1	Space Charge Behavior:	91
7.3.	Comparison between PEA and TSM:.....	92
7.4.	Partial Discharge Monitoring:	93
7.4.1	Leakage Current Measurement:	96
7.4.2	DC Breakdown Voltage	97
7.5.	Co-Relation between Space Charge and PDIV-DC:	99
7.6.	Relation between Applied Pressure and PDIV:.....	100
7.6.1	Partial Discharge Inception Measurements:	100
8.	CONCLUSION	104
9.	FUTURE SCOPE.....	105
10.	REFERENCES	106

List of Figures

Fig:2. 1 Single-core cable with bonded or strippable insulation screen and copper wire earth screen	19
Fig:2. 2 Power Cable Components	20
Fig:2. 3 Partial Discharge (PD) Sensor Terminal Box	20
Fig:2. 4 Partial Discharge accumulation in cables.....	21
Fig:2. 5. Shrinking joint insulation	22
Fig:2. 6 Installation of a cold-shrink joint sleeve with spiral tape holdout.....	22
Fig:2. 7 Screened separable ‘T’ connectors (or elbows).....	23
Fig:2. 8 Mass Impregnated HVDC Cable.....	24
Fig:2. 9 Oil-Filled HVDC Cable.....	25
Fig:2. 10 PPL	25
Fig:2. 11 Electric field distribution at a cable end using stress control materials is illustrated here by the pattern of equipotential lines that are graded smoothly between the coaxial cable region at the right and the open HV conductor at the left.....	26
Fig:2. 12 Polypropylene Cable	28
Fig:3. 1 Discharges for Internal, Corona and Surface.....	32
Fig:3. 2 The a-b-c equivalent circuit for describing PD recurrence process	33
Fig:3. 3 The principle of PD pulses occurrence for a-b-c circuit.....	34
Fig:3. 4 Positive and Negative streamer with a thin space charge layer at their tip	36
Fig:3. 5 Basic PD parameters for AC (left) and DC (right) excitation voltages. The magnitudes of PD pulses are represented by q_i while the phase and time differences between successive pulses are represented by ϕ_i and Δt_i	38
Fig:3. 6 Ramp test profile for DC testing. VR is the peak value of the AC PD inception voltage.....	39
Fig:3. 7 PD test cell with HFCT sensor	41
Fig:3. 8 PD-Analyzer software	42
Fig:3. 9 Voltage Measurement.....	43
Fig:3. 10 Oscilloscope	43
Fig:3. 11 Phase-resolved plot of PD activity accumulated voids	44

Fig: 4. 1 Accumulation of charges	45
Fig: 4. 2 PEA and TSM space charge measuring range in cable samples.	46
Fig: 4. 3 Electric Representation of TSM	511
Fig: 4. 4 Double Capacitor.....	51
Fig: 4. 5 Experimental set-up.....	52
Fig: 4. 6. Propagation of the pressure wave.....	54
Fig: 4. 7 Left Working principle of the PEA method and Right Principle diagram	555
Fig: 4. 8 An example of PEA measurement results from a sample containing no space charge	56
Fig: 4. 9 Ideal charge profile detected by the piezoelectric transducer.	57
Fig: 4. 10 Real output signal after amplification	57
Fig: 4. 11 Example of deconvolution.....	57
Fig: 5. 1 Tension and Compression.....	61
Fig: 5. 2 Air filled capacities in two dimensional.....	62
Fig: 5. 3 Conceptual diagram of the parameters having an influence on solid-solid interface.....	63
Fig: 5. 4 Indicates the relation between interface strength and pressure.	64
Fig: 5. 5Simplified contact model of two rough surfaces in contact according to the Greenwood-Williamson contact model.	64
Fig: 5. 6 The electrical model of interface and field strength inside the voids.....	66
Fig: 5.7 Paschen Curve and Weibull plot.....	67
Fig: 6. 1 XLPE-3D specimen.....	68
Fig: 6. 2 Experimental set-up of TSM	68
Fig: 6. 3 Thermal diffuser	69
Fig: 6. 4 Keithley 428 Current Amplifier	69
Fig: 6. 5 DC supply system with the connections for the circuit.....	70
Fig: 6. 6 Software used for TSM	70
Fig: 6. 7 Illustration of sample preparation.....	71
Fig: 6. 8 Experimental Set up of PEA Measurement.....	72
Fig: 6. 9 Block diagram of the PEA cell.....	72
Fig: 6. 10 Pulse generator	73

Fig: 6. 11 PEA System.....	74
Fig: 6. 12. The measuring setup.....	76
Fig: 6. 13. DC voltage power supply	76
Fig: 6. 14. Current measurement equipment.....	77
Fig: 6. 15 Oscilloscope TEXTRONIX 5 Series.....	78
Fig: 6. 16 PD Waveform Viewer	79
Fig: 6. 17. 3D Specimen configuration.....	80
Fig: 6. 18 Test object nylon bolt type	81
Fig: 6. 19 Test object steel bolt type.....	82
Fig: 6. 20 Bolt and nut dimension specification	83
Fig: 7. 1 Experimental set up of TSM.....	85
Fig: 7. 2 3D Specimen with 2a configuration	86
Fig: 7. 3 Space charge Measurement using TSM Method for (left) negative and (right) positive applied field for Type-2a Sample.....	86
Fig: 7. 4 Space charge Measurement using TSM Method for (left) negative and (right) positive applied field for Type-2b Sample.....	87
Fig: 7. 5 Space charge Measurement using TSM Method for Negative field	88
Fig: 7. 6 Circuit connection of TSM.....	89
Fig: 7. 7 Space charge Measurement using TSM Method for Positive field on PP sample.....	90
Fig: 7. 8 Field dependent Space charge characteristic on XLPE.....	91
Fig: 7. 9 Thermal Step Method (TSM) (a) conditioning phase, (b) measurement phase .	92
Fig: 7. 10 Partial Discharge Appearance 1a on 14kV@8 bar pressure Leakage current characteristics.....	95
Fig: 7. 11 Partial Discharge Appearance 1a on 14kV@5 bar pressure Leakage current characteristics.....	95
Fig: 7. 12 Partial Discharge Appearance 1a on 11kV@3 bar pressure Leakage current characteristics.....	96
Fig: 7. 13 Dependence of leakage current on clamping ressure	97
Fig: 7. 14 Different specimen on breakdown voltage measurement	98
Fig: 7. 15 Mechanical pressure influence on breakdown voltage XLPE – LDPE interface	98
Fig: 7. 16 Illustration of void on solid-solid interface	99

Fig: 7. 17 Illustration of an interface, showing voids and contact spots air-filled cavities at the interface..... 100

Fig: 7. 18 An electrical model of voltage drops at the interface..... 100

Fig: 7. 19 Breakdown Mechanism 101

Fig: 7. 20 Software for PD in AC 102

Fig: 7. 21 AC PD inception stress of interface surface..... 103

List of Tables

Table :4. 1 Information output of space charge monitoring techniques	46
Table :4. 2 Overview of methods its resolution and the sample thickness	48
Table :4. 3 Acoustic methods for non-destructive space charge measurement	53
Table: 6. 1 Test pressure range.....	84
Table: 7. 1 Indicates the PP poling field with temperature.....	89
Table: 7. 2 It indicates the Applied Field with Charge accumulation in the sample.	90
Table: 7. 3 XLPE – XLPE PD monitoring results	94
Table: 7. 4 XLPE – XLPE leakage current.....	97
Table: 7. 5. Breakdown voltage result	98
Table: 7. 6 PDIV voltage result	102

1. INTRODUCTION

Electric power network is one among the foremost vital and sophisticated pieces of infrastructure. Electric systems operators must maintain network robustness. Polymer insulated HVDC cables and their accessories are a key to achieve flexible DC power transmission and space charge inhibition is usually a drag to unravel by science and engineering of electrical insulation. Since the 1980's, there are many papers on space charge in cables reported, and there are few papers on electric insulation of accessory. Most of researchers and engineers focus on the way to suppress the space charge in cable insulation. And there are few reports on the dielectric properties of accessory insulation. According to the Maxwell Wagner model, there will be amount of space charge present near the interface. The more difference of the ratio between dielectric constant and conductivity of both insulations, the higher amount of space charge emerges at the interface. And therefore, the higher amount of space charge stores at the interface, the more distortion of electrical field occurs. Therefore, its necessary to investigate the conductivity of accessory insulation intimately. Since the conductivity of polymer insulation relates closely to the temperature and electrical stress, much attention should be paid to the quantitative effect of electrical stress on the conductivity of accessory insulation.

Furthermore, the compatibility of cable and its accessory insulation on the conductivity should even be investigated. Severe defects in insulation systems are common case of failure in electrical equipment. These defects often have a lower electrical breakdown strength than the encompassing insulation material, which suggests that discharges can occur inside them. If the discharge does not bridge the gap between electrodes, it is defined as a partial discharge (PD). Measurements of PD activity are a non-invasive tool that can be used to quantify defect severity prior to failure. Despite sustained research interest, much remains unknown from the underlying discharge physics to the precise interpretation of phase resolved partial discharge (PRPD) patterns. In conjunction with experiments, modelling PD activity has also received attention to investigate whether complex PD data are often described by a simple system of equations, with the aim of using simulations to gain insight into the PD system.

For ages, insulation breakdown has been a crucial concern for manufacturers and users of electrical engineering components. One among the leading causes of the electrical weakness is that the existence of solid-solid interfaces in cable apparatus and joints. An interface contains microscopic imperfections like cavities, protrusions, and contaminants which will reduce the

tangential AC electric breakdown strength (BDS) of the interface since these imperfections cause local field enhancements. Local fields are likely to initiate partial discharges (PD) and trigger electrical discharge which will cause tracking failure eventually. An inherent problem of any cable connector and termination is that the presence of interface between the materials. If the BDS at some extent on the interface is exceeded by local field enhancement, partial discharges are going to be initiated. The interfacial breakdown (BD) between the contacting surfaces of two dielectric materials was reported to represent one among the principal causes of failure for power line joints and connectors, where coefficient of elasticity plays a critical role. Under varying interfacial pressures, the coefficient of elasticity features a significant influence on the structure of the cavities at the interfaces, and hence on the BDS of the interface. Since the combination of two solid dielectrics increases the risk of existence of microscopic activities and imperfections on the interface reducing the BDS of the interface considerably particularly when the electrical field has tangential component.

Important failure of such sort of interface is that the tracking failure defined as the formation of a conductive path. Even though the magnitude of electrical field is much lower compared to the dielectric strength of the majority insulation. The effect of the contact pressure on the surface roughness on the tangential BDS and therefore the higher the interfacial pressure and smooth surface results in higher breakdown. In this experiments, AC breakdown testing of solid-solid interfaces was carried out were subjected to varied contact pressures.

The improvement of insulating system performance and therefore the present tendency to develop materials for HVDC cables require a radical knowledge of the physical phenomena which happen within the dielectrics submitted to high electric fields. It seems more and more probable today that a decrease of dielectric performance might be associated with the electric charges which tend to accumulate in insulating materials, commonly referred to as 'space charge'. Thus, when an insulator is submitted to high electric stress, charged regions develop in its bulk and modify the repartition of the constraints. The residual field created by the space charge can locally increase the applied stress, overstressing the insulator. Local augmentation of the internal energy of the dielectric by the stored charge also likely to accelerate degradation by lowering the activation barrier of undesired chemical processed.

During the past years, many research groups have developed different techniques which are useful for detecting space charges accumulation in dielectric materials. Most of those

techniques are often grouped as thermal and acoustic methods. One among these techniques which the experimentation is carried with thermal step method (TSM) and Pulsed Electro Acoustic (PEA), in which TSM is predicted on the propagation of a thermal wave, which generates a temporary local displacement of the space charge. This is often reflected at the electrodes by a variation of the induced charges, which allows a determination of the distribution of the residual field and charge density across the sample. The TSM is applicable to any sample presenting a geometry that the spatiotemporal distribution of the temperature is often calculated, like material specimens and industrial components (power cables, capacitors, printed boards and stator windings).

TSM has been used on short circuited specimens via a current amplifier, which measures the signal generated by the thermal wave propagation (thermal step (TS) current). The fundamentals of the short circuit experiment are reviewed first, the principle and theoretical basis resulting in the TS signal being addressed intimately. The core of the work is dedicated to an evolution of TSM which allows the distribution of space charge in flat samples and in power cables while submitted to an external dc field.

The 'voltage-on' measurements supply useful information for calibration and therefore the proposed principle might be used for industrial applications. The experimental setup, the validation and therefore the perspectives opened by the 'under field' TSM are presented and discussed. Comparatively simple measurement system and a good spatial resolution, the Pulsed Electro Acoustic (PEA) method is currently the foremost reliable way to detect space charge accumulation in the dielectric material of HVDC cables. Since 1985, the year demonstrated the possibility of measuring space charge accumulation with a non-destructive method, the scientific community has made important progress within the use of the PEA method. The presence of space charge in the dielectric is a typical phenomenon occurring in HVDC cables. This is due to the DC high voltage supply of the cable line, which determines the application of an electric field for a long time in the dielectric region: this enables space charge accumulation phenomenon PEA method to carry out space charge measurements on flat samples of dielectric materials and more recently on HVDC mini and full size cables. Much progress has been made in the knowledge of performance and applicability of the PEA method. However, further improvements to the PEA method are needed to obtain a universally accepted measurement protocol and to achieve the possibility of measuring on-site the aging of HVDC cables during their lifetime.

1.1. The Aims of thesis were as follows:

1. Analyzing the behavior of space charge using TSM on 3D specimen in which the electrodes are deposited inside the layer of XLPE.
2. Developing the improved model of PD activity in DC.
3. Investigating the PD activity and space charge to find seek out some relation between them.
4. Investigating the PD activity in AC by using the mechanical stress.
5. Analyzing the behavior of space charge using TSM on XLPE sample.

1.2. Contributions:

According to the literature review a PD model and space charge model was developed. The key improvements of the model over earlier work in the literature were as follows:

- **Inception and Generation Points** - The model considers the inception of a discharge and therefore the electron generation processes governing PD activity at a variety of locations within the PD system.
- **Two Electron Trap Depths** - The detrappable electron population is split between two trap depths. This is often different to other approaches within the PD modelling.
- **Surface Charge Density Distributions:** Surface charge density distributions, due to discharge activity, in an earlier Poisson PD model were discrete, which results in discontinuities in the electric field at the surface.
- **Depolarization time:** Time starting after voltage removal as soon as the cable conductor has been short-circuited and grounded.
- **Poling Time:** Time starting as soon as the voltage applied between cable conductor and ground cable metal sheaths reaches the rated voltage V_0 of the tested cable system.
- **Trapped charge density:** This is the density of charge trapped within the volume of the material just after voltage off, after having been energized at a given DC field (above threshold field). The average value of the charge density trapped is calculated from the spatial distribution of charge measured using PEA.
- **Trap Depth:** Traps are potential wells, where a free charge loses its energy and continues to reside until it acquires the energy to escape. Therefore, the minimum energy which a charge must acquire to escape from a potential well is defined as the trap depth. After voltage off, charge decay characteristics obtained from PEA measurements are used to estimate trap depth.

- **Apparent trap-controlled Mobility:** Charges trapped within the volume of the material start de-trapping, after voltage off on short circuiting the electrodes. These charges contribute to decay current. The charge de-trapping occurs from different trap energy levels and with certain mobilities. The value of charge decay mobility depends on the energy levels of trapped charge and is called apparent trap-controlled mobility.
- **PDIV:** Applied voltage at which repetitive PD are first observed in the test object when the applied voltage to the test object is gradually increased from a lower value to no PD.
- **Repetitive PD:** Pulses exceeding a prescribed magnitude.

1.3. Context:

The work is split into chapters as follows:

Chapter 1 - A brief introduction, outlining the research conducted for the project.

Chapter 2 - HVDC power cables, power transmission and the structure of cable mainly in Joints in XLPE/PP materials.

Chapter 3 - An analysis of the literature is undertaken, an introduction to PD phenomena of existing PD models and a summary of PD data analysis.

Chapter 4 - Space charge measurement systems and the working principle of TSM and PEA cell is described.

Chapter 5 - Interfacial charge in dielectric/dielectric interfaces is described.

Chapter 6 – Test set up of space charge measurements in TSM and PEA, Partial discharge in AC/DC and the leakage Measurement Current.

Chapter 7 - The results showed that of Space charge, PD activity models.

Chapter 8 - The conclusions of the work are presented, and future projects that could be developed from this work discussed.

2. DESIGN AND STRUCTURE OF HVDC CABLE

2.1. Preface:

Until the 1980s, most of the MV cables installed by utilities and industry were paper-insulated type in which the insulation over the conductors is built up by applying multiple layers of special cellulose paper. This paper insulation must be impregnated with insulating oil or compound to exclude air and impart good electrical properties. Fig. 2.1. Indicates a common feature of all paper cables is a metallic sheath, normally extruded Lead or Aluminum, enclosing the paper-insulated core. The main purpose of the metallic sheath is to give the paper insulated cores complete protection from the environment outside the cable.

With the objective to improve long-term reliability of XLPE power cables, it is essential to understand the mechanisms of degradation and breakdown of XLPE solid insulation material and interfacial phenomena. The insulation performance of polymers usually decreases quickly with high voltage application if partial discharges PD occurs in voids or by defects. Hence, PD detection and diagnosis are one of the most important means to test HV cables. In the recent years, PD tests have been widely conducted after XLPE cables were completed, and the importance of PD test has been already recognized. Moreover, we have investigated physical phenomena and degradation processes by PD. However, identification of defects and degradation processes of XLPE power cable joints have not been fully understood yet. From this viewpoint, we have been trying to identify the types of defects and elucidate the degradation processes of XLPE cable joint by measuring patterns and PD statistic parameters, etc.

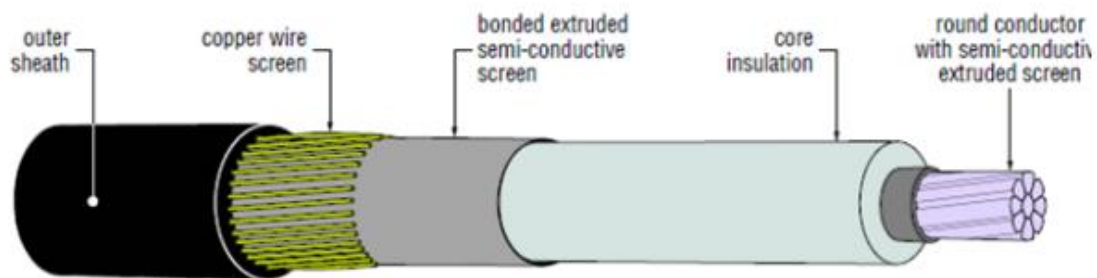


Fig:2. 1 Single-core cable with bonded or strippable insulation screen and copper wire earth screen

The functions of cable components are as follows:

- Conductor: Transports electric current
- Conductor screen: Provide for uniform electric field in cable insulation

- XLPE insulation: Electrical separation between the cable conductor at high voltage and cable sheath at ground potential
- Insulation screen: Containment of electric field
- Metallic sheath: Water barrier and mechanical protection of cable-core provide for the flow of fault currents
- Anti-corrosion and anti-termites` jackets: Protect cable metallic sheath and insulate the sheath to withstand induced and transient voltages.

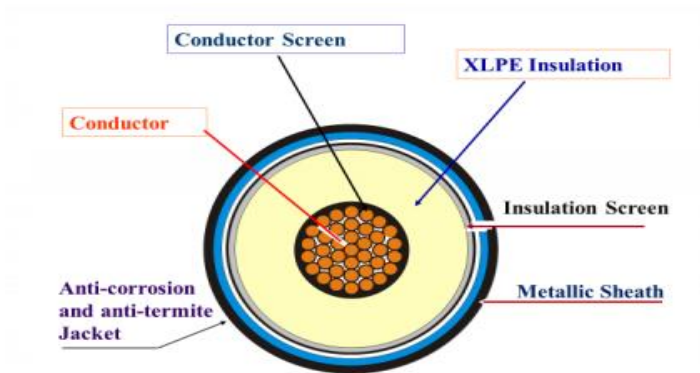


Fig:2. 2 Power Cable Components

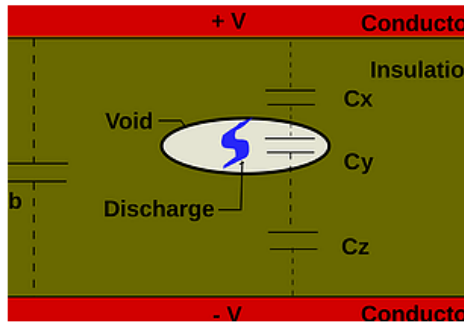
2.2. HV Underground Cable Partial Discharge (PD) Box:

Major function of a cable PD box is to provide a waterproof, accessible, enclosure for electrical wiring connected to PD detectors at cable joints and terminations which is shown in Fig.2.3



Fig:2. 3 Partial Discharge (PD) Sensor Terminal Box

HVDC polymeric insulation showed that significant space charge builds up starts when the applied field is above a critical value, the so-called threshold for space charge accumulation. In fig.2.4 which explains about the voids and discharge of PD in airgaps on HVDC cables and the percentage of insulation failure with different components.



Component	Percentage of insulation failure
Transformers	84%
Circuit Breakers	21%
Disconnect Switches	15%
Insulated Switchgear Bus	95%
Bus duct	90%
Cable	89%
Cable Joints (splices)	91%
Cable Terminations	87%

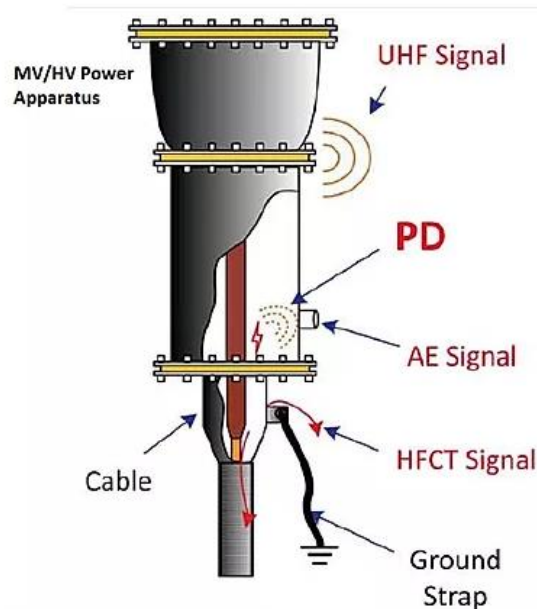


Fig:2. 4 Partial Discharge accumulation in cables.

2.3. Technologies for HVDC Cable Accessories

2.3.1 Heat Shrink Accessories:

Heat-shrinkable sleeves and molded parts are made of special crosslinked plastic materials that are heated and stretched expanded and then cooled whilst held expanded as shown in the Fig.2.5. The expanded state becomes frozen into the molecular structure. Extruded tubing and

molded parts are supplied in this state. The installation process involves positioning and re-heating the expanded parts, usually with a propane or butane gas torch, until the parts shrink recover on to whatever they have been placed. Because a naked flame is involved (or perhaps a powerful hot air gun), an appropriate level of installer skill is required to ensure full recovery, avoiding faults such as voids in the interfaces of insulating layers, or burning of the material surface.



Fig:2. 5. Shrinking joint insulation

2.3.2. Cold-Shrink Accessories:

Cold-shrink sleeves and molded parts are also supplied in an expanded form but in this case on some form of rigid former or hold-out. The hold-out is removed during installation to allow the stretched part to recover into position on the joint or termination. Cold-shrink components are usually made from soft flexible materials such as silicone rubber and EPDM as shown in Fig.2.6



Fig:2. 6 Installation of a cold-shrink joint sleeve with spiral tape holdout

2.3.3 Push on Accessories:

General term referring to joints, terminations and separable connectors that are not supplied in an expanded form. Each part is sized such that it forms an interference fit with the cable and can be pushed into position, usually without the need for special tooling. These accessories are also referred to as slip-on. There are many designs of terminations and joints in this technology category as shown in Fig.2.7. Applications extend well beyond MV up to the highest system voltages. The most well-known MV push-on accessories are fully screened separable connectors for connecting cables to electrical equipment via standardized bushings.



Fig:2. 7 Screened separable ‘T’ connectors (or elbows)

2.3.4 Hybrid Accessories:

This specific type of accessories comprises a mix of heat-shrink, cold-shrink, and push-on components. The recommendations applying to each technology should be followed. Some utilities favor joints that include a pourable resin. The usual function of the resin is to provide additional mechanical protection and/or moisture sealing.

2.4. Types of Cables for HVDC transmission:

Besides there are different types of HVDC cables are available, depending mainly on cable insulation which are as follows.

- Mass-Impregnated (MI) cable
- Oil Filled cable
- Polypropylene Paper Laminate (PPL) or Lapped Thin Film Insulated Cable
- Polymer-insulated or Extruded-insulation Cable.

2.4.1 Mass-Impregnated (MI) Cable:

MI cable is mainly used in most of the applications. The copper or aluminum conductor have a compressed or a compact round shape. The conductor is covered by oil and resin-impregnated papers the resin serves for providing the oil with non-draining characteristics. The conductor semicon and insulation semicon layers are of carbon-loaded papers, whereas the outer layer consists of copper or aluminum tapes and/or woven fabrics. Fig.2.8 explains about the Mass Impregnated HVDC Cable. The fully impregnated cable is lead-sheathed to keep the outside environment away from the insulation. The next layer is the anti-corrosion protection which consists of extruded Polyethylene. Only for submarine cables, galvanized steel tapes are applied around the polyethylene layer to prevent the cable from permanent deformation during cable

loading. Over the steel tapes a polypropylene string is applied followed by galvanized steel wire armor, for protecting the cable from additional stresses associated with the sub-sea environment. Typically, this technology is available for voltages up to 500 kV and a transmission capacity of up to 800 MW in one cable with installation depths of up to 1640 m under sea level at present and nearly unlimited transmission lengths. The capacity of mass-impregnated cables is limited by the conductor temperature (in the traditional oil-paper insulation cables the maximum operation temperature of the conductor is 55 °C) which results in low overload capabilities

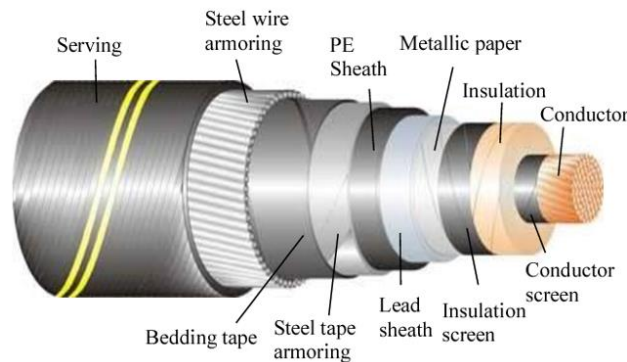


Fig:2. 8 Mass Impregnated HVDC Cable

2.4.2 Oil-Filled (OF) Cable:

The conductor is insulated by paper impregnated with a low-viscosity oil and incorporates a longitudinal duct to permit oil flow along the cable. Oil-filled cables are suitable for both AC and DC voltages with DC voltages up to 600 kV DC and great sea depths. Oil-filled cables are in turn divided into:

- I. Single core oil filled (SCOF) cables, that use low pressure oil
- II. High pressure oil filled (HPOF) cables that use high pressure oil.

Differently from SCOF cables, whose conductor is realized with a hollow shape for the oil flow, the HPOF cables are laid inside a pipe filled with oil at high pressure.

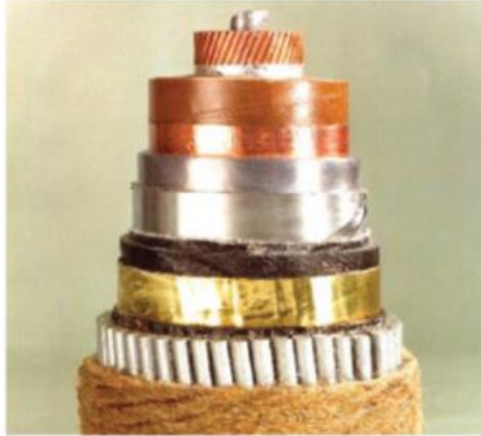


Fig:2. 9 Oil-Filled HVDC Cable

2.4.3 Polypropylene Paper Laminate (PPL) or Lapped Thin Film Insulated Cable:

Some manufacturers are developing HVDC cable systems that utilize Polypropylene Paper Laminate (PPL) insulation and impregnating compounds that have non-draining characteristics. They are claimed to operate at conductor temperatures of 80-90°C and to sustain up to 60% higher electrical stresses in operation and good for very long and deep submarine links. However, they are not yet a fully established technology.

2.4.4 Polymer-insulated or Extruded-insulation Cable:

For Higher conductor temperature Polymeric insulation is suitable than paper-oil insulation for instance, XLPE for HVAC application is suitable for a conductor temperature of 90°C and a short circuit temperature of 250°C. However, XLPE for HVDC application is suitable for a conductor temperature of 70°C at present.

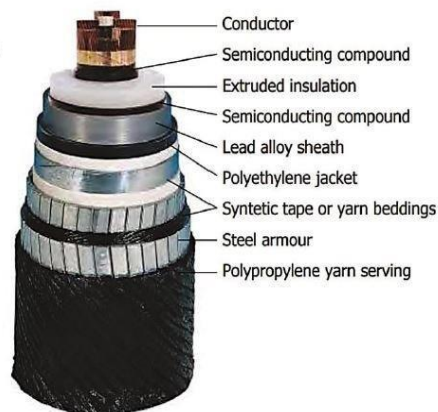


Fig:2. 10 PPL

2.5. HVDC cable insulation in AC and DC:

There is no fundamental difference in structure between AC and DC high voltage cables apart from the formulation of the polymeric insulation, which for DC may include inorganic fillers and the use of other proprietary measures to suppress the formation of space charge. Electric fields in AC cables are predominantly graded by capacitive effects on the field distribution being controlled by the design of conductor shape and by incorporating materials of different dielectric constant to avoid excessive concentrations of electric stress. In AC insulation, reversal of the electric field vector occurs so frequently that conduction via low-mobility electrical charges is usually insignificant. However, for HVDC insulation, the presence of a constant electric field across polymeric insulation causes the migration of charges through the insulation (conduction). Some of this charge becomes trapped in the insulation (space charge) in a manner that modifies the electric field pattern considerably from that expected under AC conditions, where we tend to regard the insulation as charge-free. To illustrate this point, consider the below Fig. 2.11. This is one of many studies that have shown how the electric field in an HVDC cable changes over time (usually hours) in response to both the applied voltage and temperature (i.e., load current), leading to concentrations of electric stress at unexpected locations in the cable insulation.

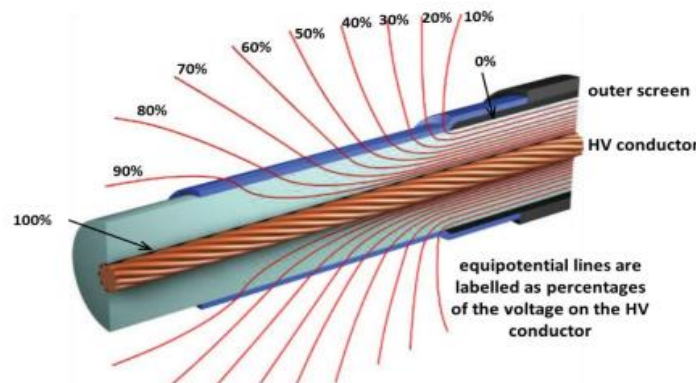


Fig.2. 11 Electric field distribution at a cable end using stress control materials is illustrated here by the pattern of equipotential lines that are graded smoothly between the coaxial cable region at the right and the open HV conductor at the left

2.6. DC Characteristics of DC-XLPE Insulation Material:

XLPE cables widely applied in AC power transmission and distribution use cross-linked polyethylene (XLPE) as the insulation material (hereafter denoted as AC-XLPE). AC-XLPE insulation material exhibits excellent insulation performance against AC voltages, but it does not exhibit adequate performance against DC voltages due to such reasons as the accumulation of

space charge. By adding nanosized filler materials in the XLPE insulator, an excellent characteristic can be obtained. The XLPE insulation material for DC usage, to which nano particles have been added.

DC-XLPE has the following features in comparison with AC-XLPE:

- High volume resistivity.
- Low space charge accumulation.
- Long DC lifetime.
- High DC breakdown strength.

2.6.1 XLPE Technology:

Rising generation XLPE material for HVDC cable insulation systems has an optimized composition with low DC conductivity, limitation of space charges effects and high impulse breakdown strength. Which is necessary when high DC voltage is applied to an insulating layer, a leakage current will flow through it producing heat and rising the insulation temperature. This will increase the insulation electrical conductivity, allowing for more current to flow and thus generating more heat, leading to thermal runaway and ultimately to electrical breakdown. It is therefore necessary to mitigate the risk of thermal runaway due to heat generation inside the insulation: XLPE cleanliness is of utmost importance to achieve good low DC conductivity. One key aspect is the reduction of peroxide content to decrease the quantity of residual by-products: it is in fact well known that cleanliness will affect both DC conductivity and the space charges properties. Peroxide is normally added to the insulation base material at high temperature and pressure right after the extrusion. Its presence is necessary to start the cross-linking process and thus peroxide content shall be enough to ensure the presence of a cross-linked polymer network. Other solutions foresee the use of nano-fillers dispersed in the XLPE insulation.

2.6.2 Polypropylene Technology:

Polypropylene is a thermoplastic resin obtained by polymerization of propylene as a monomer, which has a regular structure, high crystallinity, good corrosion resistance, and excellent heat resistance. Polypropylene can be divided into isotactic polypropylene (iPP), syndiotactic polypropylene (sPP) and atactic polypropylene (aPP) according to its methyl group position. The melting point of polypropylene can reach more than 150°C (different melting point of different brands), about 40–50% higher than that of polyethylene, and the long-term working temperature can reach 90°C. Polypropylene is a non-polar material

with high breakdown strength (mostly around 300 kV/mm), high bulk resistivity (mostly around $10^{16} \Omega \text{ m}$) and insignificant change with temperature, can be in the same insulation. Polypropylene has less space charge accumulation and the charge injection has a higher threshold electric field. Polypropylene hardly absorbs water, so its insulation properties are less affected by the ambient humidity. Polypropylene materials have high mechanical strength without cross-linking treatment and are typical thermoplastic materials that can be recycled and used in line with the development needs of environmentally friendly cable insulation. However, the polypropylene material itself also has some disadvantages, such as large low-temperature brittleness, poor aging resistance, low thermal conductivity, etc., which have certain limitations on the application of DC cable insulation.



Fig:2. 12 Polypropylene Cable

2.6.3 Mechanical properties of polypropylene Nano composites:

High-voltage DC plastic cable is working under load, the temperature distribution in the insulating layer is not uniform due to the conductor heating, and the thermo-mechanical performance changes due to thermal expansion and thermal stress can occur in the dielectric; the cable manufacturing and laying process may also cause Concentration of stress in insulating media. The role of mechanical stress can produce air gaps or micro cracks in the medium to form defects. The defects are easily discharged under the action of an electric field, causing serious breakdown of the material and threatening the operational safety of the cable. Polypropylene has high crystallinity, regularity, and excellent resistance to bending fatigue, but its high brittleness and low impact strength, especially in low temperature environments, need to be toughened and modified before it can be applied to the insulation of high-voltage DC cables.

Cable accessories such as joints and terminations have long been recognized as more likely locations for insulation defects that could give rise to PD in AC networks since they disrupt the uniform cable structure and could allow ingress of contaminants if damaged. Furthermore, there is potential for human error during their assembly, a task that must be performed with great care. Likewise, HVDC cable accessories will face similar challenges due to their complexity, which again arises from the need to control the field grading to avoid excessive concentrations of local electric stress. HVDC accessories may employ nonlinear resistive field grading materials based on ZnO (or sometimes SiC) filler compounds to produce a field-dependent conductivity so that conductivity increases at higher electric fields in order to reduce stress. These materials reversibly change their electrical properties from being highly insulating to highly conducting in regions where the field exceeds a critical value.

2.6.4 Medium Voltage Polypropylene Compounds by HV Cable:

Polypropylene insulation system together and locally available base resins has been developed for up to 36 kV with equally good or better electrical and mechanical performance compared to XLPE. The tested maximum operational temperature of the conductor is 105 °C and short circuit rating 250 °C. Our solutions have been successfully installed in grid using same joints and terminations as with XLPE cables. This will bring in world class extrusion and manufacturing technology know-how to enable off-the-shelf solutions to cable makers globally and further solutions to higher voltages. During our studies we have not identified any remarkable difference between purity of our compounds compared to commercially available medium voltage XLPE compounds. Compounds we have used seem to contain less contaminations when measured from cable than XLPE. We must address, that one additional advantage of thermoplastic polypropylene-based insulation system is related to material filtration. While there are limits in filtering XLPE, due to scorch phenomena, polypropylene can be filtered much more thoroughly, with advantages in terms of material cleanliness and cable reliability.

2.7. Power cables in High Voltages:

Power cables are designed to transport high energies over long distances with a minimum of loss. Power cables are subdivided into two classes:

1. The function of the first class is to transport the energy from a power plant to a distribution center. This is done at high voltage (20-175kV) to reduce the resistivity losses. The buried high-voltage cables (HV) are insulated with peroxide-cross-linked PE (XLPE).

2. Medium voltage (MV) and low voltage (LV) cables have the function of distributing the electrical energy to the low voltage network and to the consumers, respectively. The higher the voltage, the more important the losses through heat, hence the insulation must be temperature resistant.

2.8. Use of PP in cable applications:

Over 60% of the polymer used in cable insulation and jacketing is plasticized PVC. This is flexible and has relatively good high temperature resistance. It was also the first resin available commercially. PE comes second with approximately 35% of the world market. Crosslinked PE is the sole resin used for the insulation of HV cables and the most common also for the MV cables. PVC being polar, its insulation properties are not enough for HV cables. PP has a market share of 3-4%.

3. PARTIAL DISCHARGES IN HVDC CABLES

3.1. Preface:

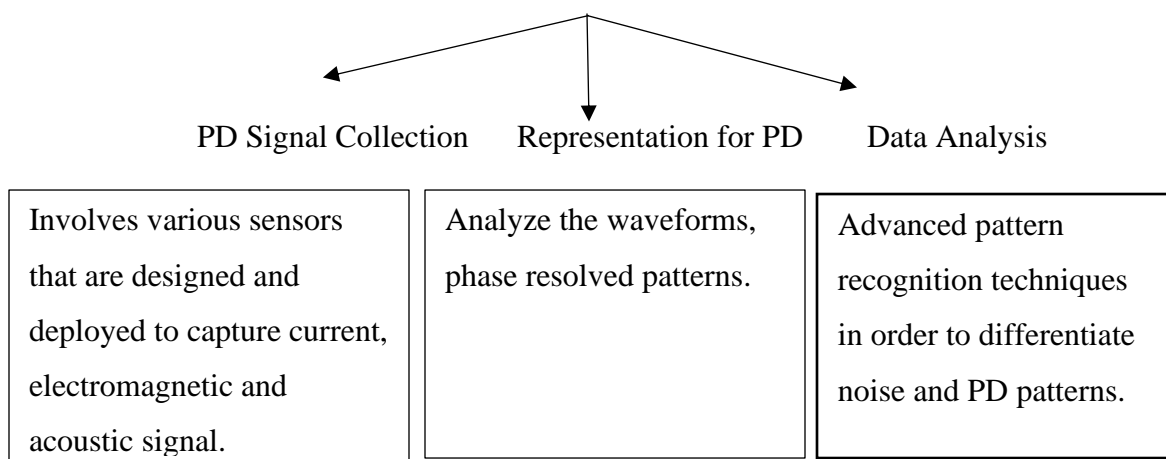
PD is an associated electrical discharge that happens across a portion of the insulation between two conductors, without completely bridging the conductors it is also used for measuring the standard of High Voltage Insulation System. PD is harmful because it causes progressive deterioration of power apparatus and insulation, ultimately resulting to equipment failure. Therefore, detecting PD and separating PD from noise are important tasks of condition monitoring to facilitate grid asset operation and timely maintenance. Additionally, PD can happen at both AC and DC voltages; however, AC voltage systems are far more common and PD at DC voltage is less harmful.

Consequently, PD measurement has become a worldwide accepted method for insulation diagnosis and a required a part of the acceptance testing for several sorts of HV equipment. PD discharges can happen in various insulation systems like corona, Internal and Surface. Corona discharges generally happen in open air and produce a current from an electrode with a high voltage. Surface discharges are produced along the surface of the insulation. Internal discharges happen inside the solid insulations with gas-filled cavities or near the contaminants. Internal discharges are more harmful than surface discharges and corona.

3.2. Detection of PD:

Perhaps by using the advanced sensing technology and Data analytic technology.

PD Monitoring System



3.3. Type of Partial Discharges:

3.3.1 Internal Discharge:

Manufacturer's defects in solid insulation. Found in Cables, Bushings, GIS Junction insulation. Highly destructive to insulation. Voids typically still grow until failure. If a void PD is discovered the insulator should get replaced. It is the silent defect where there will be no sound, smell or visual indication of a problem drag before to failure.

Sensors: UHF, HFCT, AE Contact Probe, TEV.

3.3.2 Corona Discharge:

Corona is a discharge to air from the keen surface of a conductor. Corona is typically not a problem besides the sound and therefore the radio frequency emission. Fortunately, the corona signal features a many characteristic that are much different from other forms of PD. Corona disturbances do not interfere with other PD measurements.

Sensors: AE Ultrasonic HFCT.

3.3.3 Surface Discharge:

Discharge along the surface of insulation are often very destructive also referred as "surface tracking". Usually cause by contamination or weathering of insulator surface. It is different from corona because it tends to trace to grounded metal. Corona discharges to air, this condition can evolve into surface PD as they become more severe this will happen on any MV and HV equipment. When the strength of insulation breaks down, in high humidity environments or poor maintenance of equipment can cause this kind of phenomenon. Moistures Intrusion is additionally common explanation for surface PD.

Sensors: AE Ultrasonic and Contact Probe, UHF, HFCT, TEV (low magnitude)

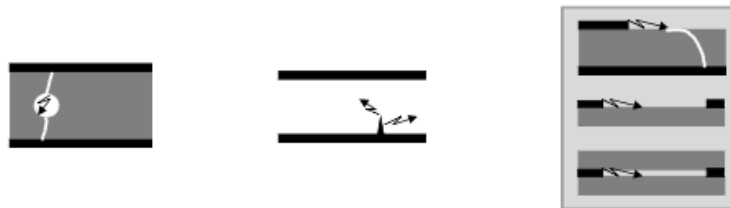


Fig:3. 1 Discharges for Internal, Corona and Surface

3.4. PD Background Noise:

1. In order to reduce the background noise frequencies and radio background frequencies analog/ digital filters are used.
2. To reject interferences, hardware and/or software gating and digital signal analysis (e.g., time-frequency map, multi-phase/frequency relation diagram) are found available in PD systems from different manufacturers.

Likewise, rejection methods are mainly based on phase characteristics of PD. Severe noise and interferences are encountered on-line PD testing under DC voltages. Noise signals detected on-line often occur from the power conversion equipment. The coupling of these signals will depend on sensor attachment point to the Cable under Test.

3.5. Performance of Insulation to PD:

There is a considerable difference between PD tolerance of XLPE and laminated (oil impregnated paper) cables. Whereas the insulation is intended to be PD free and can resist the PD magnitudes up to 1000 pC. Over a long period of time. Common sources of defects in extruded cable system are voids between cables and accessory, voids in insulation, semiconductor protrusion. The location and the severity of the PD are important factors when considering the PD risk. Not all PDs end up with the failure.

3.6. Partial Discharge Recurrence Pulses:

Analysis of PD process is important for the detection and measurement of the PD pulses created by PD activities. For describing the PD process, a well-known a-b-c circuit is used. This electrical model can be used to describe the PD recurrence process of three types of PD which mentioned. The a-b-c circuit is shown in Figure 3.2. The capacitance c represents the capacitance of the defect. The capacitance of the dielectric in series with the defect is represented by capacitance b and the sound part of the dielectric is represented by capacitance a .

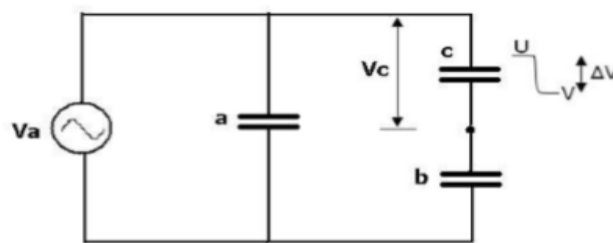


Fig:3. 2 The a-b-c equivalent circuit for describing PD recurrence process

The recurrence process of PD pulses is shown in Figure 3.3. The high voltage applied to the insulation system is V_a and the voltage across the defect is V_c . A discharge will occur in the defect when the voltage V_c reaches the breakdown voltage U_+ , the voltage V_c then drops to V_+ and the current impulse i is produced. The voltage drop ΔV takes place in extremely short time compared to the duration of 50 Hz sine wave so this can be regarded as a step function.

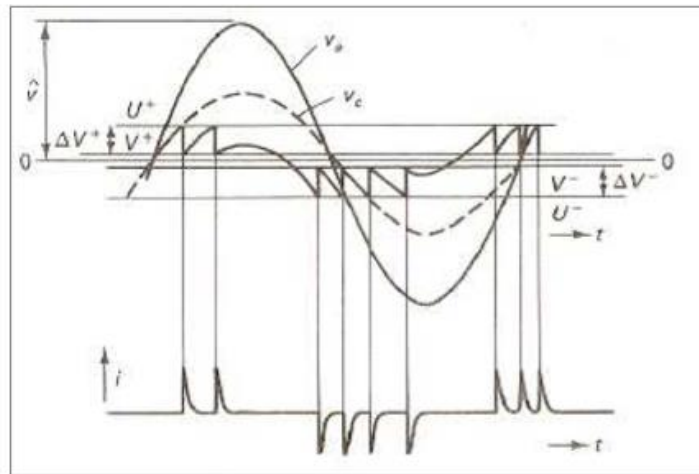


Fig:3. 3 The principle of PD pulses occurrence for a-b-c circuit

After the discharge has occurred, the voltage V_c increases again and when this voltage reaches U_+ a new discharge will occur. This process will happen several times until the voltage V_a decreases and the voltage V_c reaches U_- and a new discharge occurs. Recurrence discharges and current impulses will occur when the AC voltage is applied to the dielectric system which contain of defect.

Charge q_1 , which is transferred in defect c when the PD occurs, will be equal to:

$$q_1 = (b + c) \Delta V$$

Degradation of the dielectric due to PD activity is certainly related to this charge. However, this charge quantity cannot be measured with discharge detector in practical situation. The value that can be measured is the charge displacement q in the leads to the sample; this charge quantity is expressed in picocoulombs (pC) and equal to:

$$q = b * \Delta V$$

This charge displacement is related to the discharge in the defect; however, this quantity is not directly representing the charge transfer in the defect. There are several reasons that make the charge displacement quantity q are reasonable for the PD measurements.

- The discharge magnitude q is proportional to the energy dissipation in the partial discharge.

- The discharge magnitude q is proportional to the size of the defect.
- This transfer of charge q can be measured by electrical PD detector.
- The order of discharge magnitude q in powers of ten can be used to determine the harmfulness of discharge.

Disruption time of voltage pulse caused by the discharge process is determined by the type of defects that produce PD pulses. For internal cavity, the voltage pulses collapse in a time of at most few nanoseconds, consequently the resulting voltage pulses that travel in both directions from the PD source will have pulse width in nanoseconds region. For surface discharge, the voltage pulse from the PD source will have pulse width in some tens nanoseconds, therefore resulting pulses from PD process will have corresponding frequency up to few hundreds of MHz or 1 GHz. Furthermore, this high frequency component of PD pulses will attenuate due to losses in semiconducting shields in XPLE power cable. As a result of this attenuation, the magnitude of PD pulses will decrease, and their width will increase as a function of propagation distance.

3.7. Plasma PD Models:

PD models are typically interested in reproducing experimental measurements for many PDs. As such, the discharge process is heavily simplified. A more rigorous approach is to use models that explicitly consider the plasma dynamics of the discharge. A well-established approach is to use drift diffusion equations that describe the dynamics of electrons, positive and negative ions. Many of these simulations have been used in the literature, typically to model discharges from a needle-plane electrode configuration with no solid dielectric materials present. Investigations have also been made into dielectric barrier discharges. These simulations have often been used to provide insight into systems where discharge activity is desired, such as sterilization, or material processing. This means that most of these investigations offer limited insight into PD activity for systems of interest as they are conducted under significantly different physical conditions. Most notably discharges often take place applied voltage frequencies in the order of kHz, whereas PD systems of interest are typically at power frequencies of 50-60 Hz.

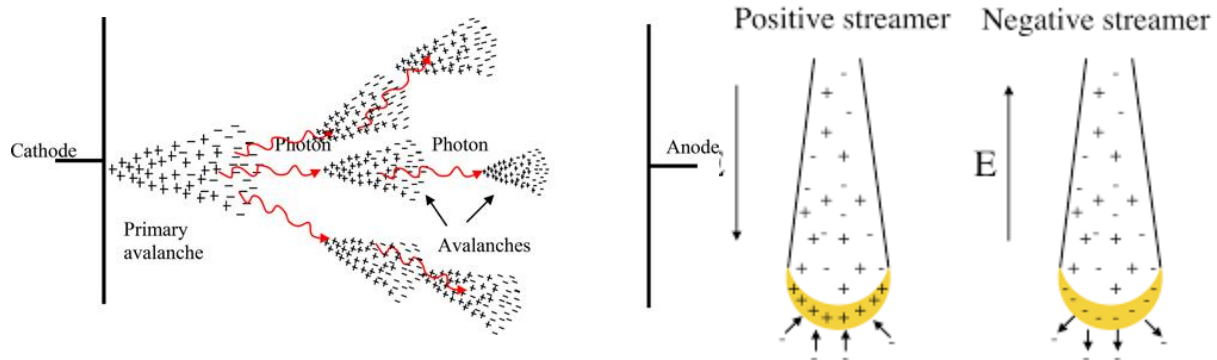


Fig:3. 4 Positive and Negative streamer with a thin space charge layer at their tip

However, there are some models of PD using plasma models in the literature which is shown in Fig:3.4. Serdyuk et al. showed that a single discharge in an airgap between electrodes covered in polyethylene consisted of an electron avalanche transitioning into a positive streamer. Testa et al. presented a one-dimensional model for single PDs that considered the transport of electrons, positive ions, and electron energies for air gaps in polymers. Models that consider multiple PDs have also been developed. In drift diffusion equations were used to model many PD in an air gap bounded by an electrode above and an electrode covered with a dielectric material below.

Unfortunately, the numerical techniques used in this work, by necessity to reduce the computational cost, mean that its results must be approached with some caution. Recently a more rigorous model was successful at modelling several discharges in a spherical air void. It should be noted that the emphasis of this work was in the development of numerical techniques to solve the governing equations, the analysis of the results at is pertains to PD activity is somewhat limited. Furthermore, despite axisymmetric physics and geometry, the presented results, solved in a three-dimensional geometry, display a high level of asymmetry, the reasons for which are unclear.

3.8. Partial Discharges in DC Insulation:

PD is well-known to be an indicator of defective insulation and an explanation for insulation ageing and degradation. The tool used for predictive maintenance is On-line PD monitoring of HVAC equipment which is widely used for testing. Historically, PD under DC conditions has received less attention for the subsequent reasons:

- For couple of years, HVDC was mainly used for non-energy applications (e.g. television, radar, X-ray equipment, etc.) where the failure of an individual component didn't affect large numbers of individuals.
- PD under DC is small amount directly related to causing insulation damage (i.e., it is an indicator of weakness instead of a primary cause of degradation in itself). One main difference in PD phenomena under DC conditions is that current is flowing in one direction, which suggests that the PD are usually all are with the equivalent polarity. Another difference is that the build-up of charges either within the bulk material, on surfaces or at material interfaces can suppress further activity until the externally applied voltage changes. This effect results in PD pulses occurring much less frequently under DC conditions, which suggests that the physical damage caused by PD itself could also be minimal.
- Although, the build-up of charges in the insulation poses a hidden threat that would cause sudden breakdown in abnormal circumstances, without exhibiting a previous growth in PD activity which may be expected under AC conditions.
- Hence, although DC PD pulses could also be sparse, they ought to still be considered as indicators of potential insulation weakness and techniques must be developed to deal with the demanding task of interpreting DC PD activity.
- PD detection and analysis under DC conditions is growing interest and research the work is progressing. For detection purposes, an equivalent sorts of PD sensor are often used as for AC since an equivalent current pulse is flowing in the external circuit. Hence the sophisticated measurement techniques developed for AC PD testing remain applicable under DC conditions.
- For DC PD analysis, no standard method of representation exists unlike the AC case where phase resolved patterns are often obtained for several different tests. There are two parameters in DC PD tests mainly, the discharge magnitude q_i and time interval between two consecutive pulses Δt_i , which are analogous to PD magnitude q_i and difference in phase ϕ_i in AC tests which is shown in Fig.3.5.
- In AC testing, these quantities PD magnitude and phase difference feed into the “apparent charge” measure of PD magnitude defined in the measurement standard IEC 60270. For DC testing, there's not yet an internationally agreed standard for assigning a magnitude to

PD severity the PD pulses under steady state DC conditions may occur very infrequently. However, proposals made during ongoing revisions to the IEC 60270 partial discharge standard are mentioned, which describes some methods for evaluating PD data from DC tests.

- Typically, the pattern of consecutive PD pulses at a constant DC test voltage is recorded over a long period (typically 30 minutes). Since the slope of the cumulative charge plot is proportional to the mean PD current, this is often a useful quantity because it relates to whether the PD current is growing or diminishing over time.
- Two simple methods for presenting the distribution of PD pulse amplitudes graphically also are suggested: The primary representation counts the entire number of PD pulses whose charge lies within consecutive bands of PD magnitude – these are termed the class frequencies of PD pulses. Secondly (and closely associated with primary representation), the amount of pulses whose apparent charge exceeds a defined series of threshold level is counted – these are termed the exceeding frequencies of PD pulses.
- An important aspect of HVDC testing that must be defined in the ramp test profile, for which one option is to use the peak value V_R of the AC PD inception voltage as a basis for outlining the voltage variation with reference to time. The ramp test consists of three voltage increments, as shown in Fig. 3.6. Following each increment, the voltage is held constant at $V_R/2$, V_R and $3V_R/2$ respectively for half-hour minutes each, after which the recorded PD pulses are often represented using the statistical analysis mentioned above. At the conclusion of the test, the voltage is decreased down (from $3V_R/2$ to 0 V) within 30 seconds.

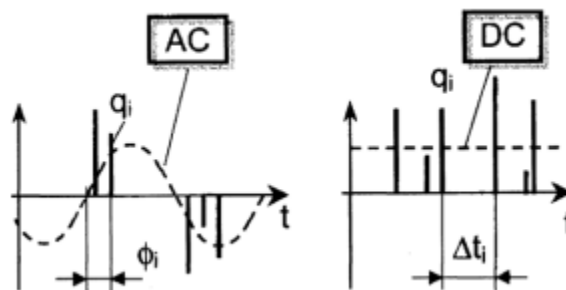


Fig:3. 5 Basic PD parameters for AC (left) and DC (right) excitation voltages. The magnitudes of PD pulses are represented by q_i while the phase and time differences between successive pulses are represented by ϕ_i and Δt_i .

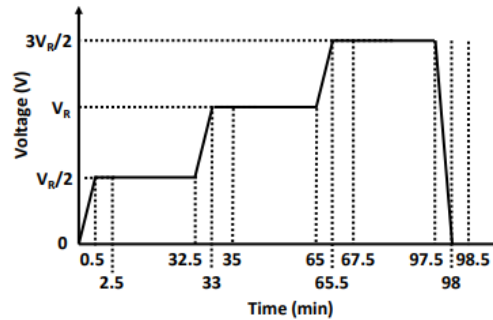


Fig:3. 6 Ramp test profile for DC testing. V_R is the peak value of the AC PD inception voltage.

3.9. Surface Discharge Distribution:

When the applied voltage is increased, the numbers of PDs per cycle, total charge per cycle and therefore the maximum charge magnitude become higher. When the electric field at the surface of the electrode exceeds the breakdown strength of gas, ionizations of air near the surface of electrode occur. This is due to the tangential field on the insulation surface is high enough to cause PDs along the surface of the substance. The surface discharges until the transient activity stops. When the applied voltage is increased, the number of electrons ionization increases, and electron avalanche can grow longer along the material surface. It is commonly assumed that when the dielectric surfaces at each side of a discharge channel are symmetric, such as in spherical, cylindrical, or ellipsoidal voids, the surface charge distribution at the dielectric surfaces are bipolar. Earlier numerical studies and experimental work investigating PD in cylindrical voids suggest that the distribution is in fact not bipolar and that the negative surface charge distribution has a greater spread due to the higher mobility of electrons compared to ions. Both studies have looked at PD for electric fields that just exceed the breakdown threshold. In previous models of PD activity, it has been assumed that the PD surface charge is deposited directly over the surface charge of previous PDs. However, it is likely that field due to the charge of previous PDs will influence the charge deployed by subsequent PDs.

3.10. Measurement Set-up:

Partial discharges were sensed through a high frequency current transformer (HFTC) clamped around the ground connection of the test objects. The test object, HV supply, sensor and PD detector could be all segregated within a metal cabinet to minimize noise and disturbance from other PD sources.

3.10.1 Discussion of PD Monitoring for HVDC equipment:

Testing of HVDC components, conventional AC PD measurements may retain a role as a part of the manufacturer's quality assurance. However, once HVDC system has been constructed in the field, it will be of value to apply monitoring as far as is possible practical, and economical during the various phases of its life. Doing so is expected to offer the following benefits:

- Competency to detect and rectify manufacturing or assembly defects at commissioning, before they cause component failure or secondary damage. This might include, for instance, detecting partial discharges at inception, below the normal operating voltage during commissioning tests.
- Ability to detect equipment defects or deficiencies.
- Possibility to scale back operators' repair costs and regulatory fines (imposed as a result of outages or power quality issues) through enabling condition-based and predictive maintenance to be exploited to a greater extent using the holistic monitoring system approach.
- Expertness to plan capital investment for replacement or upgrade of assets based on a better understanding of plant health and prognosis of its future rate of degradation.
- Given the characteristics of PD activity under HVDC conditions it is possible to outline an approach to the monitoring of PD in HVDC equipment under various headings as follows:

3.10.2 Sensors:

Partial discharge sensors should be installed at suitable, accessible locations on the HVDC network to be monitored, in accordance with practice for HVAC equipment. Sensors can include HFCTs, coupling capacitors, all of which must be appropriately rated for HVDC use and comply with safety requirements to ensure that HV clearances are not compromised as shown in Fig.3.7. In this respect, it should be noted that ideally, facilities for condition monitoring sensors should be included at the design stage for new equipment as this will help to ensure that monitoring equipment are often installed more effectively than could be the case during a retro-fit scenario. HFCT is most used for on-line PD measurement on cables.



Fig:3. 7 PD test cell with HFCT sensor

3.10.3 Signal acquisition:

The challenge in terms of sampling rate for signals from the PD sensors is to optimize the trade-off between hardware cost, volume of data and signal fidelity, all of which increase with sampling rate. Since an accurate representation of the PD pulse detail in the time-domain is preferable to enable discrimination between different types of pulses from different sources, it is considered that a sampling rate of 100 MHz is optimal at present. This may in fact change in future, as analogue-to-digital sampling technology continues to advance. As described in the discussions ‘Voltage measurement’ below, the length of sampled time-domain data recorded in a single acquisition could benefit from being dynamically variable and governed by measurements of HVDC system parameters, as well as the characteristics of the PD activity itself.

3.10.4 PD Analyzer:

Foremost important difference between HVAC and HVDC (On-Line Partial Discharge and Off-line Partial Discharge) systems is that the latter should normally be ‘event driven’, rather than triggering repetitively on the AC power frequency cycle. This change is necessary due to the scarcity of PD pulses under DC conditions shown in Fig.3.8. which means that the conventional AC operation of the digitizing, data transfer and rearming cycle of the acquisition hardware could lead on to a high probability of PD pulses being missed. Instead, the monitoring system should be set to trigger on the detection of a PD pulse and then to record and transfer the signal data only for the period of time necessary for the PD events to be captured in full with sufficient fidelity for pulse characterization.

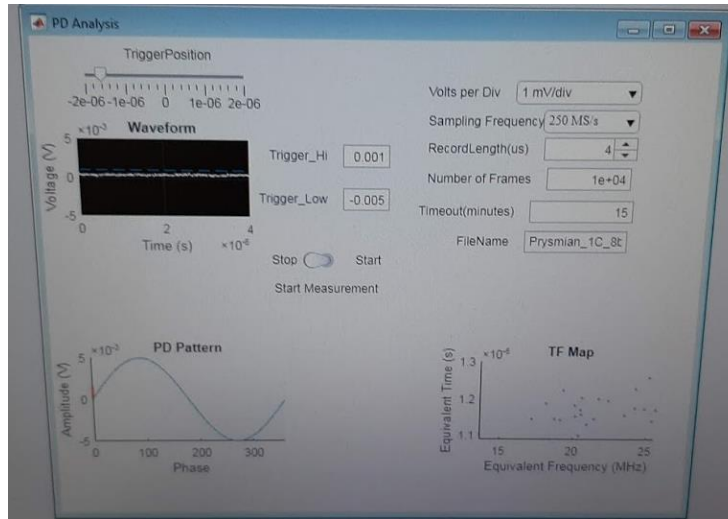


Fig:3. 8 PD-Analyzer software

3.10.5 Synchronous timestamping:

A valuable feature expected of HVDC-OLPD monitoring system functionality is that PD signals acquired from all the sensors in a locality of the HVDC network should be captured in a time synchronized manner. This enables the use of pulse amplitude and time-of-arrival comparisons among sensor outputs when the detected pulses can be attributed to a common source. Both comparison methods are important tools for locating the origin of pulses and discriminating between different signal sources be they PD or interference. An extension of this requirement is that the recorded timing of PD pulses should not simply be traceable across other sensors but should also be known relative to the phase of the AC cycle of the converter station (where this is nearby and accessible). During monitoring of an HVDC transmission cable, this functionality has been found to offer a considerable improvement in the discrimination between PD and non-PD transients detected by the sensors. In addition, it provides diagnostic information concerning PD that is associated with repetitive, system-generated transients.

3.10.6 Voltage measurement:

The HVDC-OLPD system should preferably have access to a measurement channel /sensor that allows it to monitor the instantaneous voltage level on the HVDC system. Superimposed on the HVDC conductor will be ripple and transients, which are known to play a significant role in influencing PD activity in HVDC systems. The incorporation of an instantaneous voltage measurement channel into the OLPD monitor enables dynamic optimization of signal acquisition settings. This allows the monitoring system to operate in an adaptive mode, in which system triggering and record length are dynamically optimized to capture PD activity in a manner

appropriate to changing system conditions, such as: voltage ramping (increasing / decreasing during energizing /de-energizing), VSC ripple, voltage spikes, switching transients, etc.



Fig:3. 9 Voltage Measurement

3.10.7 Environmental sensors:

Considering modern trends and cycles in parameters such as temperature and humidity have the potential to modify both PD activity and PD like interference signals, it is important to log such parameters so that their influence can be taken into account within the holistic diagnostic process. While ambient sensors have considerable value, it is equally important to possess additional sensing where local effects are dominant (for example, load-dependent heating of components such as cables).

3.10.8 Oscilloscope:

An oscilloscope is in a research laboratory instrument commonly used to display and analyze the waveform of electronic signals which is designed in University of Bologna. In effect, the device plots a graph between instantaneous signal voltages as a function of time. Here we have used Tektronix 5series Oscilloscope It is 15.6-inch-high resolution capacitive touch screen. A new method to detect partial discharge in high-voltage cables with splices and terminations as shown in Fig.3.10



Fig:3. 10 Oscilloscope

3.10.9 Phase Resolved PD:

AC tests were performed by gradually increasing the applied voltage in steps until sustained PD became perceptible at the inception voltage, which was 20 kV rms for this sample. At this voltage, the PD level indicated by the measurement system and the PD activity is shown below in phase-resolved form was recorded over a 10 second period. Note that the PD pulses tend to occur beforehand of the test voltage peaks, which is typical for internal discharges. While the PD level appears quite large for tiny voids, this is often because the electrodes are strongly coupled to the PD currents due to their proximity.

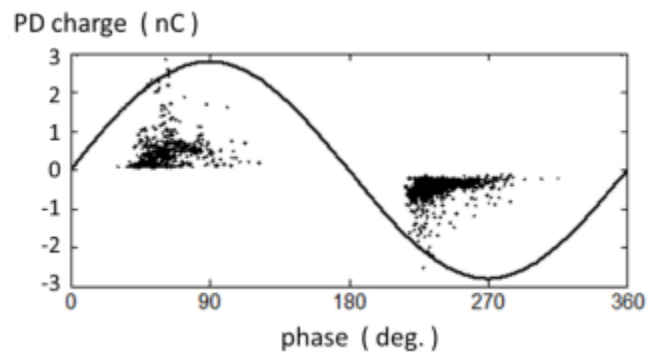


Fig:3. 11 Phase-resolved plot of PD activity accumulated voids

4. REVIEW OF SPACE CHARGE MEASUREMENTS

4.1. Preface:

In the subsequent years the research has focused in the development of non-destructive methods. In particular, the techniques were divided into three main groups in relation to the physical principle on which they are based on acoustic, thermal and optical methods. Of these groups, methods based on acoustic and the thermal phenomena have been largely used in industrial applications while, the methods based on optical phenomena have not had much success due to the complexity of the measuring cell. For these reasons, a more detailed description will be given for acoustic and thermal methods, in particular for the Thermal Step Method (TSM) technique and for the Pulsed Electro Acoustic (PEA) belonging to the groups of thermal and acoustic methods, respectively. These two techniques have had the greater success for measures of space charge on a flat specimens but also on a full-size cables. During the years, their measuring cell has been modified in order to make measurements on samples with different shapes and sizes. The below are explained about the principles of operation, about different configurations, the thicknesses is analyzed and the spatial resolution will be discussed. Accumulation of charges in a region is referred to as space charge as mentioned in Fig.4.1. The space in which the charges concentrate can be either free space or a dielectric. Further, this cloud of charges might be mobile or immobile in nature.

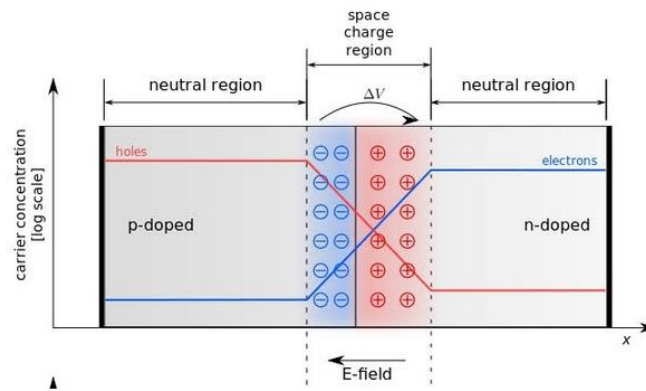


Fig: 4. 1 Accumulation of charges

The two online space charge monitoring techniques that have already been tested on HVDC transmission cable. These are Thermal Step Method (TSM) and the Pulse-Electro-Acoustic (PEA) method. Both online techniques enable the measurement of space charge distribution in extruded cable insulation. The two techniques have traditionally been used in dielectric material to

understand space charge characteristics and material properties. In full size cables both techniques can be used to derive the Poissonian electric field as well as the localized charge accumulation, as shown in Table below.

Output	TSM	PEA
Charge Density C/m^3	Yes	Yes
Poissonian E-field (kV/mm)	Yes	Yes

Table :4. 1 Information output of space charge monitoring techniques

Benefit of the PEA technique is that the charge distribution can be visualized easier from the unprocessed signal profiles. However, the PEA technique is only able to measure the charge distribution over a thin cross section of the cable, see Figure 4.2. On the other hand, the TSM technique when applied on full size cables can measure the average space charge distribution over a 50cm cable section longitudinally and axially. TSM technique can measure the space charge distribution is dictated by the internal dimension of the thermal diffuser. PEA technique is capable of measuring is dictated by the acoustic contact of the PEA aluminum block and the size of the piezoelectric sensor.

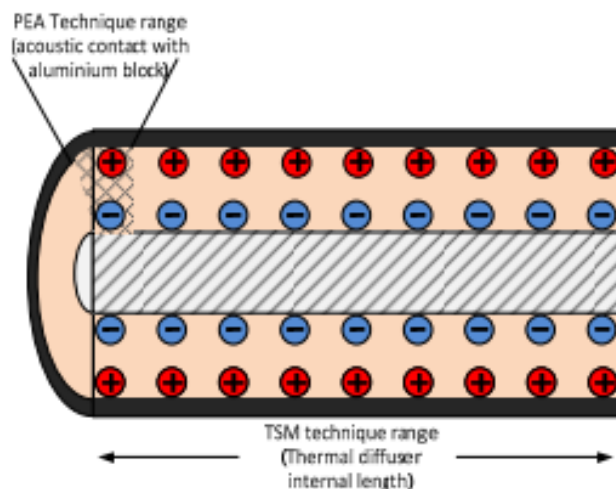


Fig: 4. 2 PEA and TSM space charge measuring range in cable samples.

4.2. History behind the Thermal Step Measurement:

Many efforts were made in order to determine the space charge and the electric field distribution in an insulating material. The main methods belonging to this group are the Thermal Pulse Method (TPM), the Thermal Step Method (TSM) and the Laser Intensity Modulation Method (LIMM). The main difference between these categories consists in the modality of

application of the thermal gradient to the sample. More in detail, this gradient can either be a thermal pulse from a flash of light or a thermal step by using a thermal diffuser or a sinusoidal modulated heating by means of a laser beam. In the TPM case, the output signal is a voltage response related to the charge and polarization distribution and temperature change. The method which is used is Thermal Step Method, which is applied across the insulator, due to the thermal expansion of the insulator the current response is created across the sample. These following methods have a common satisfactory value of spatial resolution, which can further improve greater accuracy through the measurements over the surface, internal temperature mechanism and detection process are explained in the below table:

Method	Disturbance	Scan Mechanism	Detection Process	Methods Resolution (μm)	Sample Thickness (μm)	Comments
Thermal Pulse Method	Absorption short light impulse in front electrode	Diffusion according to heat conduction equations	Voltage change across sample	≥ 2	~ 200	High resolution requires deconvolution
Laser intensity modulation method	Absorption of modulated light in front electrode	Frequency-dependent steady state heat profile	Current between sample electrodes	≥ 2	~ 25	Numerical deconvolution is required
Laser induced pressure pulse method	Absorption short light impulse in front electrode	Propagation with longitudinal sound velocity	Current between sample electrodes	1	100-1000	No deconvolution is required
Thermo elastically generated LIPP	Absorption short laser light pulse in thin electrode	Propagation with longitudinal sound velocity	Current or voltage between sample electrodes	1	50-70	Deconvolution is required
Pressure wave propagation method	Absorption of short laser light pulse in metal target	Propagation with longitudinal sound velocity	Voltage or current between sample electrodes	10	5-200	Resolution improved with deconvolution

Non-structured acoustic pulse method	HV spark between conductor and metal diaphragm	Propagation with longitudinal sound velocity	Voltage between sample electrodes	1000	≤ 10000	Higher resolution with deconvolution
Laser generated acoustic pulse method	Absorption short laser light in thin paper target	Propagation with longitudinal sound velocity	Voltage between sample electrodes	50	≤ 3000	Deconvolution is required
Acoustic probe method	Absorption of laser light pulse in front electrode	Propagation with longitudinal sound velocity	Voltage between sample electrodes	200	2000-6000	
Piezoelectrically-generated pressure step method	Electrical excitation of piezoelectric quartz plate	Propagation with longitudinal sound velocity	Current between sample electrodes	1	25	Deconvolution is required
Thermal step method	Applying two isothermal sources across sample	Thermal expansion of the sample	Current between sample electrodes	150	2000-20000	Deconvolution is required
Electro-acoustic stress pulse method	Force of modulated electric field on charge in sample	Propagation with longitudinal sound velocity	Piezoelectric transducer at sample electrode	100	≤ 10000	Deconvolution is required
Photo conductivity method	Absorption of narrow light beam in sample	External movement of light beam	Current between sample electrodes	≥ 1.5	-	Nondestructive for short illumination time
Space charge mapping	Interaction of polarized light with field	Parallel illumination of sample volume	Photographic record	200	-	Mostly used in transparent dielectric liquids
Spectroscopy	Absorption of exciting radiation in sample	External movement of radiation source	Relative change in the observed spectrum	≥ 50	-	Few applications
Field probe	None	Capacitive coupling to the field	Current	1000	≤ 20000	Destructive

Table :4. 2 Overview of methods its resolution and the sample thickness

4.3. Thermal methods:

This non-destructive measurement systems can be classified into mainly 3 categories.

- Thermal Pulse Method.
- Thermal Step Method.
- Laser Intensity Modulation Method (LIMM)

Particular difference between these categories consists in the modality of application of the thermal gradient to the sample. More in detail, this gradient can either be a thermal pulse from a flash of light or a 5 thermal step by using a thermal diffuser or a sinusoidal modulated heating by means of a laser beam. In the TPM case, the output signal is a voltage response related to the charge and polarization distribution to the temperature change. The output signal is current response for TSM and LIMM methods. In the first method, the current is connected to the electric field and to the thermal step. In the second method, this current is related to the temperature, characteristics of material, and accumulated space charge.

Only in the case of TPM, the output signal is a response of voltage related to the distribution of charge, polarization and the change in temperature. Rather, the output signal is a current response in the TSM and LIMM methods. The generated current is related to the electrical field and the thermal pulse. This current is related in the second method due to the temperature characteristics and the space charge.

4.4. Principle of the Thermal Step Method:

Amongst all the techniques, in this Thermal Step Method is introduced it mainly works with the difference in temperature which generates the fluctuations in the space charge. This change is shown on the surface of the sample i.e., charge in the sample.

Tourelle designed the thermal step method in 1988, and its operating principle is based on the application of a thermal step to the ends of the sample, to calculate the current response due to the sample's thermal expansion. Mainly there are various methods for measuring nondestructive (because the maximum temperature reached is close to room temperature) space charge measurements.

Thermal step is provided by the thermal diffuser, which creates a thermal wave. This wave will diffuse through the thickness of the dielectric, which determines either an expansion or contraction of the material, this will create a variation in the permittivity of the insulation and causes a temporary and reversible displacement of the sample's space charge. Such displacement

is shown on the electrodes, which will determine a difference in the induced charge and therefore a current between electrodes. The value of this current $I(t)$ read by a pico-ammeter (pA) is related to the electrical field distribution as well as the space charge.

The variation of the induced charges is reflected in the external circuit by the appearance of a current $I(t)$, called the thermal step (TS) current:

$$I(t) = - \frac{dQ_2(t)}{dt}$$

Once the Electric field $E(x)$ and the dielectric constant are known from the Poisson's equation the distribution of space charge is determined:

$$\rho = \epsilon \frac{\partial E(x)}{\partial t}$$

Specimen is used in Sandwich configuration, the charges which are induced in the Q_i are the image charges as shown in Fig.4.3. When the change in temperature ΔT_0 is applied on one side of the sample there will be imbalance in the charges, Electrical Permittivity and there will be changes in the direction of the charges in the sample. This is due to the thermal contraction or expansion. As there is imbalance in the system, the charges on the Q_i are re-distributed on to the electrodes. Hence, there will be transfer of charges from one electrode to the other. This change of charge will correspond to an external current it is given by,

$$I(t) = -\alpha \cdot C \int_0^d E(x) \frac{\partial \Delta T_0(x, t)}{\partial t} dx$$

Where d is the thickness of the sample

α is the constant of the material (expansion/ contraction)

C is the capacitance of the sample

$E(x)$ is the remaining Electric Field Distribution.

$\Delta T_0(x, t)$ is the relative temperature distribution in the sample.

$\Delta T_0(x, t) = T(x, t) - T_0$ (T_0 is the temperature of the sample before applying the thermal step).

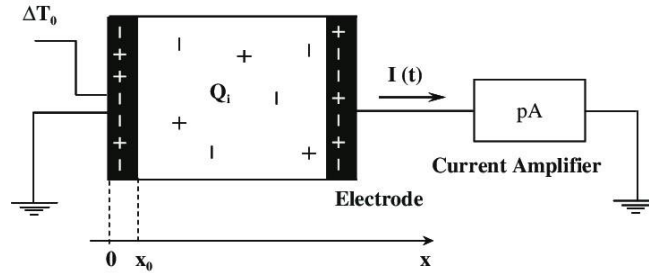


Fig: 4. 3 Electric Representation of TSM

4.5. The thermal step method under applied DC field:

In year 2000 Agnel et al. developed a work finalized to perform measurements under the application of a DC electric field. However, the above Fig.4.3 was not completely suitable for the measurements under electric field, because of the use of the current amplifier. To overcome this challenge, a compensation sample in front of the specimen was placed, obtaining the so called “double capacitor” configuration, which is represented in Figure 4.4.

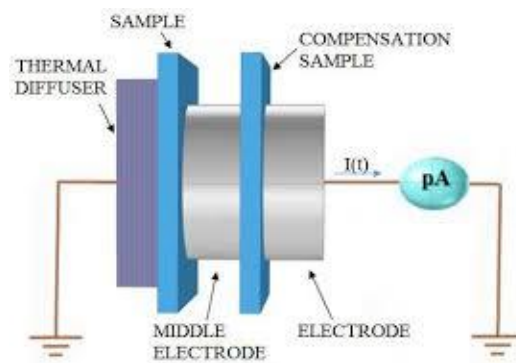


Fig: 4. 4 Double Capacitor

In order to measure space charge distribution, the testing procedure requires two steps:

- Firstly, the high voltage is applied to the middle electrode, while the pA is short circuited.
- Secondly, the high voltage is disconnected in order to avoid the carriage of charges through the electrodes, compromising the correct measurement.

Space charge can be assessed in the same manner contactless configuration in order to measure both the space charge inside the dielectric and the surface charge. In this configuration the upper face of the specimen is isolated from the upper electrode through a thin layer of air, avoiding disturbances. The spatial resolution decreases when the distance between the space charge inside the sample and the electrode in contact with the thermal diffuser increases which is comprised between 50 and 100 μm for a polyethylene terephthalate (PET) sample of thickness of 100 μm . In order to evaluate the influence of the electric field gradient and temperature in the

charges distribution, space charge profiles were carried out in 0.5 mm of a XLPE sample, under different DC electrical stress (from 2 to 60 kV/mm) and temperatures (from 70 to 90C).

4.5.1 Experimental Set up:

The Thermal Step signal is generated by circulating the cold liquid within a radiator in contact with the sample which is shown in Fig.4.5. The electrodes between the samples are connected to current amplifier. The last is associated with a PC, which records the current data and does the numerical information handling. After performing a measurement, the sample can be reheated using a warm liquid, and the experiment can be repeated.

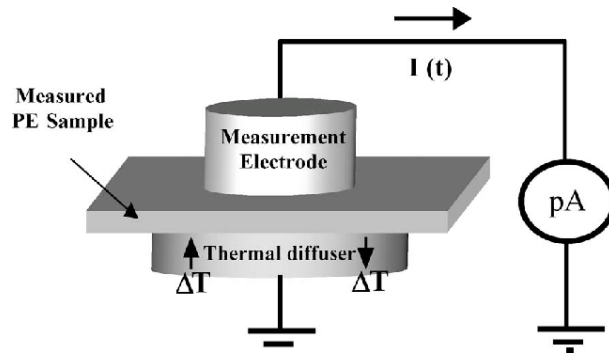


Fig: 4. 5 Experimental set-up

4.6. Space Charge in PEA Method:

The PEA technique was developed in 1981 to measure the space charge profile in dielectrics. Since then it has become one of the most widely used techniques by researchers from industry and academy. The title space charge, which occurs so frequently into polymeric HVDC cables originates in the historical context of vacuum diodes where it described the electronic charge that accumulates in the space between anode and cathode as a result of electron emission from the cathode. Space charge may also accumulate in a solid dielectric in the presence of a DC field. As it does so, this charge modifies and distorts the electric field pattern. If the space charge density becomes sufficiently high, the local electric field strength can exceed the dielectric strength of the insulation, leading to failure. This is particularly the case following a reversal in polarity of the externally applied voltage because under these circumstances, space charge distributions that were generating a local field in opposition to the external field will be oriented so as to enhance the externally-generated field following polarity reversal. In recent years, the development of HVDC cable technologies can minimize the accumulation of space charge in the insulation. Approaches include structural modification of the insulation polymer to reduce its propensity for trapping

charges and further reducing the conductivity of the insulation by maintaining extreme cleanliness and material purity during manufacture.

4.6.1 Acoustic group:

Predominant methods belonging to this group are the Pulsed Electro Acoustic (PEA) method and the Pressure Wave Propagation (PWP) method. The latter includes the Piezoelectric Induced Pressure Wave Propagation method (PIPWP or Piezo-PWP) and the Laser Intensity Pressure Pulse (LIPP) method. The below table 4.3 shows the Excitation methods and Measurement signals for different measuring methods.

Measurement Method	Excitation Method	Measurement Signal
PIPWP	Pressure wave by piezoelectric device	Displacement Current
LIPP	Pressure wave by pulsed laser irradiation	Displacement Current
PEA	Electric pulse	Pressure Signal
TSM	Thermal step	Electric Current
TPM	Thermal pulse	Electric signal
LIM	Thermal pulse by laser intensity modulation	Electric Current
EBM	Electron Beam irradiation	Electric Current

Table :4. 3. Acoustic methods for non-destructive space charge measurement

Working principle of the different configurations of the PEA method remains the same, the main differences are in the measuring cells, which have been modified in order to carry out tests for flat specimen for cables, Portable PEA for measure simultaneously both the space charges inside the dielectric and the surface charges. All acoustic methods use the same physical principle based on the propagation through the sample of acoustic waves. The pressure waves are generated in different ways for different methods. Considering a single wave, it starts from the inside of the sample in the case of the PEA method, while it starts from the outside of the sample in the case of the PWP method. In each case the pressure pulse propagates in which a sample of perfect insulating material, with thickness d and relative permittivity, interposed between two metallic electrodes A and B is considered as shown in Fig.4.6. Analyzing the evolution over time of the voltage or

current, it is possible to finally get information on the distribution of space charge within the sample. In the PEA method, the output signal is a voltage, while, in the PIPWP and LIPP methods the output is a current signal.

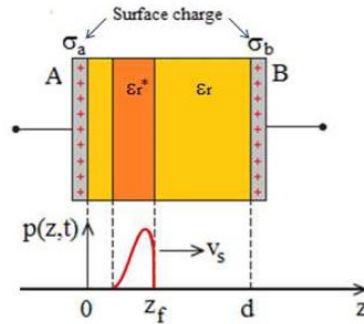


Fig: 4. 6. Propagation of the pressure wave.

4.7. The Pulsed Electro Acoustic method:

4.7.1 Basic principle of PEA:

The PEA method is physically based on the measurement of the acoustic waves generated by the vibrations of charge carriers, laying into the dielectric material, by means of a superimposed pulsed voltage applied between the electrodes. The fig.4.7 left indicates the path of the pressure waves generated by the vibration of the charge carriers within the dielectric is illustrated. After having reached one of the specimen interfaces, the pressure waves propagate toward a metallic grounded electrode and are converted into an electric signal by a piezoelectric membrane. Downstream of the latter, an absorbent material avoids the reflection of the pressure waves. In order to minimize the pressure waves reflection before their detection with the piezoelectric sensor, the adherence of the contact surfaces between the crossed materials should be optimized.

Operating principle is based on the one-dimension Coulomb force law and the principle diagram for a flat specimen is shown in Fig.4.7.1. It consists essentially of a high voltage direct current generator, which is used in order to create a constant electric field within the sample and then allow the accumulation of the space charges. These charges subjected to the pulse voltage will move slightly, this movement generates pressure waves that reach the piezoelectric sensor which allows the conversion from an acoustic signal to a voltage signal proportional to the space charges. The absorber is used in order to avoid reflections and the amplifier to increase the amplification of the signal. Finally, the output voltage signal $V(t)$, viewed in the oscilloscope, is sent to the computer to be processed.

$$V(f) = s(f) \left[\frac{\sigma(0)}{v\Delta\tau} + R(f) + \frac{\sigma(d)}{v\Delta\tau} \exp\left(-\frac{i2\pi fd}{v}\right) \right]$$

where $S(f)$ is the system response function that depends on the properties of the transducer and amplifier, while the terms in square brackets represent the pressure wave. In which, the first component is the surface charge at the ground electrode that corresponds to the electrode in the right side of Fig:4.7.1 near the transducer, the second component is the accumulated charge in the sample and the third component is the surface charge at the upper electrode. The sampling time is denoted by $\Delta\tau$, while v_s is the speed of sound of the sample with thickness from 0 to d .

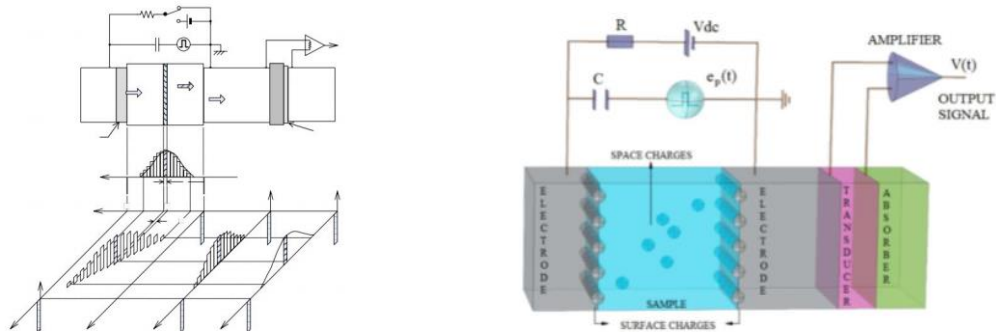


Fig: 4. 7 Left Working principle of the PEA method and Right Principle diagram

PEA method is used, both for flat specimens and for other type of tests in this mainly focused on flat specimens an important aspect concerns the material homogeneity. Indeed, if a material is not acoustically uniform, the acoustic wave generated from the charge can be distorted in which they proposed a numerical model for estimating the effect of acoustic mismatching in a sample which will represent on the output of PEA signals.

Although Holè et al. analyzed the case of complex geometries and the case in which filler particles are present inside the sample. In these works, it was found that if the diameter of the filler particles is larger than the smaller resolution of the measurement system, the output signal is distorted. The method can be used to directly obtain the space charge distribution $\rho(x)$, along with the electric field distribution $E(x)$ and potential distribution $U(x)$ along the thickness of the sample. Fig.4.8 shows typical experimental results using the PEA method.

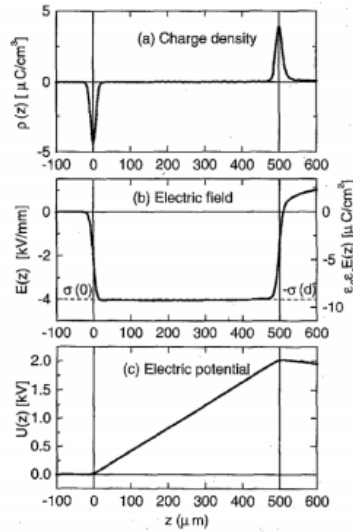


Fig: 4. 8 An example of PEA measurement results from a sample containing no space charge

4.8. De-Convolution process:

For the purpose to obtain a reliable space charge pattern at the output of the PEA setup, the outgoing signal of the amplifier measured by the oscilloscope, must be deconvoluted and calibrated. The signal at the amplifier is affected by distortion because of the acoustic reflection and due to characteristic nature of the detection circuit. A deconvolution technique is therefore applied in order to obtain the waveform with two peaks shown in Figure 4.9 below.

Because the presence of the amplifier after the transducer, and thus the presence of an RC filter, the real output signal results distorted, as shown in Figure 4.10. As can be seen in this last figure, the distortion causes a signal which seems an accumulation of charge with opposite polarity compared to that accumulated in the negative electrode/sample interface (red circle on the Fig:4.10). Also, in the space comprised between the two main peaks the signal is different from zero, as in the case of space charge accumulation in the bulk of the sample. While, the red circle of the same figure highlights the signal distortion after the main signal, therefore its correction can be avoided after signal processing by means of deconvolution technique, the final space charge profile becomes very similar, in which between the main peaks, but also on the right of the positive one, the signal is equal to zero.

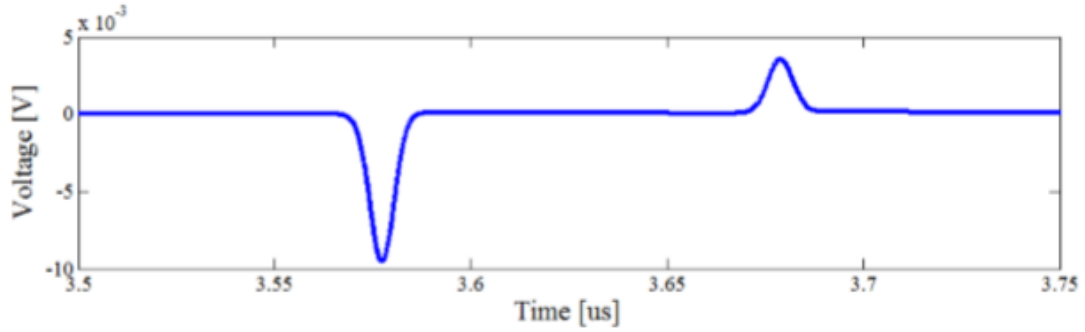


Fig: 4. 9 Ideal charge profile detected by the piezoelectric transducer.

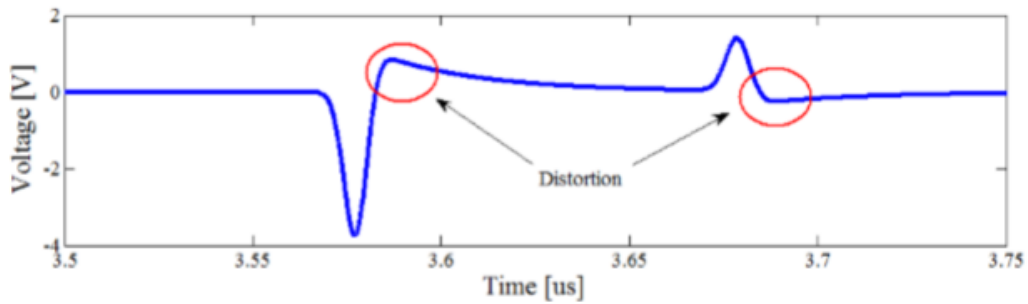


Fig: 4. 10 Real output signal after amplification

Considering the above-mentioned distortion can be considered as a systematic error, the deconvolution can be based on the signal obtained by applying a small electric field at the sample. In this condition, it can be assumed that the charges lay exclusively at the electrode interfaces while no charge is in the bulk of the dielectric. Where V_{dc} is the applied voltage, T_s is the sampling time due to the resolution of the oscilloscope, and u_{sa} is the sound speed into the sample.

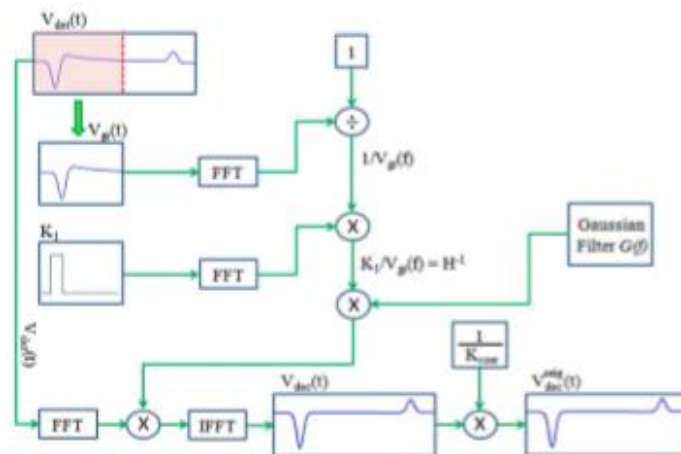


Fig: 4. 11 Example of deconvolution

The measurement output in the above described conditions involves two peaks with different heights due to the partial absorption of the pulse generated at the farthest electrode. The

higher peak measured at the oscilloscope can be compared with the calculated value of ρ_0 in order to evaluate the transfer function. Once the output deconvoluted signal which is explained in the above example Fig.4.11 is obtained in millivolts, a further operation is necessary in order to calculate the value of volume density charge. By assuming that the pulsed voltage is square shaped, the following expression can be used in order to convert the output deconvoluted signal in space charge.

$$v_{decon}(t) = k_p$$

where K is calculated based on a comparison with the signal obtained from a known value of space charge.

4.9. Measurement Errors:

We observe several types of error sources in the space charge measurement. Here we look on the different types of error and a rough estimation of their role in the system is provided.

4.9.1 Random error:

Random error is due to white noise in the system. The main source for white noise is thermal fluctuations inside the measurement system. Other possible source is external RF noise disturbance. The former cannot be avoided, but its influence on measurement accuracy is not significant. The latter can be eliminated by good designing a good electrical shielding case for the signal detection parts.

4.9.2 Systematic error:

The system calibration parameters can only be determined with a limited accuracy, giving rise to some error in the measurement. Sample thickness was measured with accuracy of $\pm 5\mu\text{m}$. The HV DC voltage supply output has an accuracy of ca. $\pm 1\%$. Material parameters include the acoustic velocity and vacuum permittivity ϵ_r , which are based on absolute values found in literature and contain some margin of error

4.9.3 Errors in signal detection and data acquisition:

The space charge is detected with the help of voltage impulse that has a limited width. That inherently limits the measurement resolution which makes it difficult to detect slight changes in the real charge profile. Another factor is slight ringing present in the voltage pulse, which leads to unwanted response in the dielectric. The limited bandwidth of different parts of the signal detection system causes them to function as low-pass filters further reducing the measurement resolution.

This causes inaccuracy in determining the sample properties in spatial dimension. Acoustic mismatching in different material.

4.9.4 Errors in numerical processing of the signal:

Numerical signal recovery techniques can be used to eliminate some of the error sources originating from the physical limits of the system. However, often the algorithms are unable to restore the signal accurately.

5. INTERFACES IN CABLE JOINTS

5.1. Preface:

In recent times, modern plastics are widely used as electrical insulation in high voltage power cables, gradually replacing older paper/oil systems. The most favored material is polyethylene, which exhibits excellent properties for use as a high voltage cable insulation material. However, because cable insulation operates at elevated temperatures and rarely polyethylene melts at a comparatively low temperature, crosslinking is usually used to improve its high temperature properties. We set out to examine several fundamental issues associated with the practical use of crosslinked polyethylene (XLPE). In particular:

To identify the mechanical stiffness of the insulating material.

To determine the mechanical loading for the electrical integrity of the material.

5.2. Elastic modulus (Young's modulus or modulus of elasticity):

Tension or compression occurs when two antiparallel forces of equal magnitude act on an object along only one of its dimensions, in such a way that the object does not move. One way to envision such a situation is illustrated in Fig.5.1. A rod segment is either stretched or squeezed by a pair of forces acting along its length and perpendicular to its cross-section. The net effect of such forces is that the rod changes its length from the actual length L_0 before the forces appeared, to a new replacement length L that it is under the action of forces. This change in length $\Delta L = L - L_0$ may be either elongation (when L is larger than the original length L_0) or contraction (when L is smaller than the original length L_0). Tensile stress and strain occur when the forces are stretching an object, causing its elongation, and the length change ΔL is positive. Compressive stress and strain occur when the forces are contracting an object, causing its shortening, and the length change ΔL is negative.

Young's modulus describes the relative stiffness of a material, which can be measured by the slope of elasticity of the stress and strain graph. It is calculated by the ratio of stress and strain value. A constant of proportionality will result, which is also called as the modulus of elasticity, or Young's modulus (E).

$$E = \frac{\text{Stress}}{\text{Strain}}$$

stress as the ratio of the deforming force F_{\perp} to the cross-sectional area A of the object being deformed. The symbol F_{\perp} that we reserve for the deforming force means that this force acts

perpendicularly to the cross-section of the object. Forces that act parallel to the cross-section does not change the original length of an object. The tensile strength is defined as

$$\text{Stress } \sigma = F/A$$

Tensile strain is the measure of deformation of an object under tensile stress and is defined as the fractional change of the object's length when the object is subjected to tensile stress.

$$\text{Tensile strain } \epsilon = \Delta l/l_0$$

Elastic modulus describes the relative rigidity of the material i.e., stiffness of the material which has high module of elasticity, while a versatile material will have low module of elasticity. The unit of Elastic modulus is giga-newton/m² (GN/m²). This phenomenon can play an important role in burnishing the margins of a crown (high elasticity), but the impression materials should have a low modulus of elasticity in order to enable removal from the undercut. The mod of elasticity should not be so low. Enamel features a coefficient of elasticity (3–4 times) than dentin and is stiffer and more brittle. Although dentin is more flexible and tougher, ceramic features a higher modulus than polymers and composites.

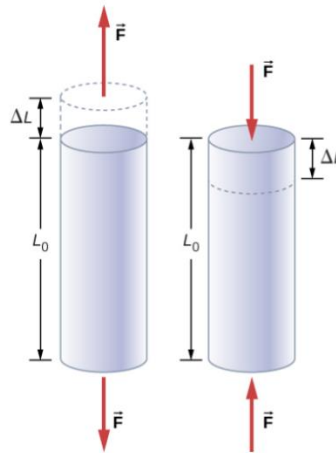


Fig: 5. 1 Tension and Compression

5.3. Solid-Solid interfaces:

Presence of solid-solid interfaces between polymers causes many problems since the dielectric strength of an interface is weaker than that of a bulk insulation due to the presence of microscopic imperfections such as cavities see Fig.5.2 protrusions, and interfaces. Such defects will reduce the tangential AC electric breakdown strength (BDS) of the interface. Even in cases when the magnitude of the tangential electric field is much lower than the dielectric strength of the bulk insulation, the imperfections at the interface cause local electric field enhancements. They are, thus, likely to initiate partial discharges (PD), electrical treeing, and an entire flashover might

eventually follow. Elastomers and polymers as insulating materials and BDS thereof have been studied to a large extent in the literature. The interfacial breakdown between two dielectric surfaces is one among the principal causes for the failure of power line joints and connectors, during which surface roughness, applied contact pressure, and elastic modulus of the dielectric material play an important role. There is, however, still a lack of knowledge on the theoretical correlation between the elastic modulus and the BDS of the interfacial surfaces. Therefore, the primary objective is to theoretically and experimentally examine the influence of the elastic modulus on the tangential AC breakdown strength of assembled solid-solid interfaces under various contact pressures.

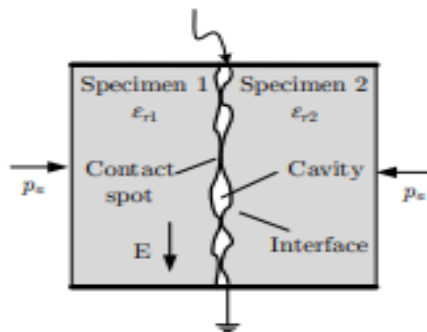


Fig: 5. 2 Air filled capacities in two dimensional

The PD activity presumably commences at the largest cavities whereas there is no activity in average sized cavities. Hence, it is still possible that PD inception in compressed average-sized cavities evolve to a flashover instantly. Secondly, when the contact pressure is considerably increased, the cavities might become much smaller in practice than the predicted average size. Therefore, an improved model estimating the largest cavities while providing a more intricate contact analysis is likely to perform better. Thirdly, as suggests, the interfacial BDS might also be influenced by the breakdown of the total area of contact, at high contact pressures. The coexistence of vented cavities, enclosed cavities and large contact spots at the interface are likely to occur in real life. Depending on the contact pressure, elastic modulus, and surface roughness, any of these mechanisms might predominate the rest or be equally dominant. One of the main reasons of solid interfaces being weaker than the bulk solid material is caused by the inhomogeneous electric field distribution at the interface since interfaces mostly arise between different materials with different relative permittivity. Besides, interfaces are generally mated during assembly at the site in sub-optimal and less controllable conditions, which renders them rather vulnerable to bad installations.

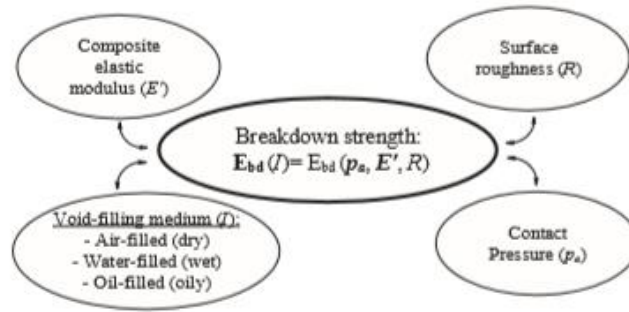


Fig: 5.3 Conceptual diagram of the parameters having an influence on solid-solid interface

In the above shown Fig.5.3 Applied contact pressure P_a surface roughness R and the composite elastic modulus of the interface E' are the key parameters affecting the size and number of voids on contact surface that in turn affects the tangential AC breakdown strength interface. The composite elastic modulus E' expresses the aggregate elastic modulus E of the combination of two materials. The properties of dielectric filling the cavities (air, water, oil, particles etc.) has also a substantial impact on BDS of the interface.

5.4. Co-Relation between the surface and Breakdown strength:

Thorough approach modeling the electrical breakdown phenomenon between two dielectric surfaces is far-fetched since the number of parameters involved varies significantly depending on the test environment and the test set-up itself. The length, number of channels and cavities are unknown which mainly depends on the elasticity of the material, the applied interfacial pressure and the surface roughness. The correlation between interfacial BDS and each of the parameters is studied.

As shown in the Fig.5.4 when the electric field traverses the interface tangentially the increased contact pressure i.e., interfacial pressure renders the interfacial BDS higher. The reason for this is the increased pressure which pushes the tips of the protrusions and the cavities smaller that in turns the interfacial BDS. Likewise, smoother surfaces show as similar an influence on the BDS because of the increased pressure, due to the reduced cavity size at the interface. It is worth mentioning that the interfacial BDS is higher than that of air, whereas it is not as strong as the bulk material strength even under a higher contact pressure or a smoother surface. The impact of the surface roughness and therefore the interfacial pressure on the BDS are going to be interpreted.

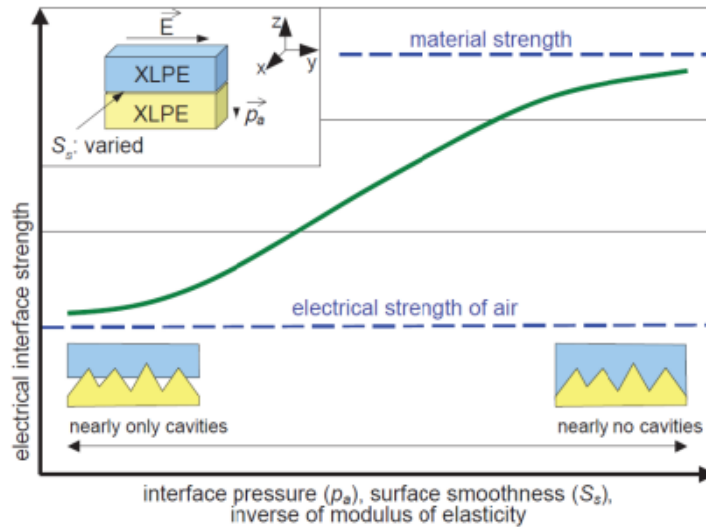


Fig. 5. 4 Indicates the relation between interface strength and pressure.

5.5. Interface Contact Model:

In accordance with the Greenwood-Williamson contact model shown in Fig.5.5 using probabilistic methods, the contact problems between two rough surfaces are calculated using the roughness parameters of the two contact surfaces. The contact problems associated with two rough surfaces are highly complex. Thus, the assumption of an equivalent surface, whose roughness parameters are the superpositions of the roughness parameters of the two surfaces is introduced, and the complex contact problems of two rough surfaces are simplified to problems of the equivalent surface and an ideal surface.

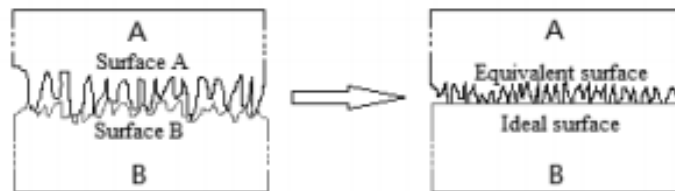


Fig. 5. 5Simplified contact model of two rough surfaces in contact according to the Greenwood-Williamson contact model.

Protuberances of the rough surface are assumed to follow a Gaussian distribution in height, and the probability density distribution function of the asperities' height z is:

$$\phi(z) = \frac{1}{\sigma\sqrt{2\pi}} e^{-\frac{z^2}{2\sigma^2}}$$

where σ is the root mean square of the asperity's height. When two surfaces are in contact, the highest asperities on both surfaces come into contact first. As the interface pressure increases,

some of the relatively lower asperities come into contact subsequently. The density of contact asperities increases with interface pressure. The real contact area is the sum of the area of all contact asperities. The density of contact asperities and the percentage of real contact area depend on the roughness, the interface pressure, and the mechanical properties of the two surfaces.

When the interface pressure is lower, the relatively highest asperities on both surfaces come into contact first. As the interface pressure increases, some of the lower asperities come into contact subsequently, and both the density of the contact asperities and the percentage of real contact area increase. The motion of electrons in the interface void consists of irregular thermal motion and the motion under the action of an electric force. The electrons are likely to collide inelastically with real contact asperities at the interface, causing the energy of the electrons to be lost during the collision. The energy of an electron is sufficiently small that the electron cannot penetrate the contact asperities during the collision. During two adjacent collisions, electrons will accumulate kinetic energy from the motion under the electric force. When the energy of electrons is sufficiently high, collision ionization will occur in the voids during the collision between electrons and gas molecules, leading to partial discharge. In addition, the asperities may also adsorb electrons with less kinetic energy, thereby reducing the number of free electrons at the interface.

During the density of the real contact asperities is small, the number of collisions between the electrons and asperities is not large. During the two adjacent collisions between electrons and asperities, the electrons can accumulate an enough energy under the action of electric force to allow collision ionization to occur in the void. When the density of the contact asperities is high, electrons cannot easily accumulate a sufficient amount of energy in the void to cause collision ionization because there are a large number of collisions between electrons and asperities and each collision will reduce the energy of electrons. Thus, the energy of electrons becomes too low to cause collision ionization in the void, making arousal of the interfacial discharge difficult. There is a probability of collision between electrons and asperities, which is influenced by the average area of asperities. The probability of collision between electrons and asperities increases with increases in the average area of real contact asperities, and the obstacle of asperities to electrons becomes quite significant. Thus, the interfacial DC voltage $U_{63.2\%}$ increases with increases in the average area of connected asperities.

Furthermore, space charge will accumulate at the interface under a DC electric field. When discharges occur in interface voids, charge will adhere to the cavity walls to form space charge, and the space charge will weaken the electric field in the voids. As the average area and density of the real contact asperities increase, the space charge accumulated on the cavity walls at the interface and weakening effect of the space charge on the interfacial electric field increase. The interfacial DC breakdown strength is related to the density and area of the contact asperities and the filler of the interface voids. If the interface is coated with high electric strength liquid, such as silicone grease, then the interfacial ramped DC breakdown voltage can be effectively improved. If the interface void is filled with air or water, then the interfacial DC breakdown strength will be reduced. Many studies show that silicone grease or silicone oil can significantly improve the interfacial breakdown strength, and the use of silicone grease or oil has been widely used in the installation of cable accessories. However, silicone grease or silicone oil can easily volatilize or dissolve into insulating material, producing interfacial voids at the interface.

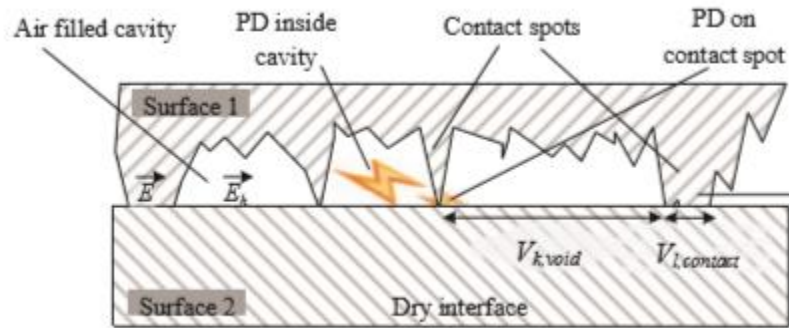


Fig: 5. 6 The electrical model of interface and field strength inside the voids

Based on the mechanical contact theory as shown in Fig.5.6 the voids are considered spherical so that the geometrical manipulation is analytically possible. The diameter of the voids can be determined by calculating the number of voids and the total area of the voids occupy. Regarding the voids, another assumption can be taken the number of voids is equal to the number of contact points. This assumption is necessarily because according to the contact theory only the number of contact spots along the interface can be analytically estimated.

The ratio between the real contact area A_{re} and the nominal contact area A .

$$\frac{A_{re}}{A} \approx 3.2 \frac{p_e}{E' \sqrt{\sigma} / \beta m}$$

5.6 XLPE-XLPE Interface:

Breakdown behavior of XLPE-XLPE interfaces under different pressure level. The Weibull plot of the BDS of the samples. The higher the applied pressure the slightly higher the BDS. This increase might be considered small, it confirms the dependency of the BDS on the interfacial pressure of XLPE samples. The pressure levels are considerably lower than that of in the case of XLPE-XLPE due to more elastic in nature.

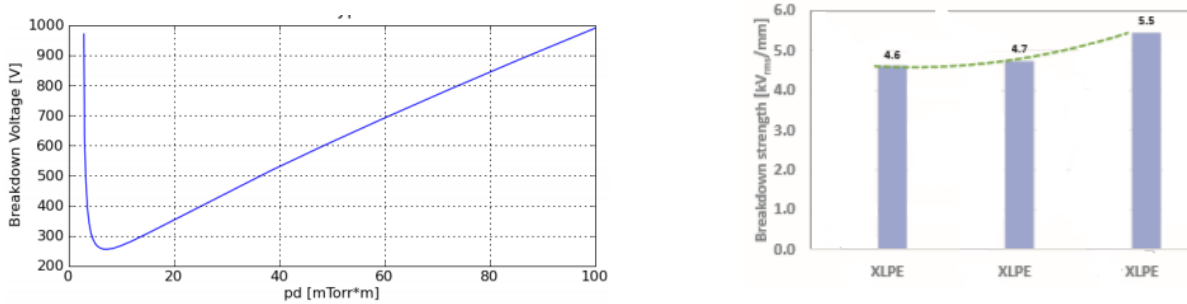


Fig: 5.7 Paschen Curve and Weibull plot

Cause of the low permittivity of the void compared to the solid, electric field enhancement is likely to cause PD initiation and breakdown of the voids at relatively low voltages. The real area of contact is generally very small compared to the nominal interface surface area even under heavy mechanical load. Thus, the electric breakdown of one void causes the breakdown of the entire interface. Since the voltage drop across contact spots is much lower where they act as barriers. Hence the breakdown strength of the interface is considered proportional to the tangential BDS of the interface on which the pressure and size of the voids will play the key role to the Panchen's curve as shown in Fig:5.7.

6. Experiment setup

This section illustrates the experimental set up made in this test procedures. It includes measuring setup, continued with the implementation procedure is performed during the test, and the specimen model.

6.1. Measuring Setup:

6.1.1 Sample Preparation:

XLPE foils with semi conductive electrodes were 3D-printed. Their appearance is shown in Fig.6.1. The electrodes cut through the XLPE and are accessible on both surfaces. The sample is made into a sandwich in which the top and bottom layers are with the XLPE and the middle layer is with the 3D electrode deposition on which the 3 layers are thermally pressed. In order to have a good contact the sample is pressed thermally (without controlling temperature). Distance between the electrodes is 0.5mm (this varies based on the electrode shape deposition) and the diameter of each electrode is 1.5mm.

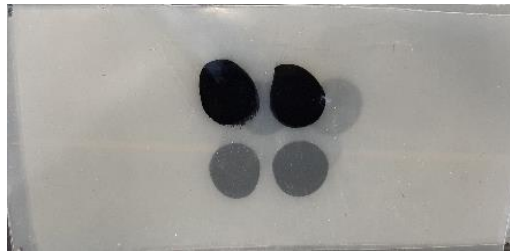


Fig: 6. 1 XLPE-3D specimen

6.1.2 Experimental Set-up:

The Thermal Step signal is generated by circulating the cold liquid within a radiator in contact with the sample. The electrodes between the sample are connected to current amplifier as shown in Fig.6.2. The last is associated with a PC which will record the current data and does the numerical information handling and the experiment procedure is repeated.

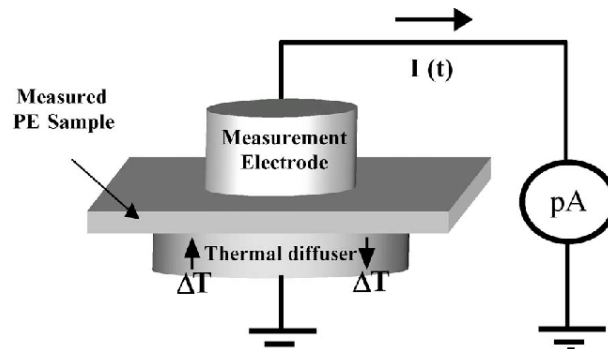


Fig: 6. 2 Experimental set-up of TSM

This measurement requires hardware along with the software. Hardware which includes the Thermal diffuser, Measurement Electrode, DC Voltage supply, pico-ammeter, Computer in which the software analyses the input data.

6.1.3 Thermal Diffuser:

Thermal diffuser provides a heat step, which creates a thermal wave. In which there is hot water which can be heated up to (25deggC) and cold water which cools down up to (-5deggC) maintaining the absolute temperature of 30deggC. This wave will diffuse through the thickness of the dielectric, which determines either an expansion or a contraction of the material, a variation of the insulation permittivity and causing a temporary and reversible displacement of the space charge located within the sample. This displacement will be, then, reflected on the electrodes, determining a variation of the induced charge and, consequently, a current between the electrodes. This setup is called TSM in short-circuit condition as shown in Fig.6.3



Fig: 6. 3 Thermal diffuser

6.1.4 pico-Amperometer:

The value of this current $I(t)$ read by a pico-ammeter (pA) is related to the distribution of both the electric field and the space charge. By setting the value for filter and the gain we can measure the Space charge which is directly connected to the Computer.



Fig: 6. 4 Keithley 428 Current Amplifier

6.1.5 DC Voltage Supply:

According to “FUG “DC Supply which is capable to measure up to 50kV in which I used until 20kV and the supply is given to the sample as Positive and Negative terminals. In which the sample is placed in the test cell which is measured at room temperature as shown in Fig.6.5. The samples are placed parallelly and given the connections accordingly. The supply is provided for an hour to the sample the starting from ideal stage until 20kV in which the voltage is increased in steps.



Fig: 6. 5 DC supply system with the connections for the circuit

6.1.6 Computer:

The Fig.6.6 shown which is used to record the data using the software of LabView. Which is easy to operate and understandable. We need to change the settings of the TSM measurement regarding the Temperature set time, Freewheel, Acquisition and the Measurement cycles. As the data is saved collect the data and try to analyse the data using the Matlab or Excel. Which will get the waveform from that we can tell whether there are homocharges or heterocharges are present.

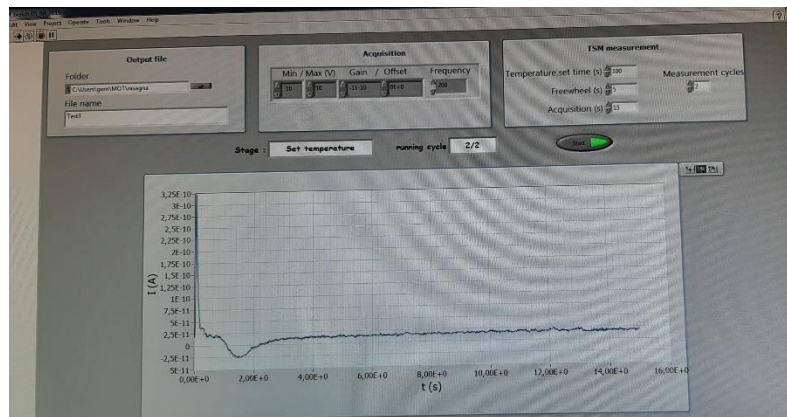


Fig: 6. 6 Software used for TSM

6.1.7 Experimental Procedure:

1. Place the sample in oven at room temperature give the connections to the sample for positive and negative supply.
2. Check the negative is grounded.
3. Applying negative or positive field to the sample of 1KV for an hour. i.e., Poling time is for an hour.
4. Removing the sample from the field that means switch off the supply by decreasing the voltage and then turn off the oven.
5. Leave the sample for 30 minutes let the space charge stabilizes thus TS current stability.
6. Then performing the measurements of TSM on the sample.
7. Recording the current values with respect to time.
8. This procedure is applied for different voltages (Ideal, 2, 5, 10 and 20 kV)

6.2. PEA Method:

6.2.1 Sample Preparation:

Cut through the central section of the cable along the axis to obtain 0.56mm-thick slices pick out slices large enough and cut them into 4x4cm squares as illustrated in Fig: 6.7 Two fresh specimens (unaged and aged) were tested directly without degassing procedure. Space charge measurement was carried out using pulsed electroacoustic (PEA) method

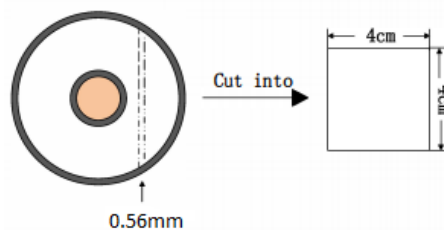


Fig: 6. 7 Illustration of sample preparation.

6.2.2 PEA System:

The space charge distribution in vertical and lateral directions of the applied pulsed electric field can be observed by using an acoustic lens sensor. The sensor can move rapidly, and the position is controlled by an X-Y positioner. While you are measuring, the location and the charge density are displayed at the same time. The output signals are deconvoluted, calibrated and displayed automatically during the measurement. Fig.6.8 illustrates about the experimental set-up.

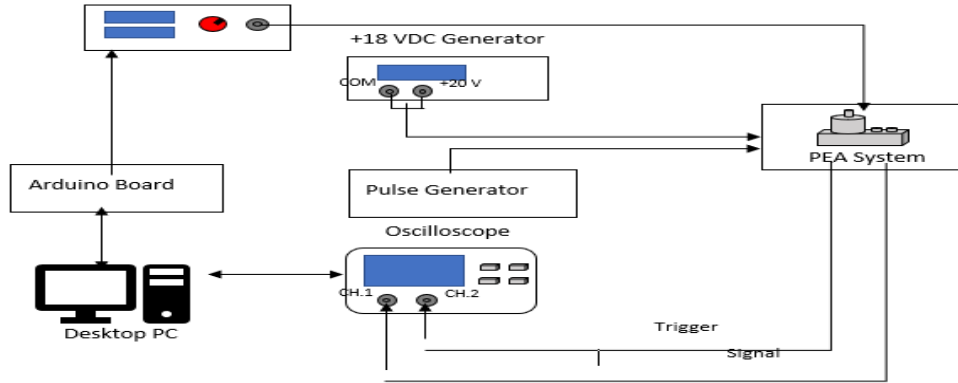


Fig: 6. 8 Experimental Set up of PEA Measurement

6.2.3 PEA Cell:

When measurements are made by the PEA cell, a sheet of semiconductor material with similar acoustic impedance of the sample under test, is placed between the high voltage electrode and the sample, with the aim to improve the acoustic matching. As shown in Fig.6.9 the system consisting of the three electrodes (HV, ground and bottom), semiconductor layer, sample, sensor, and absorber constitutes the acoustic circuit of the PEA cell. While the system, composed of resistance R, capacitance C, high voltage generator, pulse generator A and amplifier, constitutes the electrical circuit of the PEA cell. The entire system, which represents the PEA cell.

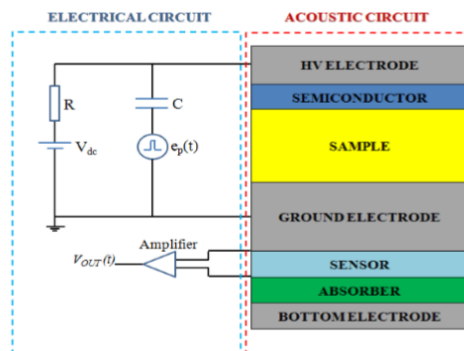


Fig: 6. 9 Block diagram of the PEA cell.

6.2.4 Pulse Generator

As described, the PEA measurement relies on a fast high-voltage pulse to stimulate space charges for producing a measurable signal. This kind of voltage pulse can be generated in several ways. Since commercial pulse generators are typically very expensive, a simple single purpose generator was designed to provide the high voltage impulse required in the measurement. Regular HV semiconductor switches would seem to be a good choice, but so far, their switching speeds are too slow for directly attaining pulse width in the order of few nanoseconds. Devices that are based on tunneling-assisted impact ionization fronts could be used to form voltage pulses with pulse width less than 100pS, a ramp up to 1 MV/ns and amplitude up to hundreds of kV have been proposed. However, so far there are no commercially available products using this novel technology. Some of the more readily available pulse generation methods found in literature include the following:

- Semiconductor switching circuit
- Marx bank pulsar with peaking switch and tail-cut switch.
- Transmission line pulsar

By the means of a semiconductor switch and fast recovery diode configuration, it is possible to gain a neat pulse output. Downside of this solution is that it is relatively complex and requires careful calculation and experimenting of several parameters. Combining a Marx bank generator with two switches as explained, an extremely fast pulse with amplitude of several kV can be attained. However, constructing a Marx bank generator requires large amount of space making the design less suitable for a compact PEA system illustrated in Fig.6.10. Of these methods, transmission line pulsing was found to be the most applicable for its simple, robust and inexpensive design.

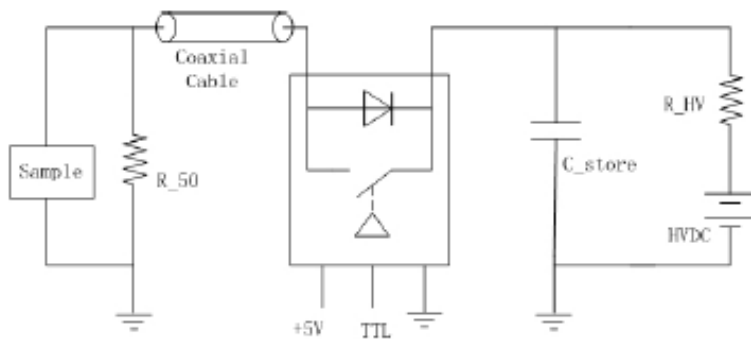


Fig: 6. 10 Pulse generator

6.2.5 Device Casing:

The pulse generator was built inside a casing to protect the circuitry from external RF noise as well as physical disturbances. Another important purpose of the casing is to isolate the user from the high voltage circuitry. The design implements separate switches for switching on the voltage supply and the pulse output. Because of low power dissipation, considerations for extra cooling measures were not necessary. The switching relay can work in ambient temperatures up to 60°C. Even though the casing is sealed, it is not likely that the inside temperature will rise to that point during normal operation. The pulse generator unit can be directly plugged into a common 220–230 V / 50 Hz power socket shown in Fig.6.11

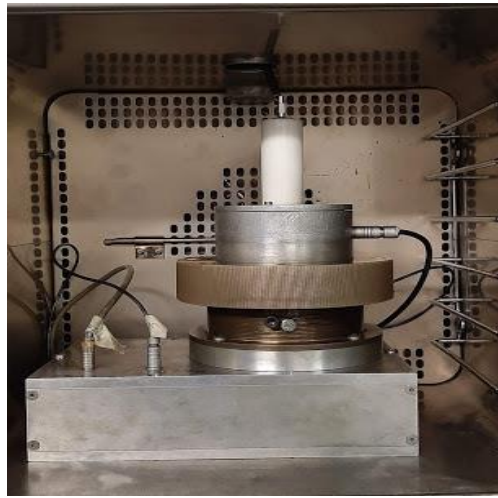


Fig: 6. 11 PEA System

6.2.6 Acoustic Signal Detector:

Piezoelectric Transducer: A piezoelectric transducer is used to receive the acoustic pulse $p(t)$ and convert it into electrical charge signal $q(t)$. The amplitude of $q(t)$ is proportional to the charge quantity and the sensitivity of the piezoelectric film while the delay indicates the position of the charge. If the transfer function of the transducer is written as $h(z = \mu_b \tau)$, the charge signal can be described as a convolution of $p(t)$ and $h(\tau)$:

$$q(t) = k \frac{u_b}{b} \int_0^{\infty} h(\tau) p(t - \tau) d\tau$$

In frequency domain the charge signal can be represented as

$$Q(f) = k \frac{\mu_b \Delta \tau}{b} H(f) P(f)$$

where $\Delta\tau$ is the sampling time, μ_b is the sound velocity in the transducer and b is the transducer thickness. The transmission coefficient K is determined by the acoustic impedance of the electrode and the transducer material and is more closely analyzed.

6.2.7 Signal Acquisition System:

The measurement also contains very wide spectrum of frequencies, and to attain high enough accuracy, the amplifier should have as large a bandwidth as possible. High bandwidth also reduces the low-pass filtering effect of the amplifier circuit, giving better measurement resolution. Among commercial wideband signal amplifiers, a broadband low noise amplifier. To minimize EMI issues originating from external radiation sources, the amplifier was placed inside an aluminum shielding case together with the piezoelectric signal detector.

6.2.8 Test Procedure:

1. Make sure the sample is stuck to the surface then tighten the brass plate.
2. Give the connections as shown in above image HV source, Vcc, Sensor, Trigger, and ground.
3. Start the software insert the applied field, thickness of the sample.
4. The software takes 4hrs in order to produce the output. 3hrs which takes for Polarization and 1hr for the Depolarization of the sample.
5. Make sure the software turns off and then save the data.
6. Collect the data then check the results in the MATLAB Software which gives the output by deconvoluting the signal.

Space charge accumulation behaviors and the electric field distributions in XLPE under various applied the charge densities are described using color scale. Red and Blue colors indicate the positive and the negative charge densities, respectively as shown in color scale bars beside the results. To show the space charge behavior in the sample clearly, the relatively lower maximum values of the color scale bars than the peak values on the electrodes are chosen.

6.3. Partial Discharges in AC/DC:

6.3.1 Measuring Setup:

The overall measuring setup consists of two parts, which is partial discharge monitoring and leakage current measurement. Both systems must monitor the specimen at the same time, the following Fig.6.12 indicates the measuring set-up of the test.

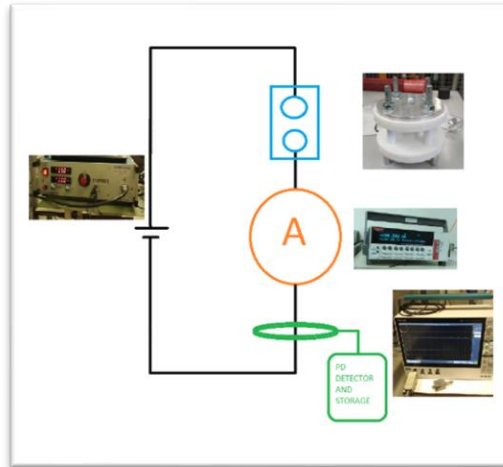


Fig: 6. 12. The measuring setup

The hardware equipment used in this research work are as follows: Voltage power supply, Test model with the specimen, leakage current measurement and Partial discharge acquisition. The hardware measuring equipment are combined with the software measuring equipment to capture the data which will be able to analyze.

6.3.2DC Voltage Power Supply:

This experiment uses F.u.G. Elektronik GmbH Series HCN 35 35000. This model can be measured up to 35 kV with positive or negative polarity with mating high voltage connectors is located on the front panel and cable high voltage connected to ensure the safety. This model also provides measurement display for the output voltage DC and the measurement display for the current when the short circuit happen. Voltage controlling with 10-turn potentiometers with precision scale, control mode indicated by LED and adjusting knob that can be lock are some feature that complete the advantage using this model.



Fig: 6. 13. DC voltage power supply

6.3.3 Leakage Current Measurement:

The experiment use KEYSIGHT model B2981A Femto / Pico ammeter as shown in Fig 6.14, due to the ability to measure very low leakage current that occur inside the circuit. Beside the accurate measurement, this model also featured with ability to read 20,000 signal per second and $< 20 \mu\text{V}$ burden voltage. With capability until $0.01 \times 10^{-15} \text{ A}$, this equipment offers high accurate data. This model also provides historical data with time domain view to capture some transient's condition. With display 4.3" color LCD, user capable to measure current trend and to monitor trend chart each pulse reading.



Fig: 6. 14. Current measurement equipment

With the advantage of this type feature, one of the most use full feature is that this model provide .csv format to be store and transfer easily using stick disc therefore user could easily took all the data measurement, collected on storage, analyze and process on the computer.

6.4. Partial discharge Acquisition:

PD acquisition Software: PDDC analyzer software is a software developed by University of Bologna and used to acquire information from oscilloscope TEXTRONIX 5 Series (Figure III-4) which connected by RJ 11 cable. This software capable to acquire necessary parameters for PD interpretation such as PD waveform, equivalent time – equivalent frequency (TF) map, PD magnitude and time length. Most of all, the main advantage of this software is its ability to perform online measurement and recorded based on the actual measurement.

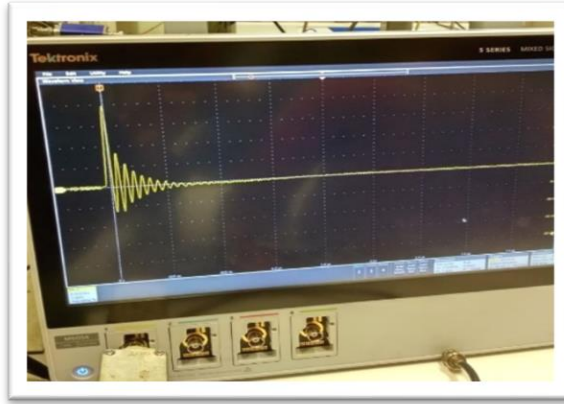


Fig: 6. 15 Oscilloscope TEXTRONIX 5 Series

Data acquisition carried out with this software able to be executed based on the specified period, number of frames, record length (μs), sampling frequency, voltage range and trigger level. This software acquires data from the oscilloscope with a maximum time of 15 minutes or reaches the maximum number of frames 10,000. After one of the thresholds is reached, the data from the oscilloscope is transferred and saved to the computer. On the time data being transferred and saved to the computer, the oscilloscope would not record any signal from HFCT. The oscilloscope repeats to acquire the signal after all the data transfer and save data already finish.

This software is able to control the trigger level of signal that is recorded by the software to minimize the external noise, with a range of trigger from 1 – 10 mV. The maximum voltage of signal is also able to be controlled based on the oscilloscope capability (Volts per Div) and signal length (μs).

6.5. PD Waveform Viewer:

PD waveform viewer is software that also developed by the University of Bologna as a tool to process the data that is saved by the PDDC analyzer software. This software could perform all necessary signal processing such as signal separation based on time and frequency and the important capabilities is the capability to identify original signal therefore the software helps to identify which signal is considered as partial discharge or external noise shown in Fig.6.16

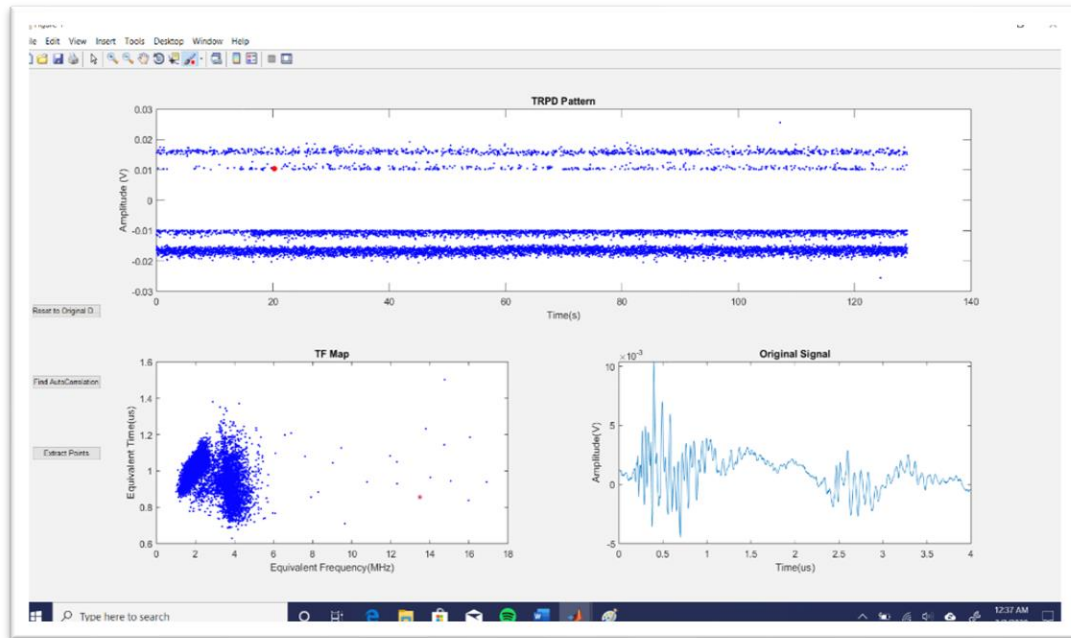


Fig: 6. 16 PD Waveform Viewer

6.6. Test Procedure:

The test procedures to conduct experiment for each of the specimens on the research are described as follows:

1. Prepare the specimen according to your test.
2. Place the sample on the test object and apply the pressure on the sample by using the torque meter.
3. Make sure all the above equipment's are available and connected according to the circuit diagram. i.e., DC voltage generator, test object, Pico-Amperometer and HFCT
4. Turn on the computer open the software PDDC analyzer as well as the oscilloscope TEXTRONIX 5 series.
5. Set the oscilloscope accordingly using software PDDC analyzer to ensure that the software could monitor PD on real time.
6. Make sure that Pico-Amperometer should be able to record the current values with unlimited time recording.
7. Before performing the experiment make sure the connections are given properly and set the storage file location and acquisition time setting in the computer.
8. Check for HV connection and the ground connection.

9. Turn on the DC generator make sure that the value of DC Generator starts with minimum value.
10. Start the PDDC analyzer to record the PD appearance.
11. Increase the voltage in steps of DC generator to reach the value that intended, and always monitor the voltage and current.
12. When the breakdown happens, immediately decrease the voltage to zero and then turn off the DC generator.
13. Switch off all the equipment's and shut down the system.
14. Check the cell with the ground wire (for safety issues) then open the cell in order to remove the sample from the test object.

Apply the same procedure for all the test specimens, in this research work we have used this procedure for all the experiments which are conducted. Based on the condition of observation variation voltage value, pressure value on the test object, length of time observation, length of time transition time changes.

6.7. Specimen:

Specimens are design to illustrate the actual cable jointing condition with variable pressure value. The specimen design is a 3D printed semi-conductive is inside the XLPE sheet with ± 500 μm thick, known as 3D specimen. XLPE sheet with diameter of semi-conductive circle is 15 mm with 5 mm separation between 2 electrodes as shown in Fig.6.17

Aluminum foil is placed on each semi-conductive electrode, in which one is connected to HVDC and the other connected to ground. The distance may vary between 2 electrodes but there will not be any deflection problem when the specimen is being press by mechanical pressure.

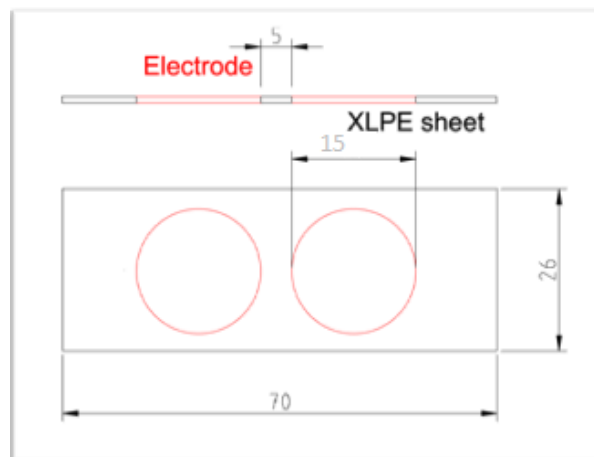


Fig: 6. 17. 3D Specimen configuration

6.8. Test Object:

According to the design of specimens, which already illustrated the condition of jointing cable, consider the specimen shape and capability of applying the equal pressure on the specimen. To produce mechanical pressure on the test object, the design utilizes 4 (four) bolts. The design also considers minimizing the usage of conductive material to minimize the influence on the measurement.

There are 2 (two) types of test objects: Nylon bolt type and Steel bolt type. Each type has pros and cons based on bolt materials. The nylon bolt type able to provide equal stress on low pressure (1 – 2 bar), on the other hand the steel bolt can be applied for high pressures from (2 – 8 bar).

The setup of nylon bolt type and steel bolt type consists of circular Teflon, that can push the specimen vertically inside and equip consists of 4 (four) screws the pressure applied on the specimen is measured in terms of torque. The other side (smooth surface) which will be in contact with the specimen, the nylon bolt type, has the axial force on 4 (four) bolts which is equally distributed on 80 diameter Teflon, on the other hand the axial force distributed on 40 mm diameter Teflon.

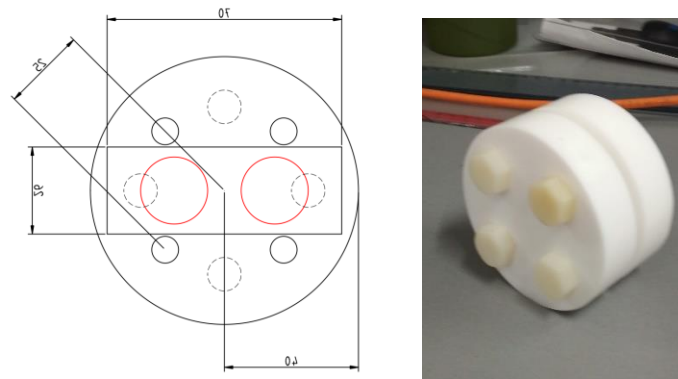


Fig: 6. 18 Test object nylon bolt type

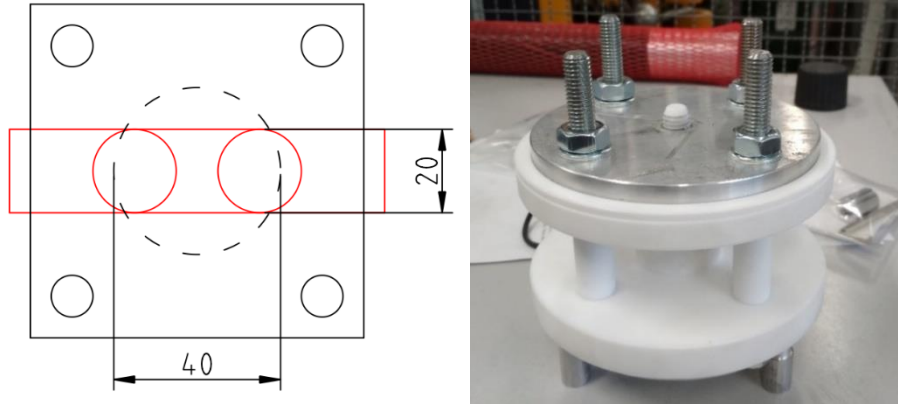


Fig: 6. 19 Test object steel bolt type

6.9. Mechanical pressure calculation:

The test object uses bolts to gain some axial pressure, therefore calculation on bolt ability is to provide enough torque which plays an important role. Based on the test object nylon type and steel type, calculation on screws torque become axial force based on reference literature: “Theory and calculation of threaded fasteners” Akira Yamamoto (Yokendo Co., Ltd) use this equation:

$$T = K \times d \times F$$

Which indicates as follows:

- T = Torque (N-m)
- K = Torque co-efficient
- d = Diameter size of screw (mm)
- F = Axial force (N)

The torque coefficient calculation based on bolt and screw dimension specification (Fig.6.20), the equation is below:

$$K = \frac{1}{2d} \left(d_2 \left(\frac{\mu}{\cos \alpha} \right) + \tan \beta \right) + \mu_n \frac{d_n}{d}$$

Indications are given below:

- d_2 = Pitch diameter (mm)
- d_n = Pitch diameter of bearing surface (mm)
- μ = Friction coefficient of threaded portion
- μ_n = Friction coefficient of bearing portion
- α = Half angle of screw thread (ISO screw 30°)
- $\tan \beta$ = Lead angle

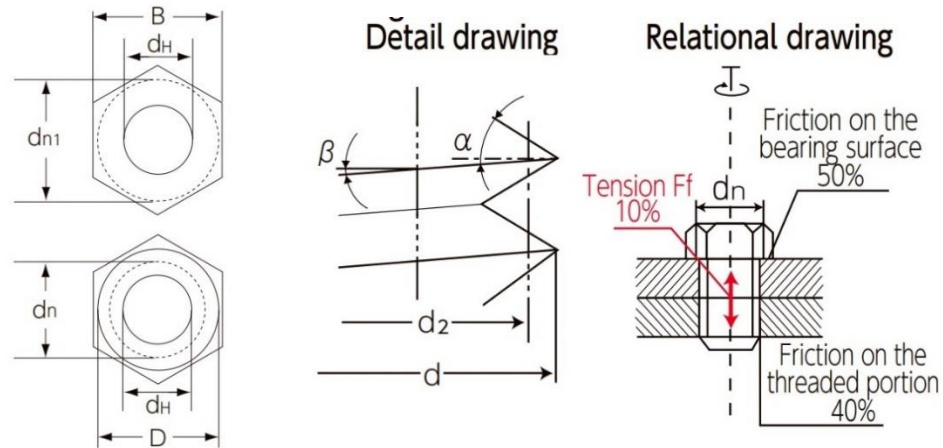


Fig: 6. 20 Bolt and nut dimension specification

Determined based on torque calculation, the torque coefficient can be calculated and prepare test range on the experiment for nylon bolt type and steel bolt type. The torque coefficient (K) for nylon bolts type is 0.2115 and with bolts diameter (d) 8 mm to produce 1 bar pressure needs 0.9 N-m torque. On the steel bolts type, torque coefficient (K) is 0.2090 and with bolts diameter (d) 10 mm to produce 1 bar pressure needs only 0.26 N-m.

Effective calculation of test objects, the test range of experiment on Table 6.1 indicates the capability of each test object and simulates the pressure level on the specimen.

<i>Pressure (bar)</i>	<i>Pressure (MPa)</i>	<i>Axial Force (N)</i>	<i>Nylon Torque (Nm)</i>	<i>Steel Torque (Nm)</i>
1	0.1	209.00	0.85	0.26
2	0.2	418.00	2.10	0.53
3	0.3	627.00	3.15	0.79
4	0.4	836.00	4.20	1.05
5	0.5	1045.00	5.25	1.31
6	0.6	1254.00	6.30	1.58
7	0.7	1463.00	7.35	1.84
8	0.8	1672.00	8.40	2.10
9	0.9	1881.00	9.45	2.36
10	1	2090.00	10.50	2.63
11	1.1	2299.00	11.55	2.89

12	1.2	2508.00	12.60	3.15
13	1.3	2717.00	13.65	3.41
14	1.4	2926.00	14.70	3.68
15	1.5	3135.00	15.75	3.94

Table: 6. 1 Test pressure range

Based on Table 6.1, the steel bolt type could produce (3 – 4 times) higher pressure compared to the nylon bolt. Therefore, on the above case study. This experiment is performed on 2nd type of object test to produce long range (1 – 8 bar) pressure measurement on the specimen.

7. Test Results and Analysis

In this section, results of measurements carried out on both XLPE and PP samples are discussed and also correlations between Space charge injection, Breakdown voltage, Leakage Measurement current and PDIV in AC and DC are sought.

7.1. Space Charge in XLPE and PP:

TSM can be used on all geometries and polymers. Here, it is used to measure the surface charge. Experiments were carried out on crosslinked polyethylene (XLPE). The sample consists of 1.5 mm-thick sheets provided by a cable manufacturer. The sheet includes carbon black electrodes, placed 0.5mm apart each other. The sample was realized by 3D printing. Samples using two different types of XLPE (Type I and II) were tested.

The specimens at different voltages have been measured at room temperature. The thermal wave has been supplied by a cold liquid (-5°C) and hot liquid (25°C) circulating in a radiator (thermal diffuser) in contact with the measured sample. The sample is connected in series with the **Keithley** current amplifier controlled by a PC via a custom-designed software.

The software interface consists of 4 panels shown in fig:7.1: (1) Output file (2) Acquisition (3) TSM Measurement and (4) A graphical output. The settings used are: Acquisition time =10s, Free wheel = 5s, Temperature set time = 80s, and Measurement cycles were set to three (The number depends on the output waveform)

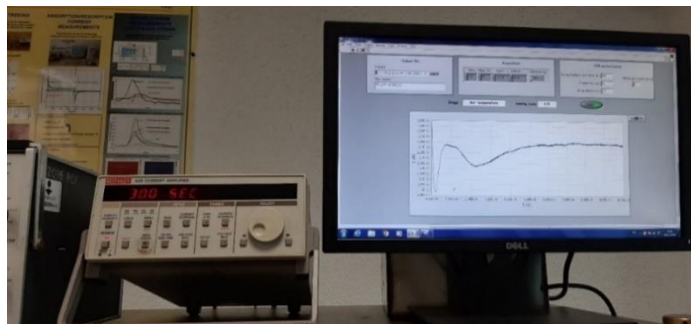


Fig: 7. 1 Experimental set up of TSM

7.1.1 Type-2:

TS currents are obtained by measuring the sample in short-circuit condition. We present the TS currents obtained prior and after DC poling.

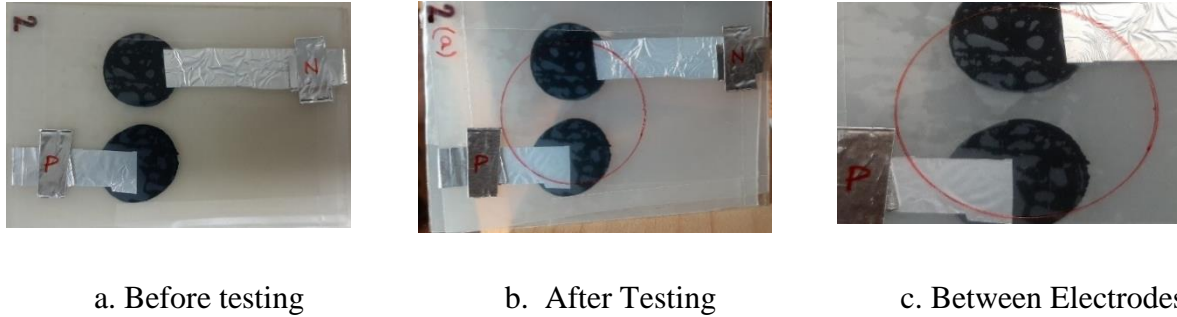


Fig: 7.2 3D Specimen with 2a configuration

To carry out the test, the specimen is placed in a ventilated test cell (**Venticell**, manufactured by MMM group) and the DC voltage applied to the sample for an hour (Poling time). After turning to zero the voltage, the sample is disconnected from the electrodes for 30minutes, for charge redistribution (Depolarization time). Subsequently, with the sample at room temperature, measurements are performed by applying a variable voltage from 0 kV to 20 kV. The test is repeated on other type of sample with same procedure the results were uploaded below we an observe in Fig:7.3. There are homo charges (charges which are accumulated with the same polarity as the neighboring electrode) and hetero charges (charges which are accumulated with the opposite polarity of the neighboring electrode) present in the sample.

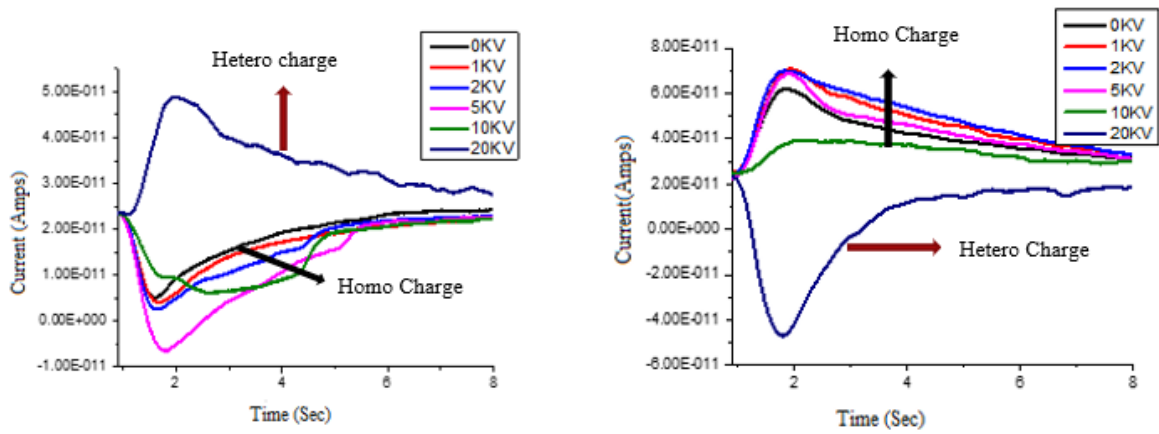
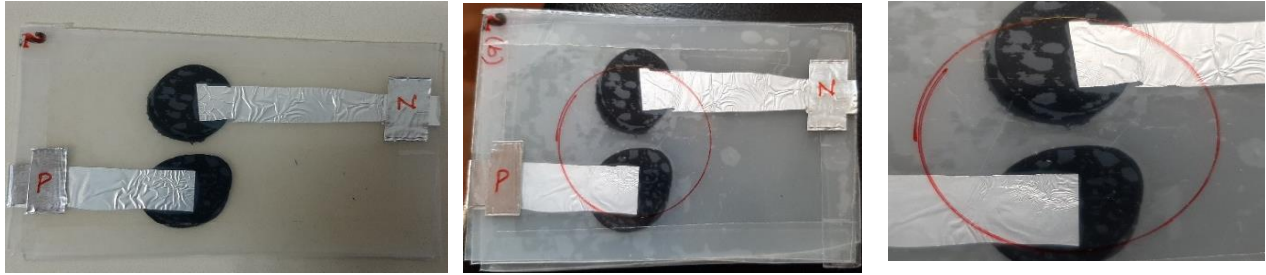


Fig: 7.3 Space charge Measurement using TSM Method for (left) negative and (right) positive applied field for Type-2a Sample



a. Before Testing

b. After Testing

c. Between Electrodes

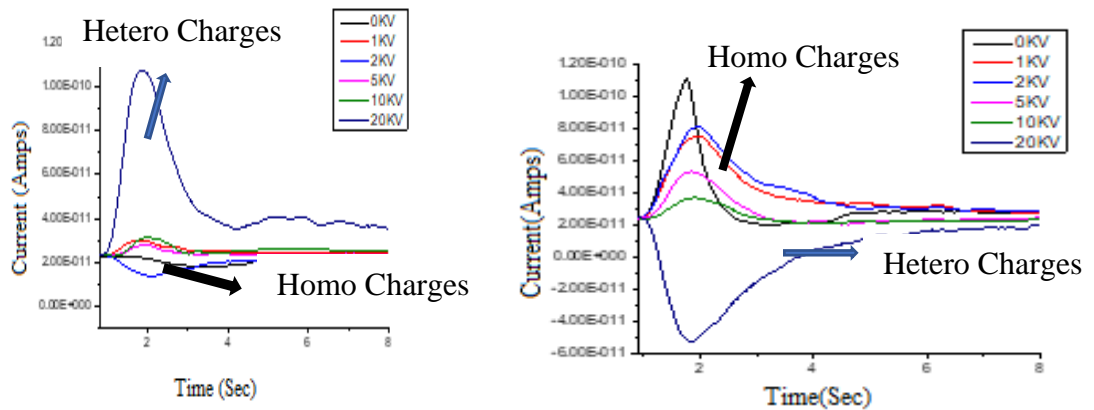


Fig: 7. 4 Space charge Measurement using TSM Method for (left) negative and (right) positive applied field for Type-2b Sample

The sample has then been submitted to several positive and negative poling voltages, as shown in Fig:7.3&7.4. The poling period is 60min, then the power source has been disconnected and the TSM measurement is performed. The negative peaks (In left graph) of TS current show a dominant trapped homo charge. These positive signals (In right graph) correspond to a same dominant charge nature and shows an increase in accumulated space charge. As the poling field increases there is a shift from dominant homo charge to dominant hetero charge.

We can note that, for applied voltages up to 10kV, the TS signals indicates homo charges. When the applied voltage is reverted, the signs of the signals also are also reverted. If we observe the above graphs, the applied voltage is for positive and negative fields 0, 2, 3, 5 and 10kV electrical conditioning the accumulation of space charge in the poling field has less homo charge. From 10 to 20kV electrical conditioning hetero charges are present in the sample.

7.1.2 Type-1:

The same procedure is performed for **Type-1**, the test results were uploaded in this case there is a break down @ 10kV. Accordingly, this type of XLPE cannot be used for cable joints, and the samples were not further used for PD tests.



Before Test

After Testing

Between Electrode

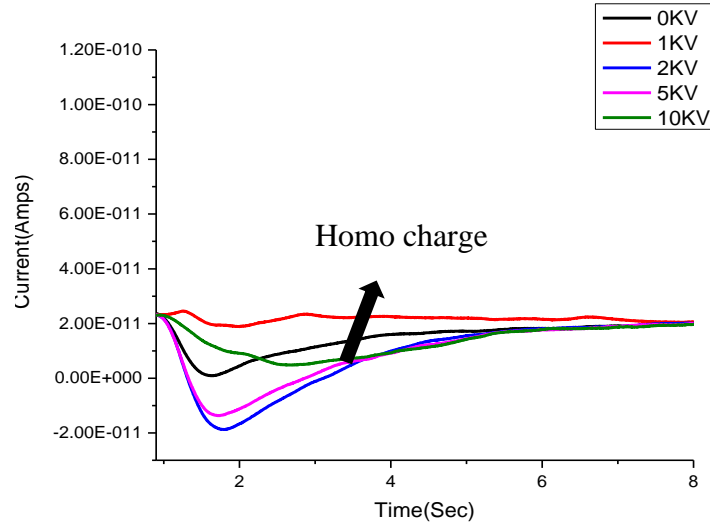


Fig: 7.5 Space charge Measurement using TSM Method for Negative field

Considering Fig.7.5, for Type-1 samples the space charge accumulation for the negative poling field is only homo charges until 10 kV. Increasing the poling field, the accumulated charge increases until breakdown @ 10 kV.

For both Type I specimens, a polarity reversal of the space charge. For Type I specimens, above 10 kV breakdown occurred. Apparently, the two phenomena can be correlated, in the sense that the shift from homo to hetero charge observed at 10 kV for Type I specimens could be the root cause for the breakdown of specimen of Type II.

7.1.3 Space charge in polypropylene samples (TSM)

In this model, charge carriers are injected from both electrodes, according to the polarity of the external fields. Table: 7.1 indicates the poling field with the temperature the charge injection process is analyzed using a Schottky mechanism and charge injection is the only source of charge carriers. After charges penetrating the material, the applied field will influence their movements across the material, and an effective mobility is proposed to study this process. During charge carrier's movement, some will be trapped in the localized states (deep trap centers) and therefore, the total amount of mobile charges across the sample will be reduced.

S.no	Poling Field (kV/mm)	Poling Temperature (°C)	Poling Time (min)
01	0	Room Temp	60
02	5	Room Temp	60
03	30	Room Temp	60
04	30	70	60
05	30	90	60

Table: 7. 1 Indicates the PP poling field with temperature

To validate experimentally Fig.7.6 which give the brief circuit connection. The principle of the under field TSM, we have used 0.5 mm thick flat sample of PP with electrode deposition of 50mm diameter with Graphite.



Fig: 7. 6 Circuit connection of TSM

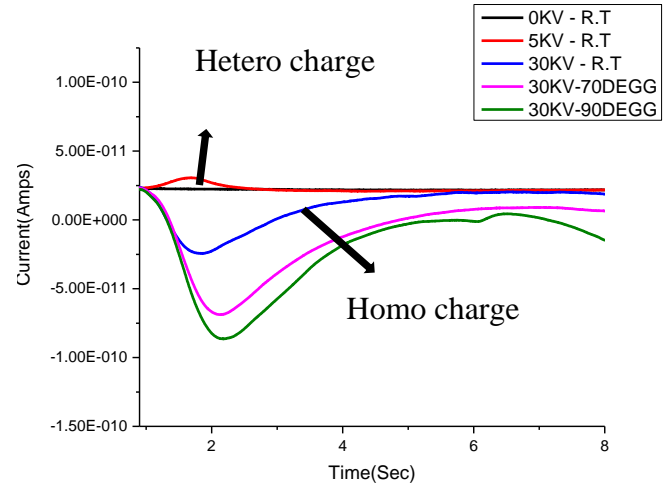
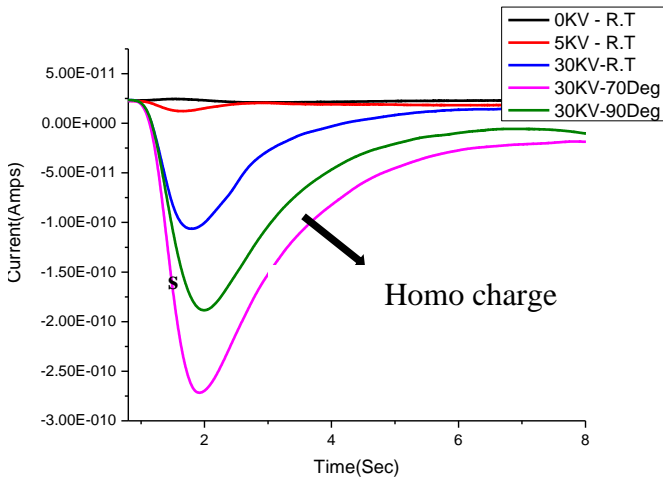


Fig: 7.7 Space charge Measurement using TSM Method for Positive field on PP samples

On considering the above graphs of the PP type insulation. The space charge accumulation is for positive poling field only. There are homo charges which are present until 30kV at room temperature. As the temperature increases for 30kV the behavior of both the samples are same.

7.2. Space charge in XLPE samples (PEA):

Space charge measurements were performed in planar XLPE samples. The results show a hetero charge distribution extending up to about one third of the insulation thickness, in the vicinity of both electrodes. The magnitude varies with temperature and electric field strength. With a constant magnitude of the applied voltage and the opposite polarity, the charge density changes the polarity, but shape and magnitude remain the same.

S.no	Applied Field (kV/mm)	Voltage (kV)	Charge (C/m ³)	Accumulated Charge (C/m ³)
01	15	7.8	0.48	0.2
02	20	10.4	0.55	0.17
03	25	13	0.76	0.19

Table: 7. 2It indicates the Applied Field with Charge accumulation in the sample.

HVDC constant application or voltage transient. Long term measurements show the establishment of several phenomena such as the migration of charges from an electrode to another or the accumulation of charges near physical or chemical defects. On the other hand, space charge accumulation is particularly dangerous during fast voltage transient such as the polarity inversion or overvoltage transient due to a fault. Indeed, Fig7.8 the experimental evaluation and the table

indicates the of the evolution of the electric field distribution into the dielectric of a HVDC cable and the Space accumulation in the test sample.

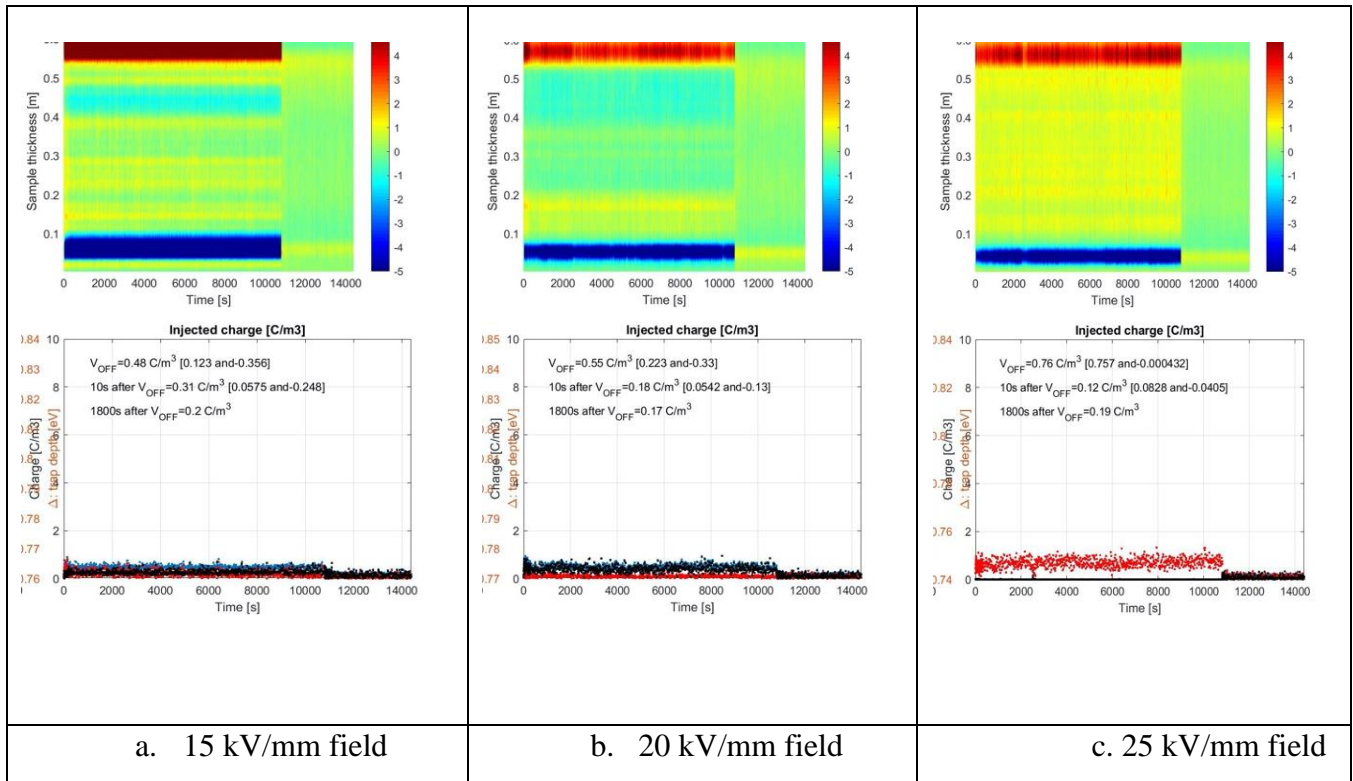


Fig: 7. 8 Field dependent Space charge characteristic on XLPE

7.2.1 Space Charge Behavior:

DC voltages are applied to the sample to understand the characteristics of space charge accumulation. Space charges are represented through a color code (blue and red for negative and positive charges respectively) that enables visualizing its evolution along the sample versus time. The negative voltage was applied to the conductor (cathode, to the bottom). Figure 7.6 shows the results of space charge behavior in XLPE under applied electric fields of 15, 20 and 25 kV/mm. During 3 hours of the polarization time at 15 kV/mm poling field, positive charges are predominantly occurring in the bulk of the sample. At the poling field of 20 kV/mm, the low level of hetero charge occurs at both electrodes, marked by light blue color near the anode while the color adjacent to the cathode are light yellow. As the field increased to 25 kV/mm, the positive charges are predominantly located at the bulk of the sample and near the cathode, suggesting the sign of the occurrence of hetero charges. During the depolarization time, it can be observed, especially right after the voltage is off ($V_{off} + 0s$), the accumulated charges are increasing as the poling field is higher, from 0.48, 0.55, to 0.76 C/m³, at the poling field of 15 kV/mm, 20 kV/mm,

and 25 kV/mm, respectively. After 30 minutes of depolarization, the accumulated charges are decreasing to 0.2, 0.17, and 0.19 C/m³, for the poling field of 15 kV/mm, 20 kV/mm, and 25 kV/mm, respectively. The very small difference value of accumulated charges meaning that the decreasing/decay rate of charges are higher as the poling field is higher. This could be related to the characteristic of the depth traps and mobility of the charge inside the samples.

7.3. Comparison between PEA and TSM:

This method was invented by Prof. Toureille in 1987 and it relies on the application of a thermal step across the insulation to generate a temporary displacement of the charges within. This influences the amount of charges at the interfaces generating a current with a typical order of magnitude of pA if the dielectric is short-circuited which is explained in the Fig.7.9. The generated current signal is then amplified, deconvoluted and calibrated to obtain the relation between the charge density and the current. The thermal step can be generated by heating the conductor or cooling the outer surface. In the first case, the short-circuited sample works as the secondary of a terminal and it is crossed by a current of several kA. Alternatively, the cooling of the outer surface is carried out by means of a cylindrical thermal diffuser crossed by a cold fluid and adjacent to the sample surface. While the inner heating method provides information about the whole sample, the outer cooling is used to get space charge measurements in a small portion of the sample.

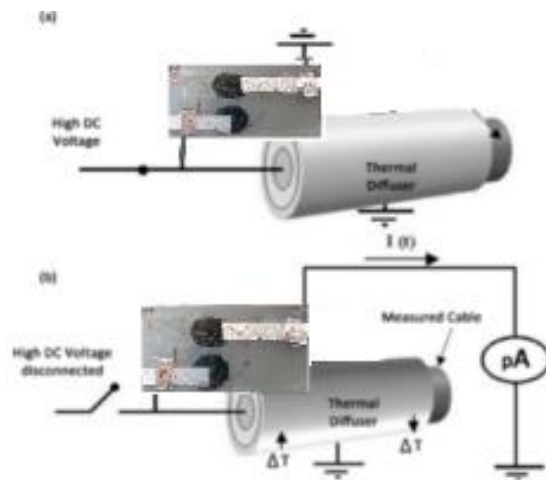


Fig: 7.9 Thermal Step Method (TSM) (a) conditioning phase (b) measurement phase

The current amplifier cannot be in contact with high voltage as well as the conduction and polarization current could mask the TS signal for these reasons, the protocol described in proposes a “double capacitor” configuration.

Unlike the PEA, the TSM provides information about space charge averaged among a sample segment and it is suitable for thick cables too. The TSM measurement setup is typically bulkier than the PEA due to the necessity to use a compensation cable. Moreover, with respect to the latter, the former requires a significantly greater measuring time due to the necessity to also perform a conditioning phase. Like the PEA, the TSM is also a partially destructive method.

7.4. Partial Discharge Monitoring:

The partial discharge detection equipment consists of hardware and software systems. A high frequency current transformers (HFCT) connected to oscilloscope Tektronix MDSO5 Series as PD analyzer hardware. PD analyzer software consist of the custom made PDDC software and the PD Waveform viewer. Partial discharge monitoring, like leakage current measurement, is not a destructive measurement therefore correlation between partial discharge behavior and breakdown voltage behavior could be one of the methods to evaluate cable jointing.

The measurement method was conducted by applied constant level pressure (4 bar, 8 bar) on the specimen and increasing the voltage level in steps of 1 kV, starting from 10 kV until PD appears. Each voltage level was hold for 15 minutes to monitor the appearance of partial discharges. The experiment is aimed at understanding the PDIV, PD magnitude and repetition rate of PDs as a function of the voltage level.

On the PDDC analyzer software, there are trigger setting to filter threshold signal which capture by the software and below the trigger will not be captured as they will be treated as noise. For every measurement of partial discharge monitoring, PDDC analyzer should be set according to the following observations:

- The positive trigger is set to 1 mV (lowest value) to capture all the signals above 1 mV.
- Since the applied voltage is positive and the PD detection circuit is of the direct type, the negative trigger is set on 10 mV (highest value) because negative PD cannot occur inside the sample.
- The volts per division are 5 mV/div considering that the maximum PD signal were not larger than 5 mV as observed through preliminary measurements.
- The Record length is 4 μ s, assuming the PD signal should last for only 2 – 3 μ s. Therefore, the record length is sufficient to capture all the PD signal within the time limit.

- Timeout was set to 15 minutes (highest value) and number of frames 10000. With these settings, the oscilloscope captures all signals on 15 minutes or 10000 signals (which reach first) then save the data to the computer.

After the data is saved on the computer, that data is transferred to visualization routines written in MATLAB. By using the PD waveform viewer, all the waveforms recorded by the oscilloscope are presented on the time and frequency map. There are three displays on the PD waveform viewer, which are: TRPD (time resolved partial discharge) pattern, TF (time frequency) map, and original signal. TRPD pattern indicate time instants of occurrence of PD signal that is captured by the HFCT. TF map will give the information of signal captured by the HFCT on equivalent frequency and signal equivalent length. The software determines through both the TF-map and a cross-correlation filter which signal can be considered as partial discharge and which should not be. The cross-correlation filter must be trained providing templates of noise signals and PD signals. Based on the experiment, the XLPE – XLPE interface for partial discharge monitoring conducted on low pressure (3 & 5bar) and high pressure (8 bar). The result measurement indicate that the partial discharge appears near to the breakdown level (8 bar) with detail describe on the Table 7.3

Voltage (kV)	3 Bars	5 Bars	8 Bars
8	-	-	-
9	-	-	-
10	-	-	-
11	1 events / 15 min	-	-
12		-	-
13		-	-
14		1 events / 15 min	4 events / 15min

Table: 7. 3XLPE – XLPE PD monitoring results

Based on XLPE – XLPE interface result with 8 bar mechanical pressure, partial discharge only occurs at 14kV voltage level. On the PD waveform viewer, the software has captured 4 points for 15 minutes, unfortunately all the signal is not partial discharge. TPRD pattern filters only positive signal. TF map filter only signal with frequency between 10 - 30 MHz considered as partial discharge. Based on all the consideration, total PD appearance are 4 times for 15 minutes observation, or PD appearance rate is 16/hr.

The measurements were performed on the Sample_1A with different applied pressures 8, 5 and 3 bar respectively which can be seen in Fig:7.10, 7.11 and 7.12. I performed measurements on Sample_1A @ 8bar pressure. The PDIV is started at 14 kV and there are just only 4 PD events at this level of voltage.

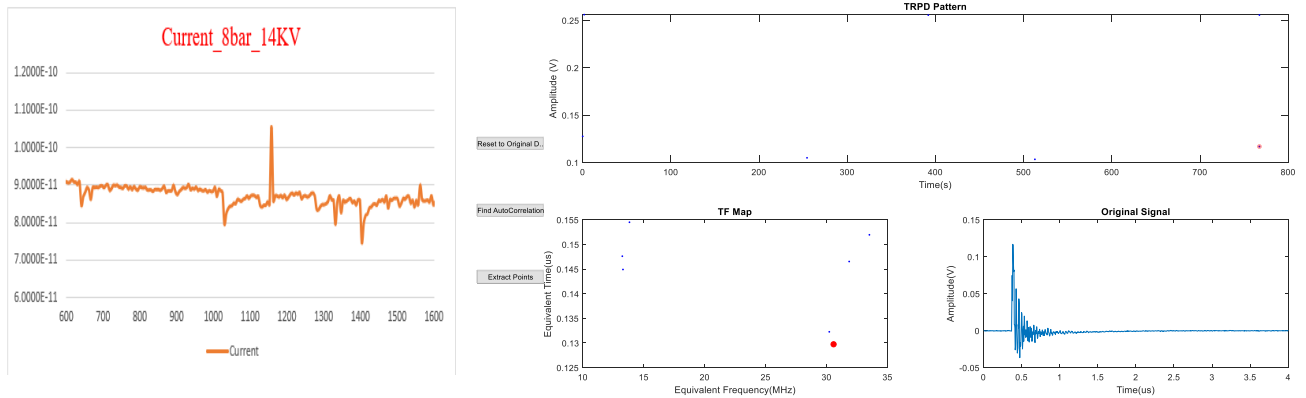


Fig: 7. 10 Partial Discharge Appearance 1a on 14kV @8 bar pressure Leakage current characteristics

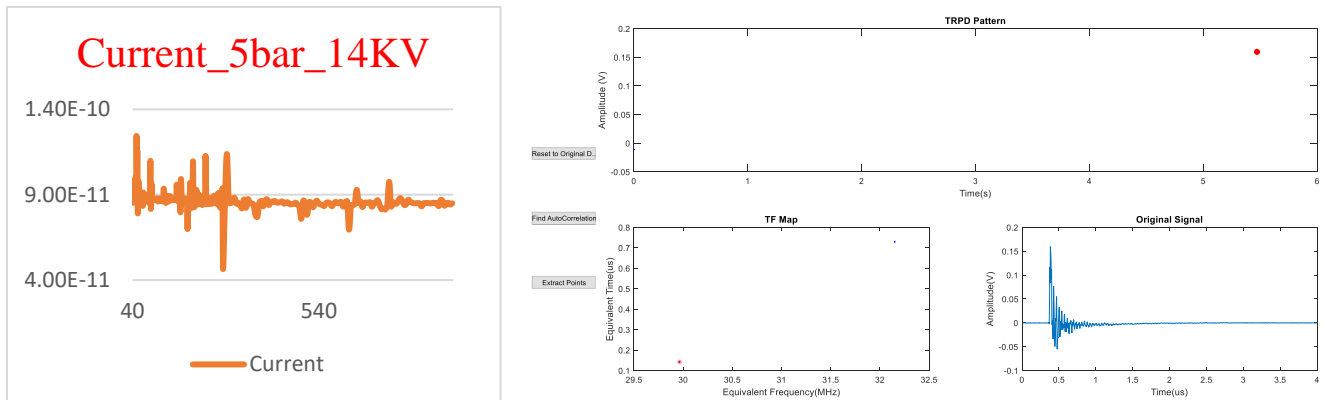


Fig: 7. 11 Partial Discharge Appearance 1a on 14kV @5 bar pressure Leakage current characteristics

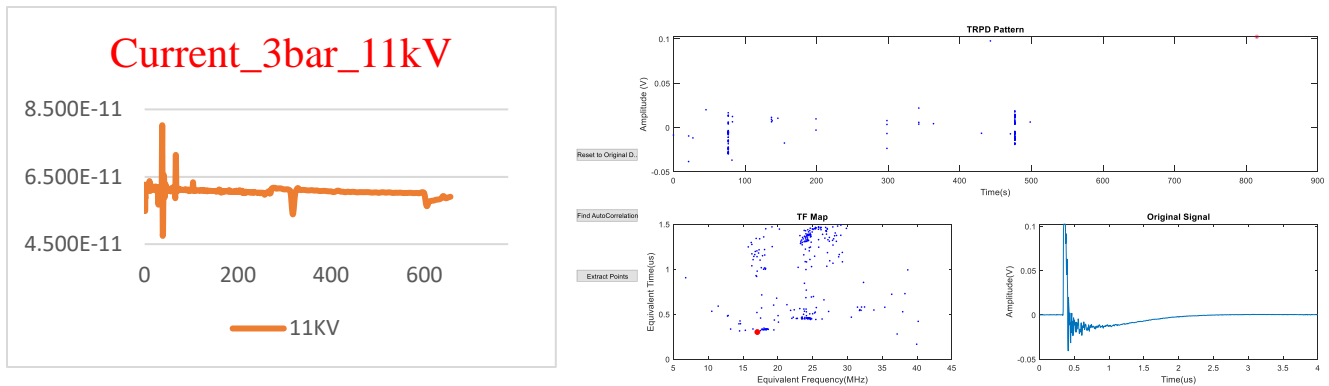


Fig: 7. 12 Partial Discharge Appearance 1a on 11kV@3 bar pressure Leakage current characteristics

7.4.1 Leakage Current Measurement:

Leakage current measurement is conducted to monitor the current that flows through the specimen when the voltage applied on the circuit. Pico-Amperometer was used to measure the current due it measures very low current (pA). Leakage current measurement was not destructive measurement, therefore correlation between leakage current behavior and breakdown voltage behavior could be one of the methods to evaluate cable jointing.

The measurement method was conducted by applying the voltage DC supply with constant level and current is recorded by the Pico-Amperometer. The electric current is generally divided into three components Charging current, Polarization current and Conduction current. The charging current component is required for charging the capacitance of the sample and the value decreases rapidly with time. The polarization current is caused by the accumulation of charge within the specimen under application of DC voltage. This polarization current is normally small and will also decrease rapidly with time. The conduction current is dependent on the applied DC voltage, the resistance of the specimen or insulation. Therefore, the measurement of leakage current requires longer time (15 minutes) due to the polarization condition need time to reach the stable condition (Figure IV-4).

Leakage current measurement is not destructive measurement, therefore the experiment able to conduct on all specimens. The measurement of leakage current was also conducted on different type of solid insulation.

Based on interface between XLPE-XLPE the Conductivity current is measured with different pressures applied with the same voltage level (11kV constant DC Voltage)

S.No	Torque (Nm)	Pressure (bar)	Leakage current (A)
1.	0.79	3	58.17×10^{-12}
2.	1.31	5	63.44×10^{-12}
3.	2.10	8	68.21×10^{-12}

Table: 7. 4 XLPE – XLPE leakage current

The above table indicates the comparison between Applied pressure and Leakage measurement current. This measurement is carried out for 15min with XLPE-XLPE solid interface the leakage measurement current increases when the specimen pressed with higher minimum surface pressure. There should be some co relation between Leakage measurement current and Applied pressure which can be further investigated.

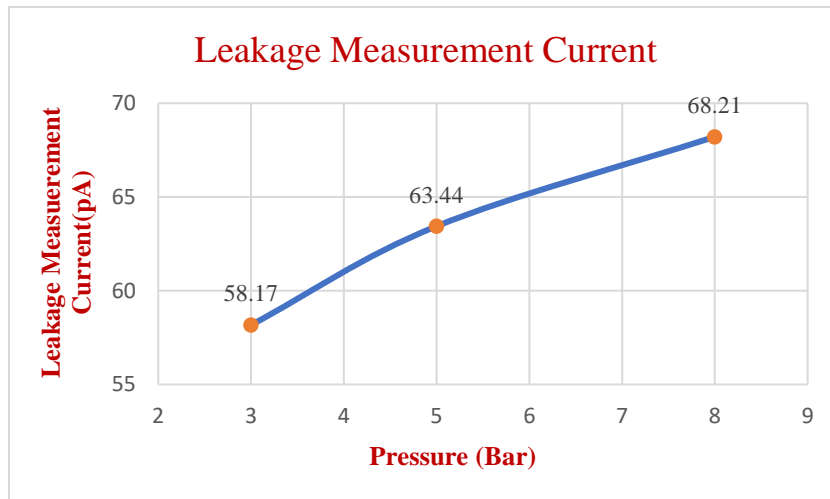


Fig: 7. 13 Dependence of leakage current on clamping pressure

7.4.2DC Breakdown Voltage

Breakdown voltage measurement conduct by applied voltage on the specimen from minimum voltage and increased each level in steps by (1 kV). Each level step requires 5 – 15 minutes to ensure the breakdown voltage or increase to higher level voltage. Due to breakdown voltage measurement method is destructive, even though specimen electrodes are not identical, overall, the semi-conductive layering, round shape, thickness, and distance between electrode are same in this case.

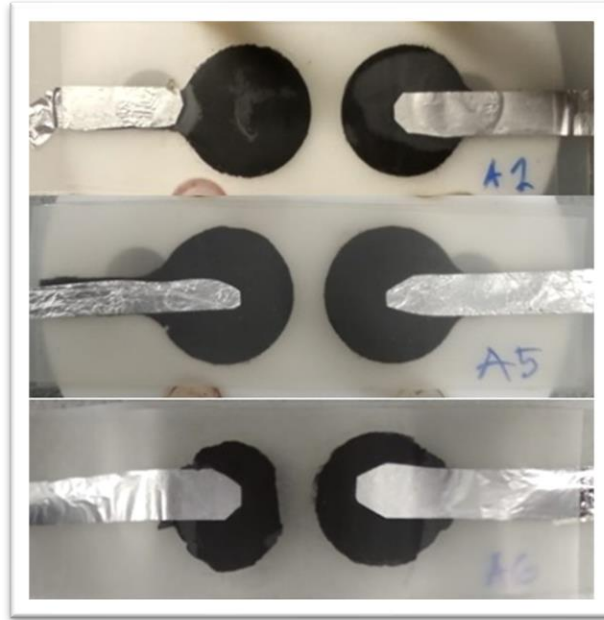


Fig: 7. 14 Different specimen on breakdown voltage measurement

Based on the experiment the breakdown voltage level on different mechanical pressure the result shown on Table 7.5.

S.no	Specimen	Pressure (bar)	Breakdown level (kV)
1.	#A1	1	9
2.	#A5	4	12
3.	#A6	8	22

Table: 7. 5. Breakdown voltage result

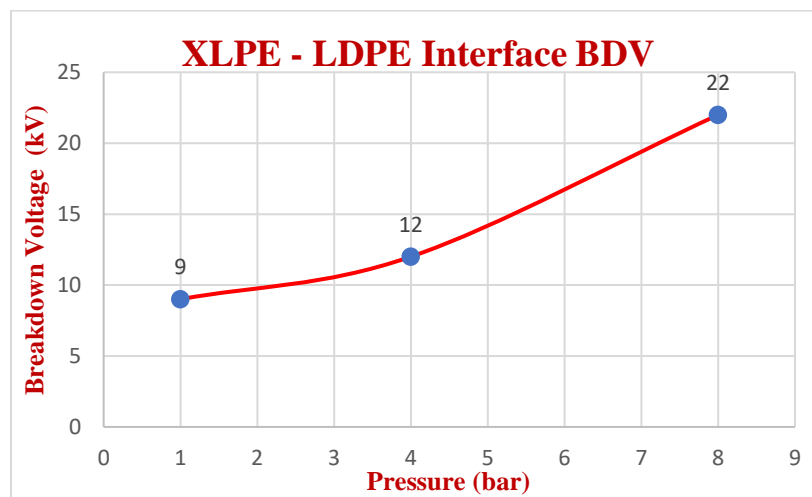


Fig: 7. 15 Mechanical pressure influence on breakdown voltage XLPE – LDPE interface

Based on the experiment of 2D specimen on XLPE – LDPE interface, the correlation between mechanical pressure on the specimen and the breakdown voltage are align (Fig 7.15). The increase of mechanical pressure on the specimen produce higher breakdown voltage level.

The correlation between mechanical pressure and electrical breakdown can be explain by the area of void that create between the XLPE – LDPE interface. When 2 (two) solid insulation contact each other, the surface of solid insulation is not contacted properly therefore voids and contact spots are formed at the interface (Fig 7.16). Voids that created on the solid-solid interface become weak when voltage applied on the circuit.

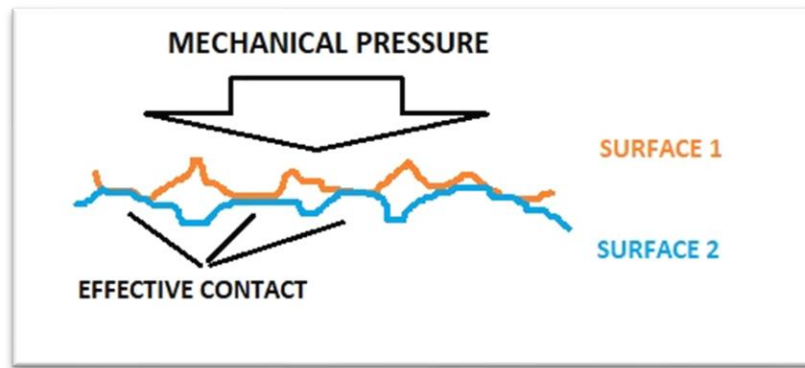


Fig: 7. 16 Illustration of void on solid-solid interface

The effect of increasing the mechanical surface pressure is to reduce the size of the void, increase the effective contact area and possibility to increase the gas pressure of the void [6]. Solid-solid interface basically a combination between air and solid insulation, where air become void and effective contact become solid insulation. The quality of insulation on solid-solid interface highly influence by the volume of void or air, higher void volume produces lower quality of insulation. Based on the last experiment, the result explain that higher pressure produces less void area on XLPE – LDPE interface therefore the breakdown voltage is higher.

7.5. Co-Relation between Space Charge and PDIV-DC:

Space charge measurements were performed through the Thermal step method TSM and pulsed electroacoustic PEA method, which is one of the most largely employed technique to detect space charges trapped in insulation. Partial discharges were measured through an innovative system which enables partial discharge pulses to be recorded and processed digitally, collecting a large number of pulses and allowing separation and identification tools, Partial discharge and space charge are closely related one affects the other accumulation of space charge can occur not only through electrode injection inside insulation bulk, but also through surface PD activity. Charges

trapped within material in shallow trapping sites at the boundary between dielectric and cavity serve as initiatory electrons. These charges may have been deposited by earlier PD events, but they can also be the result of charge transport from the electrodes towards the cavity. The results of this study could give some idea on the relation between PD and Space charge. If we consider the above results of space charge and the PDIV in DC conditions the threshold of space charge injection is 10kV and the PDIV the threshold is 11Kv.

7.6. Relation between Applied Pressure and PDIV:

7.6.1 Partial Discharge Inception Measurements:

The PD inception voltage (PDIV) of the interfaces improve understanding of the interfacial breakdown mechanism which is explained in Fig:7.15 In general, the measured inception stress of the solid-solid interface was found to increase nearly linearly with increasing contact pressure but was not significantly affected by surface roughness.

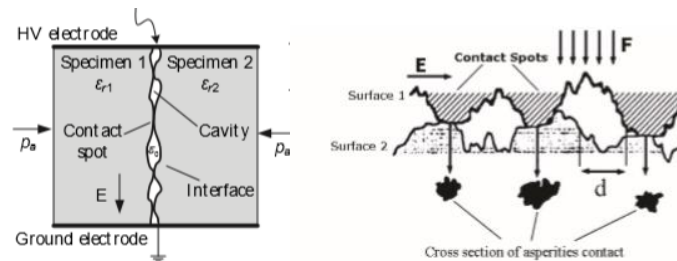


Fig: 7. 17 Illustration of an interface, showing voids and contact spots air-filled cavities at the interface

Fig.7.18 demonstrates about the interface consisting of a series connection of spherically shaped voids and contact regions. In this case, the applied voltage will be distributed along the interface. Therefore, PDs start simultaneously in all voids. Thus, electric field rises across the contact spots.

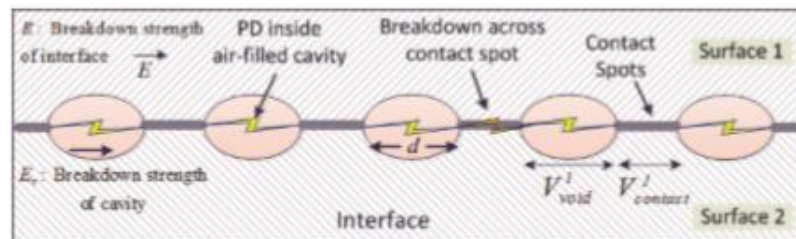


Fig: 7. 18 An electrical model of voltage drops at the interface

On-line testing equipment is connected to the power system and usually in normal operation used for condition assessment. The main challenge comes directly from the high attenuation of PD signals at high frequencies of break down mechanism in Fig.7.19.

$$v_a = \sum_{k=1}^n v_{k,void} + \sum_{i=1}^n v_{i,contact}$$

This means that quantities are not absolute but rather relative in nature. AC (50 Hz) voltage was applied with HFCT and the PD pulses were observed. The PD inception voltage (PDIV) of the interfaces was measured to examine the accuracy and understanding of the interfacial breakdown mechanism. PD is considered a major cause of the degradation at the interface and must be avoided.

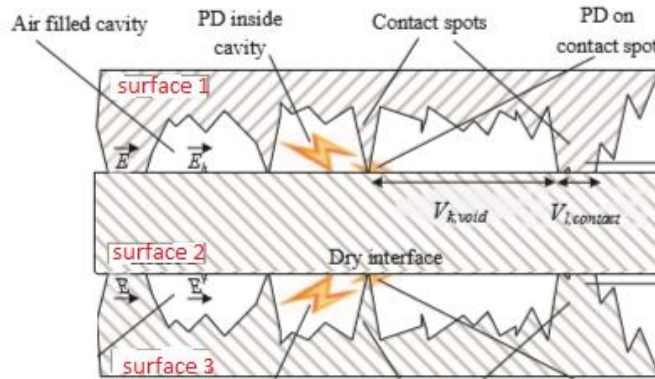


Fig: 7. 19 Breakdown Mechanism

The cavity size as a function of pressure can be estimated from PDIV measurements through the following procedure. The average electric stress in the region between the electrodes is:

$$E_{avg} = \frac{\text{PDIV (peak value in kV)}}{5\text{mm}}$$

Assuming that the cavities are spherical cavity, the field inside the cavity is the background field (assumed equal to the average field) times a factor that depends only on the geometry of the cavity (spherical) and on the relative dielectric constant of the XLPE (2.4): $E_{cavity} = 1.24 * E_{average}$

On comparing with the inception field,

$$E_{inc} = 2.52p \left(1 + \frac{19.2}{\sqrt{p} \cdot r} \right)$$

Where:

p= pressure in bars (In this case pressure is taken at 1bar)

r = radius in μcm

Equating the inception field to the estimated field in the cavity when $V = \text{PDIV}$, one obtains:

$$E_{inc} = 2.52p \left(1 + \frac{19.2}{\sqrt{r}} \right) = 1.24 \frac{\text{PDIV}}{5\text{mm}}$$

From the above calculation $1 - \frac{E_{inc}}{2.52} = \frac{19.2}{\sqrt{r}}$

Eventually, the radius of the cavity is given by:

$$r(p) = \left(\frac{19.2}{1 - \frac{1.24 \times \text{PDIV}(p)/5\text{mm}}{2.52}} \right)^2$$



Fig: 7. 20 Software for PD in AC

As it is an AC test, the software need be different, and its interface is shown in Fig: 7.20. First, we need to select the channel in which we are using and then the frequency should sync with PD Base II Synchronization to 50Hz the software has 4 portions with Waveform, Online PRPD Pattern, PRPD pattern, T-F map. In this experiment, trigger is set to 1 mV (lowest value) with consideration to capture all the signal above 1 mV to save on the software. After trigger setting, then Full scale setting to 1mV with consideration of maximum PD signal are not bigger than 5 mV amplitude while the Record length is for 5 μs setting with assumption the PD signal should last for only 2 – 3 μs length, As you observe the PD signal in Waveform column then wait for the consistency for few seconds then acquire data which will save in the computer. Timeout set on 5 minutes (highest value) then save the data to the computer. The below table 7.6 shows the PDIV voltage results.

S.no	Applied Torque (N-m)	Applied Pressure (bar)	PDIV (kV)
01	0.79	3	15.44
02	1.31	5	16.17
03	2.10	8	16.93

Table: 7. 6 PDIV voltage result

The higher the applied pressure the slightly higher the breakdown strength. This increase might be small, yet it confirms the dependency of BDS on the interfacial pressure of XLPE samples. The energy released during the breakdown, results on interfacial surface of specimens. Specific patterns of these tracks were observed for each material or interface condition. The measured PDIE for different values of applied voltage as a function of applied mechanical pressure. The measured PDIE is the average of electric field along the interface now of the observation of the first PD pulse and the estimated PDIE is the breakdown strength of corresponding void size. Graph 7.21 shows in general; the measured inception stress of interface tends to rise slowly with increasing applied mechanical pressure.

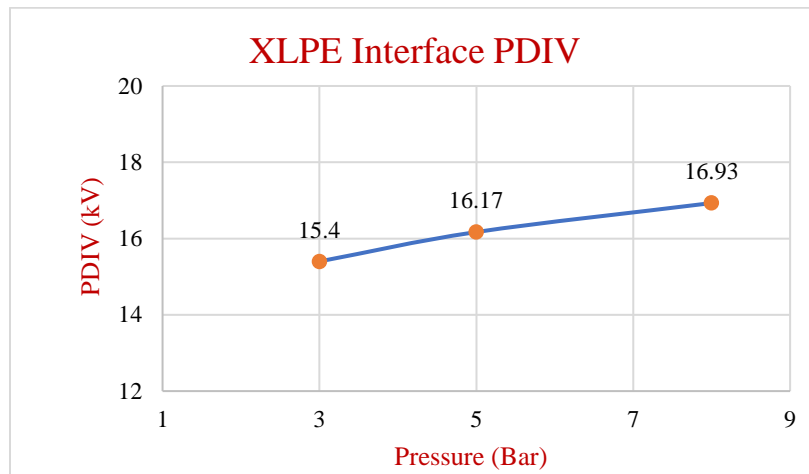


Fig: 7. 21 AC PD inception stress of interface surface

The term space charge, which occurs so frequently in research into polymeric HVDC cables (see chapters 4 & 5 in [11], for example), originates in the historical context of vacuum diodes where it described the electronic charge that accumulates in the space between anode and cathode as a result of electron emission from the cathode [14]. Space charge may also accumulate in a solid dielectric in the presence of a DC field. As it does so, this charge modifies and distorts the electric field pattern. If the space charge density becomes sufficiently high; the local electric field strength can exceed the dielectric strength of the insulation, leading to failure [14]. This is particularly the case following a reversal in polarity of the externally applied voltage because under these circumstances, space charge distributions that were generating a local field in opposition to the external field (thereby diminishing it) will be oriented so as to enhance the externally generated field following polarity reversal.

8. Conclusion

For space charge measurements, TSM and PEA techniques were used to observe any change in the space charge accumulation in XLPE sample. Then, we adapted samples of XLPE to allow either partial discharge measurements or space charge measurements after different electrical conditioning. The results obtained demonstrates the space charge injection in TSM for different electrical conditioning which is around 10 kV. Using PEA, after different electrical conditioning the space charge injection is also around 10 kV there is low level of hetero charges are injected.

Based on the experiment, higher the mechanical pressure on the solid-solid interface produce higher breakdown voltage level. DC conductivity indicates the quality of the insulation material, higher level of DC conductivity indicates higher dielectric loss that would increase the insulation temperature. The increase of insulation temperature might potentially lead to thermal runaway and thermal breakdown can occur if the DC conductivity is increasing with temperature and when the electric field sufficiently high.

In PDIV under DC electrical condition the sample which were performed with 3D configuration the PDIV-DC starts around 11 kV, as the voltage increases the repetition rate increases. As the pressure on the samples increases PD appearance voltage level changes. PDIV appears near to the breakdown voltage. Under AC conditions as the mechanical stress on the sample increases the PD appearance level of voltage also increases.

In the breakdown experiments, none or only few PD events were observed prior breakdown. Overall, it is unlikely that breakdown can be considered as PD-driven (the number of events would be insufficient to achieve breakdown by the conventional breakdown route, i.e., inception of PD, tracking, flashover of the interface) and other competing mechanisms need to be investigated. A possible mechanism could be associated with space charge injection. The tests carried out in Montpellier indicate that between 10 kV and 20 kV there might be an important change in the space charge accumulated at the interface. A large amount of space charge causes a Coulombic force exerted by the charges stored at the interface. This Coulombic force might reduce the pressure at the interface, leading to secondary mechanisms (as an example, increase of the leakage current) eventually leading to the failure of the interface.

9. Future Scope

Unfortunately, the COVID-19 pandemic prevented further tests to be carried out. Tests at different temperatures would help to acquire further information. In particular, above 90°C there is a sharp reduction of the Young modulus of XLPE. Tests showing that above 90°C there exists also a substantial drop of the breakdown voltage would prove the electro-mechanical nature of the failure.

10. References

1. C. P. Martin, A. S. Vaughan “The thermomechanical behavior of crosslinked polyethylene cable insulation material” 2003 Annual Report Conference on Electrical Insulation and Dielectric Phenomena.
2. B. X. Du, Hang Xu and Jin Li “Effects of Mechanical Stretching on Space Charge Behaviors of PP/POE Blend for HVDC Cables “B. X. Du et al.: Effects of Mechanical Stretching on Space Charge Behaviors of PP/POE Blend for HVDC Cables.
3. Hanyu Ye, Zhengyi Han, Yi Luo, Qikai Zhuang, Tobias Fechner, Haitian Wang, “Design Aspects on HVDC Cable Joints”12th IEEE International Conference on the Properties and Applications of Dielectric Materials - Xi'an – China
4. G. Hoogenraad, J. Beyer “Digital HVDC Partial Discharge Testing” Conference Record of the 2000 IEEE International Symposium on Electrical Insulation, Anaheim, CA USA, April 2-5,2000
5. Jun-Wei Zha , Yun-Hui Wu , Si-Jiao Wang , Dong-Hong Wu Hong-Da Yan1 and Zhi-Min Dang1“Improvement of Space Charge Suppression of Polypropylene for Potential Application in HVDC Cables “ IEEE Transactions on Dielectrics and Electrical Insulation Vol. 23, No. 4; August 2016
6. S. Agnel, P. Notingher jr., A. Toureille, “Space Charge Measurements Under Applied DC Field by The Thermal Step Method”, IEEE Conference on Electrical Insulation and Dielectric Phenomena, pp. 166-170, 2000.
7. Jérôme Castellon, Serge Agnel, and Petru Notingher, “Review of Space Charge Measurements in High Voltage DC Extruded Cables by the Thermal Step Method”, IEEE EIM, Vol. 33, pp. 34- 41, 2017.
8. J. Castellon, P. Notingher Jr., S. Agnel, A. Toureille, J. F. Brame, P. Mirebeau and J. Matallana, “Electric field and space charge measurements in thick power cable insulation under long term ac and dc stress using the thermal step method”, IEEE EIM, Vol.25, pp. 30-42, 2009.
9. D. Fabiani, G. C. Montanari, A. Cavallini and G. Mazzanti, “Relation between space charge accumulation and partial discharge activity in enameled wires under PWM-like voltage waveforms”, IEEE Trans. Dielectr. Electr. Insul., Vol. 11, pp. 393-405, 2004.

10. Antonino Imburgia, Rosario Miceli, Eleonora Riva Sanseverino, Pietro Romano and Fabio Viola “Review of Space Charge Measurement Systems: Acoustic, Thermal and Optical Methods” A. Imburgia et al.: Review of Space Charge Measurement Systems: Acoustic, Thermal and Optical Methods
11. Shakeel Akram, Jérôme Castellon, Serge Agnel “Space Charge Analysis of Multi-Structure Polyimide Films using TSM” 2018 IEEE Conference on Electrical Insulation and Dielectric Phenomena – Cancun – Mexico
12. R. J. Fleming “Space Charge Profile Measurement Techniques: Recent Advances and Future Directions” IEEE Transactions on Dielectrics and Electrical Insulation Vol. 12, No. 5; October 2005.
13. Giuseppe Rizzo, Pietro Romano, Antonino Imburgia and Guido Ala “Review of the PEA Method for Space Charge Measurements on HVDC Cables and Mini-Cables “Energies 2019, 12, 3512; doi:10.3390/en12183512.
14. N. A. Othmana, M. A. M. Piaha, Z. Adzisa, N. A. Ahmada “Comparative Study on Space Charge Distribution Measurements using PEA and PWP Methods on High Voltage Insulation” 64:4 (2013) 43–47 | www.jurnalteknologi.utm.my | eISSN 2180–3722 | ISSN 0127–9696.
15. B. Vissouvanadina, T.T.N.Vua, G.Teyssedrea, N.I.Sinisukab “Space Charge Measurement on XLPE Cable for HVDC Transmission using PEA Method” A.R.A. Raja et al. / Procedia Technology 11 (2013) 327 – 333
16. Pan Tang, Qiaohua Wang, Xuguang Li and Yi Yin “Investigation of Cable and its Accessory insulation in Extruded HVDC Cable Conference” Proceedings of ISEIM2011.
17. Andreas Dean Elben, Ronald Plath, “Modern Noise Rejection Methods and their Applicability in Partial Discharge Measurements on HVDC Cables” 978-1-5386-5086-8/18/\$31.00 ©2018 IEEE
18. Kreuger, F.H., Gulski, E., Krivda, A.: Classification of partial discharges. IEEE Trans. Dielectr. Electr. Insul. **28**(6), 917–931 (1993)
19. Fromm, U., Morshuis, P.H.F.: Partial discharge classification at DC voltage. In: IEEE 5th International Conference on Conduction and Breakdown in Solid Dielectrics, Leicester, UK, pp. 403–407 (1995).

20. Morshuis, P.H.F., Jeroense, M., Beyer, J.: Partial discharge part XXIV: the analysis of PD in HVDC equipment. *IEEE Electr. Insul. Mag.* **13**(2), 6–16 (1997)
21. Saadati, H., Seifert, J., Werle, P., Gockenbach, E., Borsi, H.: Partial discharge analysis under hybrid AC/DC field stress. In: *The 19th International Symposium on High Voltage Engineering*, 23–28 August 2015, Pilsen, Czech Republic (2015)
22. Emre Kantar and Erling Ildstad “Effect of Elastic Modulus on the Tangential AC Breakdown Strength of Polymer Interface” *IEEE Transactions on Dielectrics and Electrical Insulation* Vol. 26, No. 1; February 2019
23. T. L. Hanley, R. P. Burford, R. J. Fleming, “General review of polymeric insulation for use in HVDC cables,” *Electrical Insulation Magazine*, IEEE, vol. 19, No. 1, pp. 13-24, 2003
24. B. X. Du, J. G. Zhang, and D. S. Liu, “Interface charge behavior of multi-layer oil-paper insulation under DC and polarity reversal voltages,” *IEEE Trans. on Dielectr. Electr. Insul.*, vol. 22, no. 5, pp. 2628–2638, Oct. 2015.
25. E. Kantar, D. Panagiotopoulos, and E. Ildstad, "Factors Influencing the Tangential AC Breakdown Strength of Solid-Solid Interfaces," *IEEE Trans. Dielectr. Electr. Insul.*,
26. D. Panagiotopoulos, "AC Electrical Breakdown Strength of Solid Solid Interfaces: A study about the effect of elasticity, pressure and interface conditions," M.S. thesis, Dept. Elect. Eng., TU Delft, 2015.
27. Emre Kantar, Frank Mauseth, Erling Ildstad and Sverre Hvidsten “Longitudinal AC Breakdown Voltage of XLPE-XLPE Interfaces Considering Surface Roughness and Pressure “24, No. 5; October 2017.
28. Majid Hasheminezhad and Erling Ildstad “Application of Contact Analysis on Evaluation of Breakdown Strength and PD Inception Field Strength of Solid-Solid Interfaces”. *IEEE Transactions on Dielectrics and Electrical Insulation* Vol. 19, No. 1; February 2012
29. P. Notingher, S. Hole´, L. Berquez and G. Teyssedre “An Insight into Space Charge Measurements”. *International Journal of Plasma Environmental Science & Technology*, Vol.11, No.1, APRIL 2017.
30. Min Wu, Hong Cao, Jianneng Cao, Hai-Long Nguyen, João Bártolo Gomes, and Shonali Priyadarsini Krishnaswamy “An Overview of State-of-the-Art Partial Discharge Analysis Techniques for Condition Monitoring “*IEEE Electrical Insulation Magazine* 0883-7554/15/©2015.